Synthesis of 1,4-Dihydropyridines as Potential Antimalarial Chemotype

By

Nomakhwezi Mvumvu

A dissertation submitted to the University of Cape Town in fulfilment of the requirements for the degree of **Master of Science**.

Supervisors: Prof. T.J. Egan and

Prof. R. Hunter

Department of Chemistry

University of Cape Town

March 2015

Dedication

To my late great grandmother Mrs Nodilika Annie Mvumvu

and

my late Mathematics teacher Mr Thembelenkosi Shumane

Acknowledgements

To God, for every mountain, every valley every stormy sea, Thank you! *Through it all, I have learnt to trust in You. Thank you for your strength in times of my weakness and pain. Your love has never changed may your glory be seen through this work.*

To my two supervisors, Prof. Timothy Egan and Prof. Roger Hunter thank you for all your mentorship, support and patience throughout the project. Most of all, thank you for believing in me. I will forever hold that dear.

I would also like to acknowledge the following people for making the project a success:

The entire Hunter group for making my lab days the best days. I will miss the fun we had, the singing and noise we made. With you there was no sad day except when glassware was stolen. Nonetheless, thank you.

Fabrizio L'bbatte for his assistance with the project especially the previous work done on the dihydropyridine scaffold.

Kathryn Wicht, Dr. Sophie Rees-Jones for their assistance in the lab and Rudy Cozett for helping with the HPLC.

Prof. P. J. Smith and his staff at the division of Pharmacology for performing the biological tests in this project.

The Egan group thank you for your support and advice in the lab.

Roxanne Mohunlal, for her support and encouragements.

My friends for always bringing joy and happiness into my life.

The Chemistry Department staff for their friendly assistance.

A special heartfelt gratitude to my family, my parents Richard and Esther Thembeka Mvumvu; my siblings and cousins.

To Wendy Zukiswa Mvumvu, I always thank God for you. Without you my name would have never existed. Thank you for your continued moral support and love.

For financial assistance, UCTABA, NRF, Maria Lydia Schorlaship, NIH.

Finally to Hulisani Matodzi, thank you for your continued prayers, support, love and for your faith in me.

Abstract

The blood stage of the malarial parasite life-cycle is a vital stage that is believed to be a target for most antimalarial drugs. It is in this stage that host haemoglobin is degraded to provide nutrients for the survival of the parasite. However, a pathway (known as the haem detoxification pathway) that gives rise to the unique, microcrystalline ferriprotoporphryin IX [Fe(III)PPIX] dimer called haemozoin as an end-product, also arises as a result of the degradation. This haem detoxification pathway is a principal target for some of these antimalarials, especially those that contain the quinoline scaffold (e.g chloroquine), and has yielded outstanding results for the antimalarial drug discovery and development world. Even so, the spread of parasite resistance among these drugs has rendered most ineffective, resulting in a need for new scaffolds to target the pathway. However, the mode of action of chloroquine on haem may still be used as a model for identification of hits from these new scaffolds.

The project entailed the synthesis of forty 4-substituted-1,4-dihydropyridine-3,5-dicarboxylic ester derivatives (inclusive of 12 previously reported), as a new potential antimalarial chemotype. Syntheses were conducted using a Hantzsch pyridine reaction. Characterisation of these analogues was achieved using melting point, IR, ^{1}H NMR and ^{13}C NMR spectroscopy as well as HRMS. The compounds were tested against β-haematin formation as well as parasite growth, and from the data obtained, a structure-activity profile was deduced. At 95% confidence level, correlation analysis of the benzyl esters (**29**-**38**) revealed that antiplasmodium activity (decrease in logIC_{50}) increases with a decrease in molecular weight (**Mr**) of the attached ester group and an increase in unsaturation (**Fsp^3**) of the substituent. Small molecules with more unsaturated carbon bonds tend to be more drug-like because of their hydrophobic character which allows for membrane permeability and increased interaction with the hydrophobic haem macrocycle. The correlation yielded the empirical equation

$$\text{Log } IC_{50} = 0.0065\mathbf{Mr} + 8.07\mathbf{Fsp^3} - 4.78$$

All the individual parameters were statistically significant at 95% confidence level. A single correlation for the alkyl esters revealed that increasing hydrophobicity increases the

parasite activity of the analogues (**22**-**24**, **26** and **28**). The presence of the 1,4-dihydropyridine (1,4-DHP) nucleus was essential to maintain both β-haematin inhibition and parasite growth-inhibition activities of the analogues. Thus, upon oxidation to a pyridine activity was lost. Comparison of the structural alterations performed on the 1,4-DHP molecule has permitted construction of a structure-activity model for its activity against the malarial parasite. For the 4-phenyl substituents, β-haematin activity was optimum when a large, electron-withdrawing, hydrophobic *meta*,*para*-disubstituted-4-phenyl-1,4-dihydropyridine was attached. Hydrogen bond donating properties of the nitrogen atom in the dihydropyridine ring may be required to retain inhibition of β-haematin formation and the parasite *in vitro*. The presence of a basic N-heterocycle attached to the ester side chain, probably increases vacuolar accumulation but to the detriment of haemozoin inhibition. Attachment of larger alkyl groups on position 2 and 6 increase activity of the analogues.

Three compound **25**, **35** and **41** exhibited a nanomolar (nM) activity against the parasite *in vitro*, warranting further investigation of this scaffold as an antimalarial template.

List of Abbreviations

Ar	Aromatic
ArH	Aromatic proton
bs	Broad singlet
βIC_{50}	Beta-haematin inhibition IC_{50}
$CDCl_3$	Deuterochloroform
d	Doublet
dd	Doublet of doublets
DCM	Dichloromethane
DMSO	Dimethylsulfoxide
EtOAc	Ethyl acetate
EtOH	Ethanol
eq	Equivalents
EI	Electron ionisation
Fe(III)PPIX	Ferriprotoporphyrin IX
g	Grams
HOMO	Highest Occupied Molecular Orbital
HPLC	High Perfomance Liquid Chromatography
Hz	Hertz
HRMS	High Resolution Mass Spectrometry
IC_{50}	50% inhibitory concentration
IR	Infrared spectroscopy
J	Coupling constants
LUMO	Lowest Unoccupied Molecular Orbital
$[M+H]^+$	Molecular ion in a positive ion mode
$[M-H]^-$	Molecular ion in a negative ion mode
NMR	Nuclear Magnetic Resonance
Ppm	parts per million
s	Singlet
t	Triplet

TLC	Thin Layer Chromatography
µM	Micromolar
v/v	Volume by volume

Table of Content

CHAPTER 2 - Organic Synthesis

CHAPTER 3 - Inhibition of β-haematin formation and Parasite growth

1. Literature Review

1.1 Introduction to Malaria

The disease malaria has been and continues to be one of the most serious diseases to ever impact the human race, causing an intolerable burden on global human health and society. In 2013 alone, the disease affected more than 198 million people and led to 584 000 deaths.[1]This disease, for which records date back as far as 2700 BC in Chinese history got its name from the Italian phrase "mal'aria'' meaning ''spoiled air'' (when ancient Romans discovered a disease regarded similar to malaria today).[2, 3] It has been closely associated with swamps and dirty areas which are mostly found in developing countries (including Africa) where there is less or no infrastructure and the rate of poverty is high.[4, 5]

Malaria is caused by parasitic protozoans from the *Plasmodium* genus and transmitted during the feeding process on human blood by the female *Anopheles* mosquito vector. Survival of the vector is greatly increased by warm, rainy climates found in tropical and sub-tropical regions thus about 90% of malarial cases are found in these regions (Figure 1).[5-9]

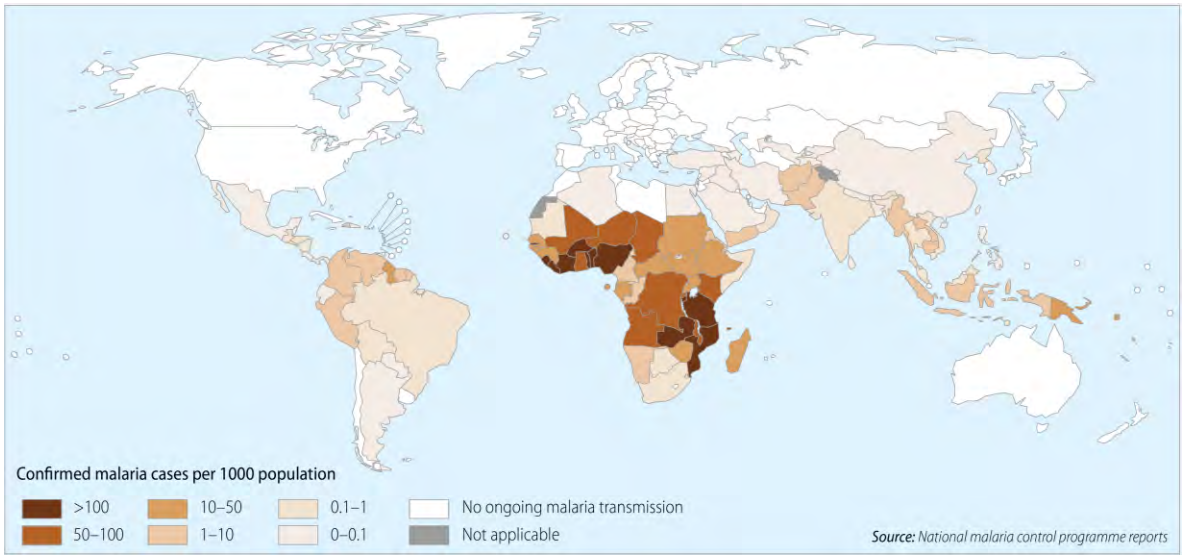

Figure 1: Distribution of malarial transmission in 2013. [1] Adapted from reference 1.

The fact that primary infection does not immediately induce immunity to the disease is the reason for predominance of the infection in young children under the age of five, who have no past exposure to the disease, as well as pregnant women. The symptoms include low birth weight (in pregnant women), severe anaemia, liver damage, coma and even death if

left untreated. Development of partial immunity (pre-immunity), which is mainly seen in older people living in malarial endemic areas, results in an uncomplicated (or asymptomatic) malaria which exhibits mild symptoms similar to normal fever and has no or less severe effects. Immunity in the older population results in an unknown disease reservoir which becomes a pool spreading the disease. Figure 2 below shows age-specific clinical incidences and proportion of infection in high malaria endemic areas with an entomological inoculation rate of 85%.[10-12]

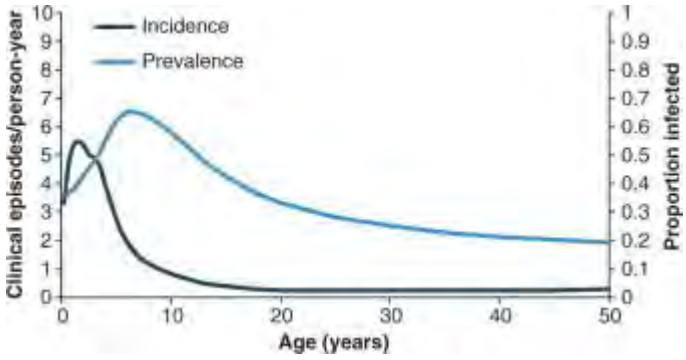

Figure 2: Model demonstrating clinical incidences and infection prevalence according to the population age in high malaria endemic areas. [10] Reprinted from Clinical Microbiology and Infection, Vol 17, Gosling, R. D. Okell, L. Mosha, J. Chandramohan, D., The role of antimalarial treatment in the elimination of malaria, 1617-1623., Copyright (2011), with permission from Elsevier.

Resistance to the cheapest and highly effective antimalarial drug chloroquine has increased the morbidity and mortality rate in the malarial regions, causing loss in economic growth thus increasing poverty .[4,13] Therefore to ensure eradication of the disease in the next few decades, research and disease control need to be intensified. These include prevention of transmission from mosquito vector to the human host (including mosquito bed nets and insecticides), biologically understanding and control of the *Anopheles* vector (this reduces survival and breeding of the mosquito as well as yielding effective controls) and research on effective novel drugs and their mechanism of action. This project focuses on the latter.

1.2 The *Plasmodium* Life Cycle and its biology

There are five *Plasmodium* species (*Plasmodium falciparum*, *Plasmodium ovale*, *Plasmodium vivax*, *Plasmodium malariae,* and *Plasmodium knowlesi*) known to infect humans. All

undergo similar life-cycle and cause malarial disease. Owing to the ability of *Plasmodium falciparum* infected red blood cells (RBCs or erythrocytes) to avoid splenic clearance by adhering to endothelial cells that line the blood vessels in various body organs it can lead to obstruction of tissues. This causes severe complications making *Plasmodium falciparum* the most virulent among the *Plasmodium* species and a major cause of human deaths. This cytoadherance process of the infected RBC, which is caused by the parasite's ability to re-shape the infected cell forming knob-like spikes on the cell's surface that assist in cell binding, is known as sequestration. It is mediated by *Plasmodium falciparum* erythrocyte membrane protein 1 (*PfEMP* 1) which is encoded by var genes. The var family is involved in clonal antigen variations which alter the parasite's surface molecules giving it the ability to re-infect humans while evading the host's acquired immune system, hence overriding the host's defence system. [6, 7, 14-16]

The parasite's complex life-cycle (Figure 3) alternates between the human vertebrate host and the mosquito vector, each with a dominating reproduction cycle.

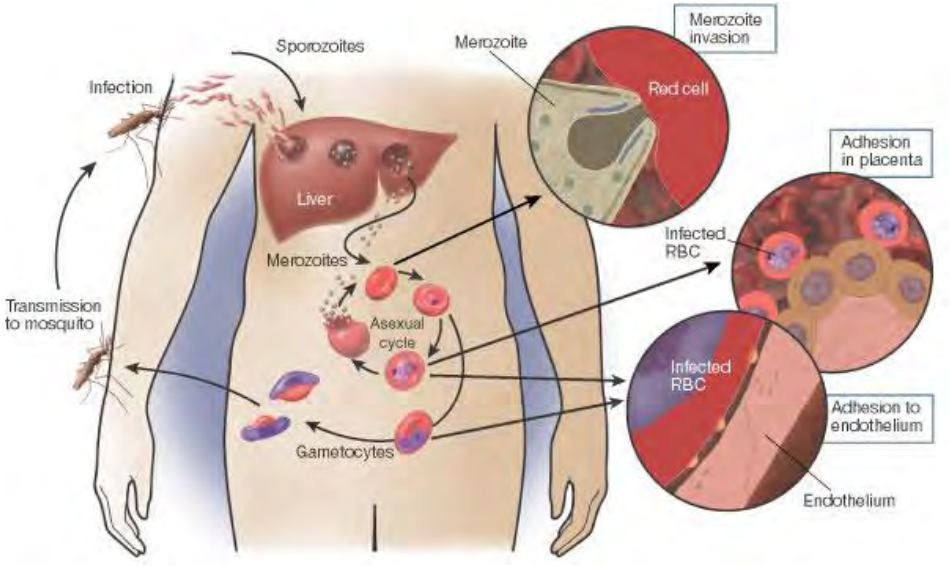

Figure 3: The life-cycle of malarial parasite (*Plasmodium* species). [7]Adapted by permission from Macmillan Publishers Ltd: [Nature] (reference 7), copyright (2002).

The vertebrate cycle, which is the asexual stage, begins when an infected *Anopheles* mosquito feeds on human blood injecting parasitic sporozoites from its salivary gland together with an anticoagulant that assists in blood flow during the feeding process. The sporozoites enter through the human skin followed by movement through the bloodstream

to the liver where they invade the liver cells (hepatocytes) and undergo sequential asexual multiplication to form schizonts in a process known as pre-erythrocytic schizogony. This initiates the liver stage which lasts up to 25 days with no recognizable immunological pathogenic response. [2, 6, 7]

Within the hepatocytes the schizonts undergo mitotic division to enlarge and then mature to produce merozoites. These burst out of the hepatocytes into the bloodstream during liver schizont rupture. Following rupture they flow through the bloodstream and then invade passing RBCs initiating the blood stage (Figure 4). The infection now manifests as periodic headaches and fever that reoccur over a period of 48-72 hours depending on the *Plasmodium* species. It is this stage that serves as an important target to most known antimalarial drugs including quinolines (e.g chloroquine) and is clinically detected and formally named malaria. Within the RBC (erythrocyte) host haemoglobin is degraded inside the parasite food vacuole for nutrients, to maintain osmotic balance and to make space in the RBC in order to form larger trophozoites that replicate asexually into blood schizonts. These schizonts again form merozoites that are released during rupture of the infected RBC invading new RBCs and so repeating the cycle therefore increasing parasite population. [7, 17, 18]

A minority of the merozoites form sexual female and male gametocytes that lie dormant in the blood stream until an *Anopheles* mosquito feeds on the infected host. During the feeding process the gametes are then transported to the digestive tract of the mosquito where sexual reproduction occurs. This results in formation of zygotes. Meiotic nuclear division of the zygote forms an oocyst, which undergoes mitotic division to form sporozoites. The new sporozoites are then transported to the salivary glands of the mosquito where they lie dormant until the next feeding, repeating the life-cycle of the parasite by infecting a healthy human being.[6, 16, 18]

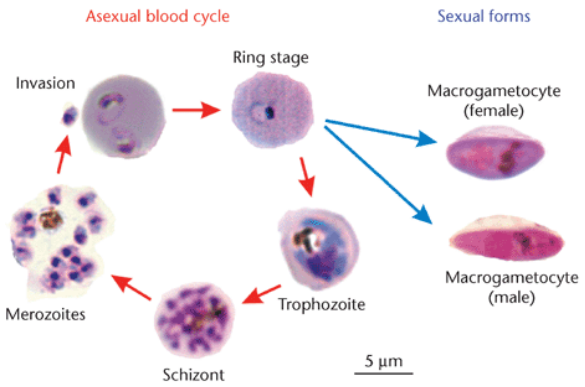

Figure 4: The blood stage of the *Plasmodium* life-cycle. The two fates for the merozoite, the formation of a trophozoite that completes the asexual cycle and the formation of gametocytes needed for the overall completion of the sexual stage of the malarial cycle.[6] Reproduced from reference 6.

1.3 The fate of haemoglobin in the *Plasmodium* life cycle

The ingestion of host haemoglobin by parasite trophozoites during the asexual blood stage is due to the parasite's need of nutrients and space required for growth and completion of the life cycle as well maintenance of osmotic balance. Degradation occurs inside a lysosome-like acid food vacuole (pH 4.8-5.2). The host haemoglobin is endocytosed from the RBC to this site. Within the food vacuole are proteolytic enzymes needed to degrade globin into peptides that are further degraded into amino acids by hydrolysis which occurs in the parasite cytoplasm.

Even though the parasites digest 60-80 % of haemoglobin only 15% of the released amino acids are used in protein synthesis, while the rest is released into the circulation. Ferrous haem (ferroprotopophyrin IX, Fe(II)PPIX) is a by-product released during this digestion process. Haem is quickly and irreversibly oxidised to soluble ferric haematin (H_2O/OH-Fe(III)PPIX, the ligand is axial to the Fe(III) centre) by an unknown process thought to involve oxygen (O_2) and generation of superoxide (O_2^-). Large quantities of haematin are cytotoxic to the parasite and have been shown to cause lipid peroxidation and membrane destabilization also inhibiting various enzymatic processes. Thus the parasite has evolved a mechanism to detoxify this into an inert-microcrystalline form known as haemozoin.[19-22] Alternative detoxification mechanisms which include neutralisation of haem with histidine rich protein 2 peroxidative degradation of haem and reduced glutathione degradation,[22-24]

have been proposed, however, physico-chemical studies showed that about 95% of haem released from haemoglobin undergoes conversion to haemozoin. This detoxification pathway is specific to the *Plasmodium* parasite. [19-22, 25] Therefore inhibition of this pathway has become an important target in antimalarial drug discovery. Figure 5 summarises the fate of haemoglobin.

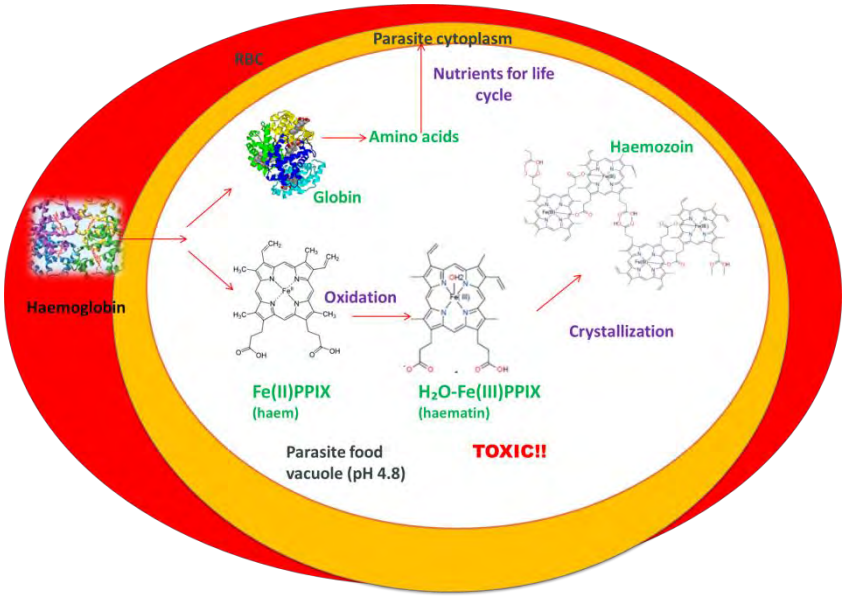

Figure 5: The pathway showing degradation of haemoglobin inside the *Plasmodium* infected red blood cell.

1.4 Formation and Structure of Haemozoin

The mechanism of haemozoin formation has been of contention in the literature, and while not fully understood, it has played a significant role in the discovery of the *Plasmodium* parasite and its life cycle as well as the role of the mosquito vector. Discovered years before the cause of malaria disease was known, scientific history shows that haemozoin played a major part in several breakthroughs in malaria research and antimalarial drug discovery. [3, 26-28] It is now strongly believed that formation of haemozoin in blood feeding organisms such as *Plasmodium* and the trematode worm *Schistosoma mansoni* is mediated by neutral lipids. The lipid mediated process was first described by Bendrat who suggested that polar lipids contaminating haemozoin extracts were the inducers of β-haematin formation. [20, 29, 30] The hypothesis was later supported by Dorn et. al using acetonitrile extracts of trophozoite lysates. [31, 32] Further work was done by other groups including Pisciotta et.al using a sucrose

cushion centrifugation for isolation and thin layer chromatography as well as mass spectrometry for identification.[20, 33-36] This demonstrated that these lipids existed as a mixture of monostearoylglycerol (MSG), monopalmitoylglycerol(MPG), 1,3-dioleoylglycerol (DOG), 1,3-dipalmitoylglycerol(DPG) and 1,3-dilineoylglycerol (DLG) in a 4:2:1:1:1 ratio in the form of neutral lipid nanospheres within the digestive vacuole (Figure 6). They further proposed that the role of these nanospheres was to protect the parasite from non-enzymatic cleavage of haem which liberates the toxic peroxide molecule (H_2O_2) by enabling crystallisation of haem to haemozoin.[19, 35, 37]

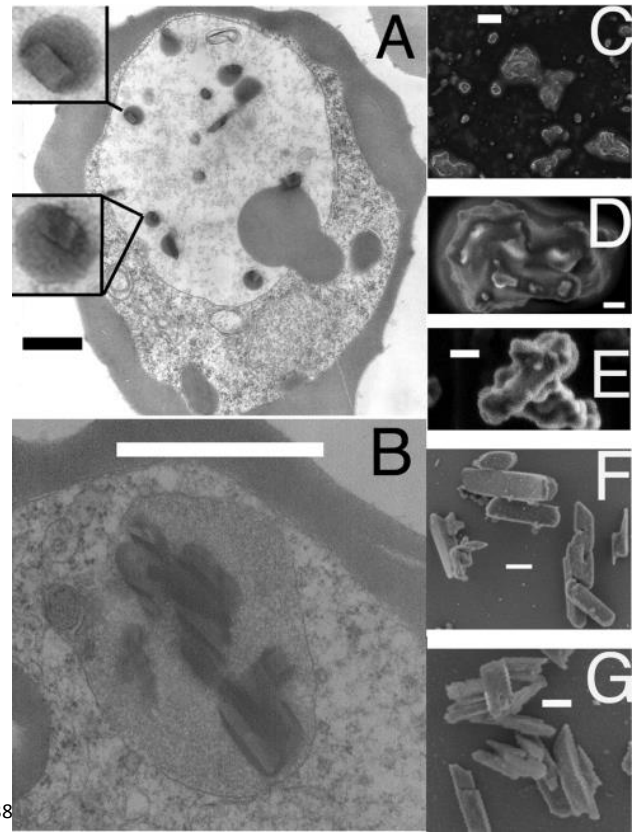

38

Figure 6: Transmission electron micrograph (TEM) of the asexual blood trophozoite stage. **A** early trophozoite with small haemozoin crystals and **B** mature stage with larger crystals (1 µm). **C**-**E** Scanning electron micrographs (SEMs) of haemozoin coated by the lipid. **F**-**G** show delipidated haemozoin crystals (100 nm). This figure was originally published in Biochemical Journal. J. M. Pisciotta, I. Coppens, A. K. Tripathi, P. F. Scholl, J. Shuman, S. Bajad, V. Shulaev and D. J. Sullivan, Jr., The role of neutral lipid nanospheres in *Plasmodium falciparum* haem crystallization. Biochemical Journal, 2007; 402: 197-204 © the Biochemical Society.

Studies performed by Hoang et. al and Ambele and Egan revealed that addition of neutral lipids (similar to the ones identified by Pisciotta et al) dissolved in acetone/methanol mixed

with haematin and layered onto an aqueous surface produced lipid droplets that efficiently mediated the formation of β-haematin (a dark-brown synthetic solid that is structurally and chemically identical to the biological haemozoin and first described by Hamsik in 1936.[39] Hoang et al. further proposed that the propionate group of ferriprotopophyrin IX extends towards the aqueous phase whilst the hydrophobic haem vinyl groups are embedded within the hydrophobic membrane layer at the interface of lipid and water. This alignment was proposed to facilitate β-haematin crystallisation.[37, 40, 41]

Formation of haemozoin crystals involves dimerization of haematin (Fe(III)PPIX Figure 7a) molecules with the propionate group of one Fe(III)PPIX molecule coordinating to the iron (Fe(III)) centre of another Fe(III)PPIX molecule. The two protoporphyrin rings interact by π-stacking interactions with other dimers in the crystal. Extension of the dimer also involves a chain of hydrogen bonds between the propionic acid groups of neighbouring dimers. The crystals are centrosymmetric and have a thin narrow shape. The smallest face (c-face) is the fastest growing face of the crystal and believed to be the site where drugs bind. Figure 7b shows the structure of haemozoin.[20, 38, 42]

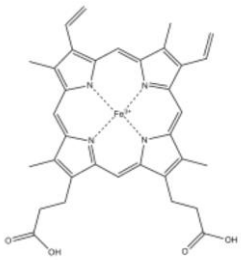

Figure 7a: The Structure of heamatin excluding coordination of the H_2O/OH^- ligand on Fe^{3+} centre.[38] Adapted by permission from Macmillan Publishers Ltd: [Nature] (reference 38), copyright (2000).

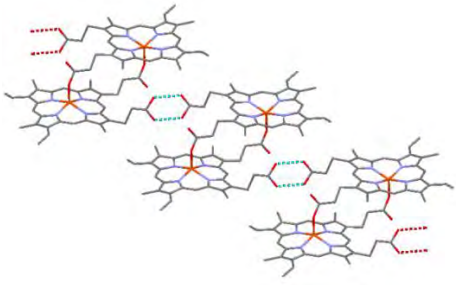

Figure 7b: The crystal structure of haemozoin; blue dots illustrate hydrogen bonding between the two dimers.[38] Made on the basis of CSD data of Pagola's structure .

1.5 Clinically used antimalarials and their mode of action.

Malarial chemotherapy begins with an appropriate diagnosis of the type of *Plasmodium* species infecting the patient. Based on this, the disease is classified according to the level of severity and the drugs to be administered are selected.[9, 12] The three major antimalarial drug classes that mainly target the asexual erythrocytic blood stage are classified according to their mechanism of action; these are the antifolates, antimitochondrial or the blood schizonticides. The latter are successful for being affordable, highly effective and safe, even though there is a lack of understanding about their mechanism of action.[43, 44]

1.5.1 The antifolates

The antifolates are known for interfering in the synthesis of folic acid and its biological pathway. This essential acid, functions as the co-factor involved in nucleic acid synthesis as well as for carrying one-carbon groups for methylation reactions and therefore limiting its synthesis inhibits parasite DNA synthesis (and amino acid metabolism through inhibition of methionine synthesis). This disrupts parasite growth and the successful completion of its life cycle.

The class is further divided into two sub-classes as the type I and type II antifolates (Figure 8). Type I which consists of pyrimethimine and proguanil (which metabolises to its active form cycloguanil once in the body) act on the schizont stage of the parasite asexual blood cycle and are dihydrofolate reductase-thymidylate synthase inhibitors. The enzyme dihydrofolate reductase-thymidylate synthase plays a bifunctional role in the synthesis of deoxythymidylate (responsible for parasite cellular DNA synthesis) and the regeneration of folic acid by catalysing the reduction of dihydrofolic acid to tetrahydrofolic acid using NADPH as an electron donor. Inhibition of the enzyme blocks the synthesis of nucleic acid precursors ultimately arresting cell division, growth and proliferation. [43, 45] The potency of the drugs is greatly enhanced when in synergetic combination with the sulfonamides such as sulfadoxine (type II antifolate class) that competitively inhibits dihydropteroate synthase, an enzyme responsible for folate biosynthesis. The combination is affordable and safe to use during pregnancy and was once also extensively used to combat chloroquine resistant malaria.[44, 46]

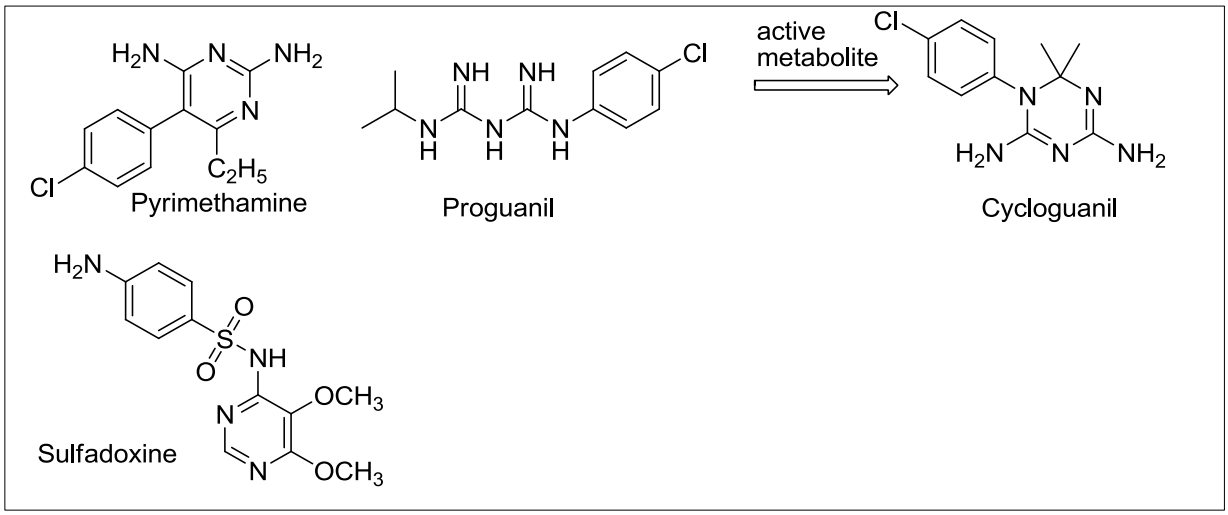

Figure 8: The antifolate class of antimalarial drugs.

The fact that most organisms, including human beings, use the folic acid-pathway as one of their key biosynthetic pathways requires specificity for the parasite enzymes in order to reduce adverse effects such as anaemia in humans. Owing to this, point mutations in genes encoding the two enzymes completely renders the drugs ineffective resulting in parasite resistance to them.[47-50]

1.5.2 The antimichondrial drugs

The malarial parasite mitochondrion is essential for various metabolic functions which include an electron transport system required for dispersement of electrons that assist in the reduction of dihydroorotate to orotate by dihydroorotate dehydrogenase during pyrimidine synthesis, a pathway essential for parasite DNA synthesis.[51-53] This metabolic route is a target for the antimalarial drug atovaquone which selectively binds to the mitochondrion by interacting with ubiquinone-cytochrome c oxidoreductase (cytochrome bc_1 complex or Coenzyme Q). This causes destabilisation, resulting in proton leakage within the complex and inhibition of the parasite mitochondrial electron transport system. The inhibition ultimately causes breakdown of the electro-potential of the mitochondrial membrane leading to oxygen consumption malfunctions and parasite death. The drug which is used in both chemoprophylaxis and treatment of mild (uncomplicated) malaria was initially administered as a monotherapeutic agent; however rapid occurrence of treatment failure (which is caused by its liphophilic character that leads to low aqueous solubility) as well as parasite resistance reduced its effectiveness.[43, 51, 54, 55] In the pursuit of a reduced

treatment failure and drug resistance a fixed-ratio combination of atovaquone and progaunil, commercially known as Malarone® is now administered. Progaunil traditionally known for its antifolate activity (section 1.5.1) as a pro-drug to its metabolite cycloguanil acts by reducing the concentration of atovaquone required to inhibit the electron transport system, hence increasing the efficacy of the drug.[51, 54, 56] Figure 9 displays the two combo-therapeutics.

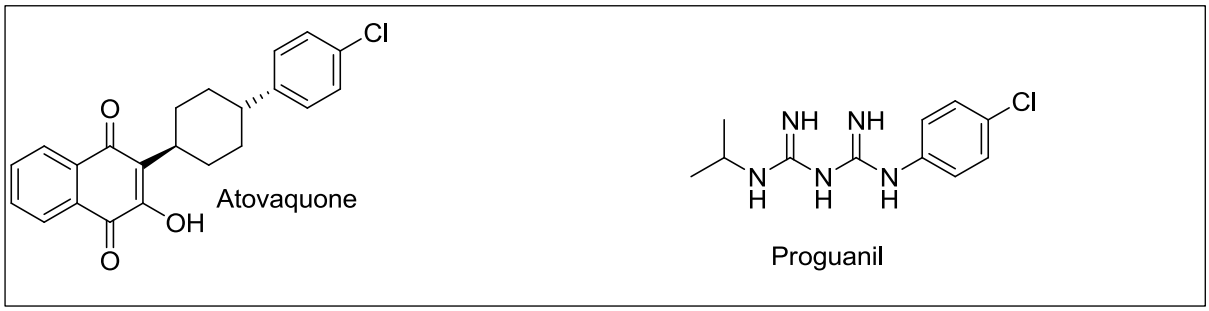

Figure 9: The mitochondrial electron transport chain inhibitors.

1.5.3 The blood schizonticides

These drugs are believed to interact with haem and work by targeting the haem detoxification process occurring in the parasite food vacuole. They consist of synthetically derived artemisinin-containing drugs (a) and quinoline derived drugs (b), Figure 10.

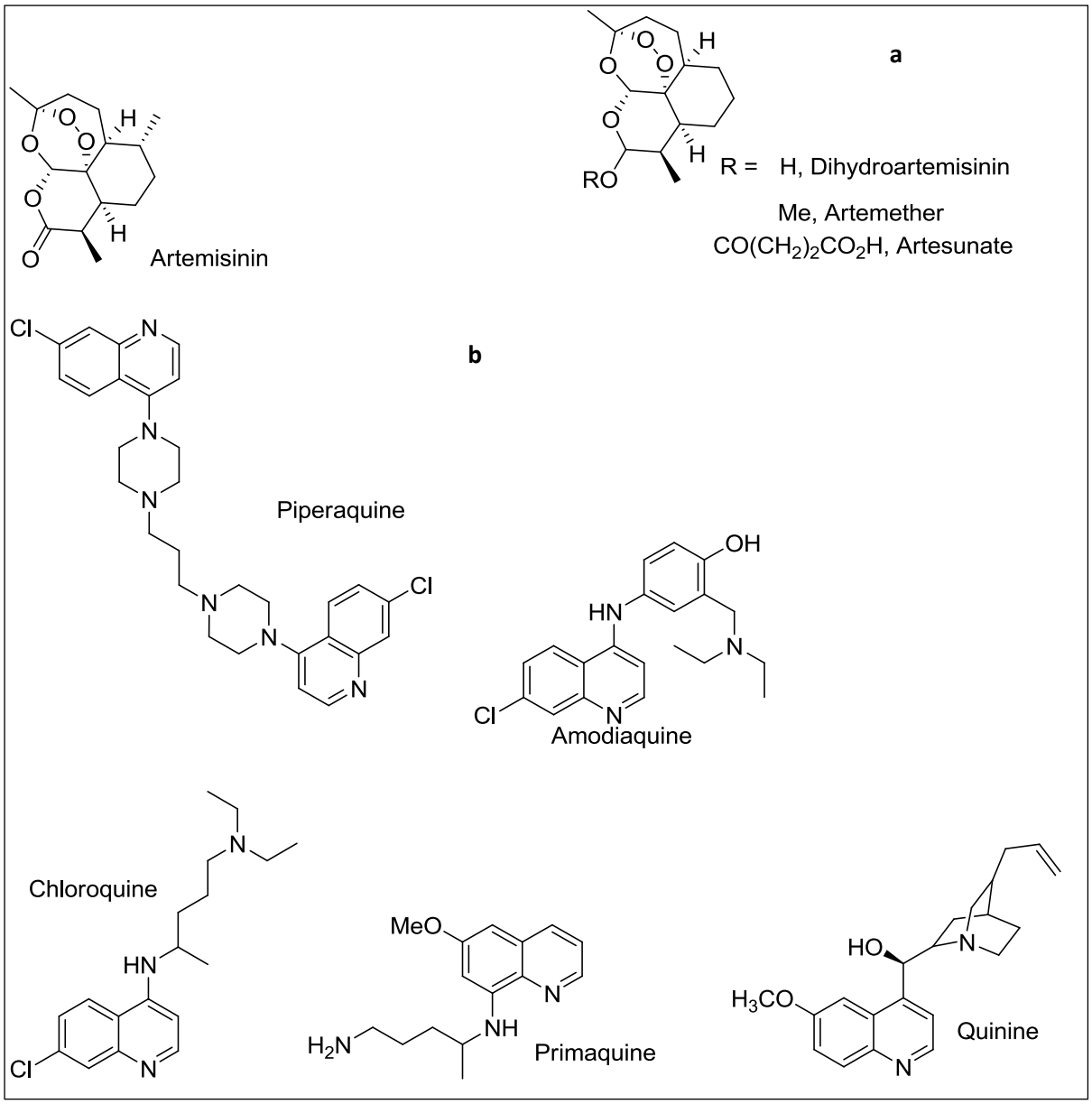

Figure 10: The blood schizontocides; **a** the artemisinin-based drugs and **b** quinine and synthetic analogues (the quinoline drugs).

1.5.3.1 The Artemisinin compounds

The mechanism of action of this class of drugs is not well understood, however both haem and free iron have been suggested to activate the endoperoxide group of the drug causing cleavage of the bond leading to radicals that alkylate essential biomoleculecular components thereby killing the parasite. The drugs are known for their short half-life, but they are so effective and potent that they rapidly reduce parasitemia. Over the last decade an artemisinin-based combination therapy (ACT) has been used as the first-line standard

treatment against uncomplicated and chloroquine resistant malaria. This multi-drug combination treatment which administers arteminisin together with a long half-life drug (such as quinoline drugs amodiquine or mefloquine) is believed to reduce the rate at which mutations confer resistance in endemic areas.[43, 57-61] Even so the emergence of resistance towards artemisinin which involves the emergence of delayed-parasite clearance phenotype has been seen in countries such as Cambodia and Thailand.[57, 62-64]

1.5.3.2 Quinine an ancient antimalarial

The discovery of quinine, an ingredient found in the bark of the chichona tree which had been known to cure malaria since the 17th century, marks one of the greatest discoveries in the medical scientific world. Developed in the 1820s, quinine became a major chemotherapeutic for treating malarial associated fevers. However, owing to the drug's toxicity and adverse effects to humans, less toxic and tolerable synthetic analogues (the quinoline-containing-compounds) such as chloroquine, piperaquine, amodiaquine, etc (Figure 10) were later discovered and used in preference to quinine.[65, 66] The exceptional efficacy (prior to the emergence of resistance), affordability and safety of chloroquine made it the most clinically used antimalarial from the class.[28, 67-69] Further discussion in this review illustrates the aspects of mode of action of the quinoline containing drugs and their structure activity relationships.

1.5.3.3 The Mode of action of chloroquine and its structure activity relationships

Although there has been advancement in the literature in understanding the mechanism by which chloroquine exerts its antimalarial potency, the exact mode of action is still not entirely understood. However, evidence supporting haem crystallisation as the target site of this drug has been the most widely accepted hypothesis (and the one with the strongest supporting evidence). In 2013, a publication by Combrinck et. al revealed that a chloroquine dose-dependent decrease of haemozoin together with a concomitant corresponding increase of cytotoxic haem correlated with parasite death (Figure 11). Other clinically used 4-aminoquinolines such as amodiaquine (see structures in Figure 10) also caused an

increase in free haem in treated *Plasmodium falciparum* in cell culture.[70] This study strongly supports the hypothesis that chloroquine is a haemozoin formation inhibitor.

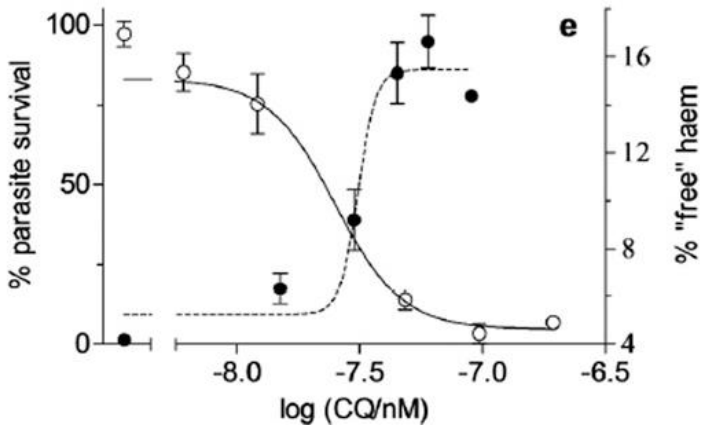

Figure 11: Dose-dependent plots of chloroquine treated parasites; **left axis** (**open circle**) parasite survival curve and percentage of haem as function of Log [chloroquine], **right axis** (**closed circle**).[70] Adapted with permission from reference 70. Copyright (2013) American Chemical Society

Chloroquine is a weak base (pK_a= 8.1 and pK_{a2}= 10.2) and has a higher proportion of the neutral species at serum pH (pH= 7.4) and can therefore diffuse across cell membrane into the food vacuole (pH=4.8) where it is more extensively protonated and trapped inside. Thisresults in its accumulation (a term known as pH trapping) and the inhibition of haemozoin formation can occur. The importance of pH trapping for inhibition is seen in chloroquine-resistant parasites strains where there is a decrease in drug accumulation in the food vacuole (see 1.5.3.4).[28, 43, 71, 72]

A detailed model of the structure-activity relationships in chloroquine with respect to haemozoin inhibition (or β-haematin since *in vitro* studies were performed) proposed by Egan et al revealed that β-haematin inhibition activity is a necessary, but not sufficient parameter for antiplasmodial activity. Moreover the amino side chain (which also assists in drug accumulation through pH trapping) is an essential requirement for strong antiplasmodial potency while the electron-withdrawing chloro group attached to the phenyl ring of quinoline assists in β-haematin inhibition. Interaction of the drug with haem occurs via noncovalent interactions that involve π-stacking interactions between the 4-aminoquinoline and the Fe(III)PPIX porphyrin macrocycle, as well as hydrogen bonds and weak electrostatic interactions between the protonated ammonium group of the quinoline

and the propionoate groups of the haem.[73] The proposed structure activity model is shown in Figure 12.

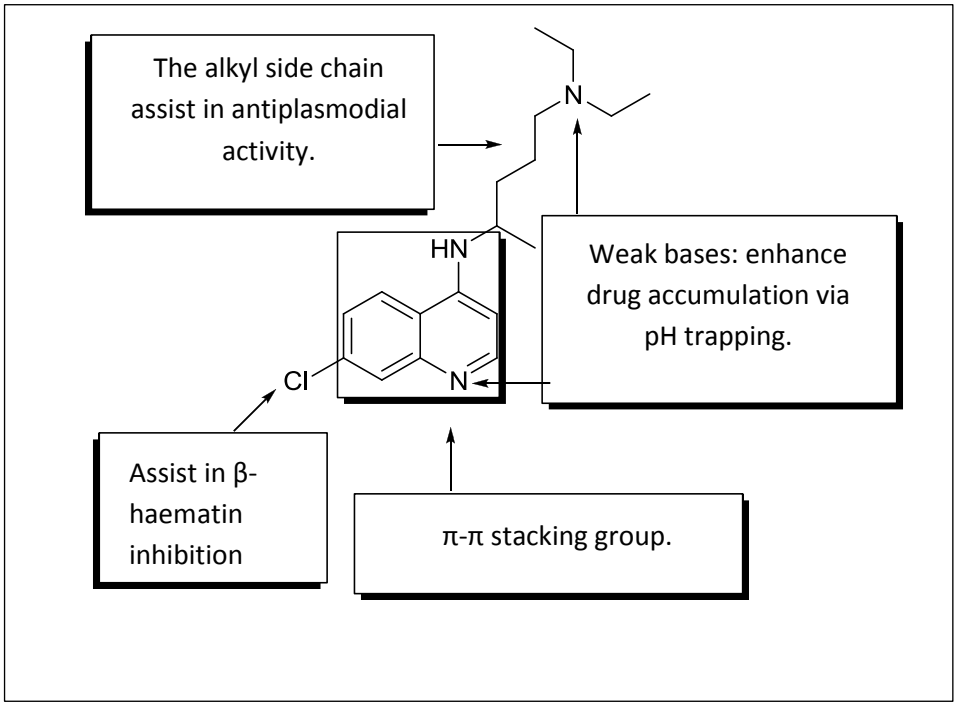

Figure 12: The proposed structure-activity relationships model of chloroquine essential for inhibition of the haem detoxification pathway. The model is based on a study performed on 19 quinoline compounds.[73]

Many years ago, the mechanism of haemozoin inhibition was thought to involve drugs binding to free haem in solution. However, more recently, evidence has pointed to the drugs inhibiting the crystal growth of haemozoin by docking onto the fastest growing crystal face of the haemozoin crystal, with intermolecular forces still playing an important role. [67, 74, 75]

1.5.3.4 Chloroquine resistance

Whilst the spread of resistance is related to the frequency at which mutations that confer resistance occur, processes such as the reduction in drug uptake and accessibility of the target, chemosentisation due to structural alterations, as well overexpression of the target site, also mediate drug resistance.[76]

The emergence and spread of chloroquine resistant *Plasmodium falciparum* parasites has left an enormous challenge on the road towards the control and ultimate eradication of malaria. Chloroquine resistance, which originated in the late 1950s in Southeast Asia, is thought to be conferred by point mutations on the gene encoding for the *Plasmodium falciparum* chloroquine resistance transporter (PCRT), a protein embedded in the parasite digestive food vacuole membrane. Conferment of resistance is a result of amino acid substitutions at position 76 of PCRT, a region thought to be involved in substrate recognition. Replacement of the amino acid lysine by threonine (K76T) at this position leads to the electrochemical downhill efflux transportation of protonated chloroquine by PCRT. This efflux causes a reduction in drug accumulation and increases the IC_{50} (concentration at which a drug exhibits 50% inhibitory effects). Inhibition of the wild type (or sensitive) strain of parasites decreases their population while simultaneously increasing any resistant mutant parasite population, a term known as drug selection.[28, 76-79] To circumvent resistance, structural alterations of 4-aminoquinolines have been performed in the literature by different groups. While some good results have been reported one also cannot ignore the toxicity of the quinoline scaffold possessed by these drugs (quinine as well as chloroquine). Some severe adverse effects (which include immune thrombocytopenia, hemolysis, blindness as well as death due to drug overdose) that led to quinine withdrawal have also been reported for chloroquine; hence a paradigm shift away from quinoline based antimalarial drug discovery has emerged.[47, 73, 80] New drug candidates in this class should preferably be non-quinoline haem detoxification pathway inhibitors.

1.6 Some approaches to drug discovery relevant to this project

Understanding the mechanism of action of quinoline-based antimalarial drugs acting on the haem detoxification pathway is of great importance for the rational design of novel haemozoin inhibiting compounds. Drugs inhibiting this process require precise structure, shape and alignment of functional groups that will promote haemozoin (or possibly haem) binding in order for effective recognition and association to take place leading to inhibition of haemozoin formation. Furthermore, factors affecting properties such as lipophilicity and pH trapping are important in the context of recognition and cellular uptake of the potential drug.[81, 82] While rational design of such inhibitors is not currently possible, an understanding

of the properties of chloroquine and its intermolecular interactions with haem (discussed in section 1.5.3.3) nonetheless has assisted in hit identification.

In general, techniques such as high-throughput screening and computer-aided molecular modelling have been successfully used to identify potential hits (as well as their druggable targets) in order to quantify and further develop them into novel drugs via hit-to-lead beneficiation. The optimisation of physicochemical parameters of the hit compound results in the optimisation of interactions between substrate and the receptor (target) molecule leading to maximum activity, an approach underpinning the quantitative structure-activity relationships method. This method identifies properties related to the activity of the molecule using a series of analogues of the same scaffold.[81, 83-86] Careful selection and evaluation of substitutional patterns performed on the template is essential for generating a meaningful set of rational design data as well as having implications for synthesis. One of the approaches often employed for this selection (also used for selection of some analogues synthesised in this study) is the Topliss decision tree method.[87-89] The approach consists of a flow diagram which differentiates alkyl and phenyl substituents ultimately based on descriptors such as electrostatic effects, electron-withdrawing/releasing effects and lipophilicity of the compound as parameters describing the activity of the analogue. A compound is more potent (M), equivalent (E) or less potent (L) than the previous analogue and this forms the basis of selection of the next derivative for synthesis. In case of an increase in activity with increasing logP and minimal steric factor in alkyl side chains, the trend moves from the isopropyl to the benzyl and 2-ethylphenyl groups respectively. However where potency stays the same or is reduced, electronic effects also play a role. If the activity stays the same when moving from isopropyl to ethyl group, the pathway suggests more electron-withdrawing groups should be synthesised to improve the activity, while in a case of a reduction in potency further lead development must be undertaken. A similar rationale is applied for the aromatic substituents. Figure 13 demonstrates the Topliss pathways for alkyl side chains and aromatic substituents. This formed a basis on which diverse analogues were chosen, taking substituents from different branches of the tree (rather than sequentially progressing through the flow chart).

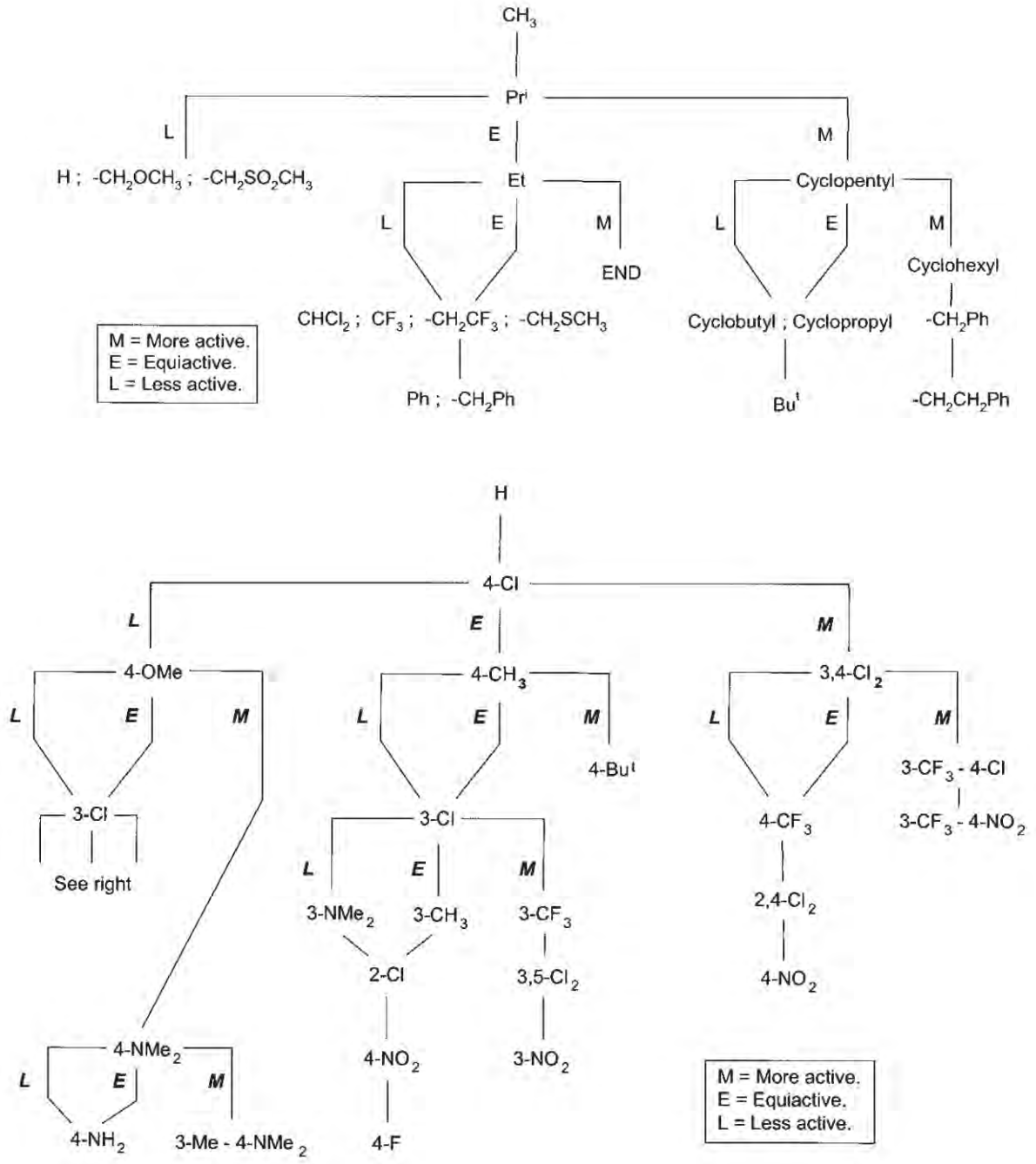

Figure 13: The Topliss scheme for **a**) The aliphatic side chains and **b**) the aromatic substituents.[87, 88] Reprinted with permission from (reference 87), copyright (1972), American Chemical Society.

1.7 The 1,4-dihydropyridine (1,4-DHP) scaffold as an alternative antimalarial template

A high-throughput screening study conducted by Vanderbilt University (Nashville, TN, USA) in collaboration with the University of Cape Town screened over 140000 compounds against parasite growth and haemozoin formation.[90, 91] From this, a dihydropyridine compound (Figure 14) was found as the most active non-quinoline containing hit.

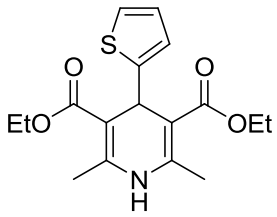

Figure 14: Structure of the dihydropyridine, hit molecule from high-throughput screening.

The dihydropyridine scaffold has proven to be of remarkable pharmacological importance, notably providing the basis of L-type calcium-channel blockers that have been utilised in the treatment of cardiovascular diseases such as hypertension and exemplified by the commercial drugs nifedipine, amlodipine or nilvadipine, Figure 15. The drugs act as antagonists of the voltage-dependent calcium channel, disrupting calcium ion movement through the channel into cells. These ions are responsible for coupling signals that cause contraction of heart muscles (excitation state of the heart) thus inhibiting the channels that modulate heart rate which then prevents high blood pressure and chest pains. The scaffold has also provided the basis of other compounds with pharmacological activities such as antitumor, antituberculosis and antimicrobial agents. These molecules can also act as reducing agents of organic compounds by mimicking the NADH molecule shown in Figure 16.[92-94] This has drawn a lot of attention from medicinal chemists as well as evoking interest into the classical Hantzsch pyridine synthesis methodology which is a well-known way of synthesizing substituted pyridine derivatives via oxidation of the Hantzsch 1,4-dihydropyridine products.[95-97]

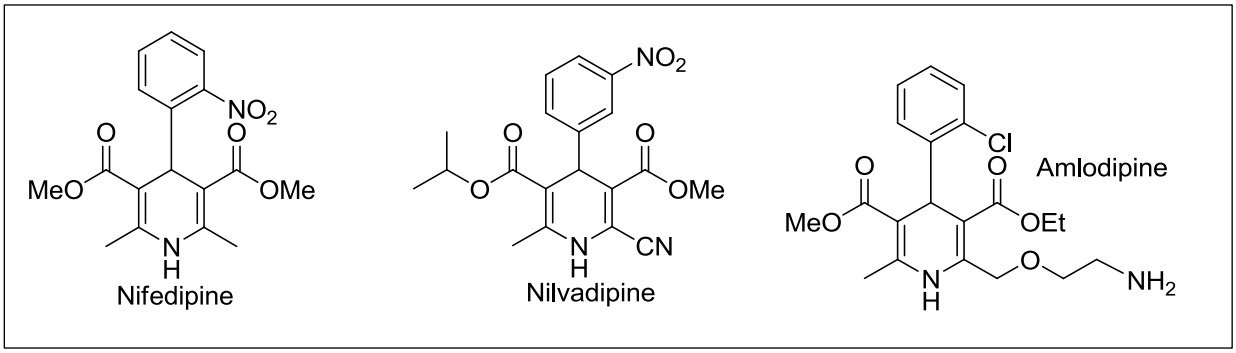

Figure 15: The L-type calcium channel blockers, 1,4-dihydropyridine drugs.

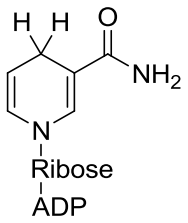

Figure 16: The NADH molecule.

This project involved the synthesis of analogues of the hit compound (Figure 14) in order to investigate structure-activity relationships necessary for inhibition of haemozoin formation and ultimately parasiteviability. The synthesis used was based on the well documented Hantzsch pyridine synthesis mentioned above. Because the thiophene ring is similar in properties to benzene, it was decided to replace the thiophene at C-4 of the hit with a phenyl substituent. This was intended to provide more opportunity for exploring substituent changes since aromatic aldehydes are more readily available than substituted thiophene 2-carboxaldehydes, Figure 17.

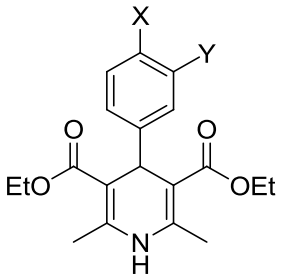

Figure 17: Structure of the 1,4-DHP molecule used as the hit for analogue design.

Previous work performed on the new aryl hit molecule had explored the effects of varying the 4-phenylsubstituents (X and Y) as part of developing structure-activity relationship profile of the template with respect to β-haematin inhibition (Mvumvu, BSc (Hons) project) (see Figure 17). Twelve 4-aryl-1,4-DHP analogues were synthesised using a microwave assisted Hantzsch pyridine reaction and their activity tested for β-haematin formation. Multiple correlation analysis performed on the anologues revealed a correlation at the 99 % confidence level between the $\log IC_{50}$ value with lipophilicity constant (π) and electronic constants, the resonance constant (**R**) and inductive constant (**I**) of X and Y. Based on the coefficient values found in the empirical equation, the substituent resonance effects had

slightly more influence than the inductive effects. Empirical equation (**1.1**) also shows a higher coefficient value for resonance constant than lipophilicity constant (**π**) denoting a greater weighting and hence influence on the activity.

$$\text{Log}IC_{50} = -0.498\mathbf{R} - 0.329\boldsymbol{\pi} + 2.548 \quad (r^2 = 0.79), \quad \ldots\ldots\ldots \text{ equ } (\mathbf{1.1})$$

$$F = 12.93 > F_{2,7} = 9.55$$

A two-tailed t-test on the individual parameters showed that both **R** and **π** significantly correlated with logIC_{50} at the 95% confidence level (t = 2.74 (R), 4.22 (π) > t_{crit} = 1.90). The linear regression plot is shown in Figure 18.

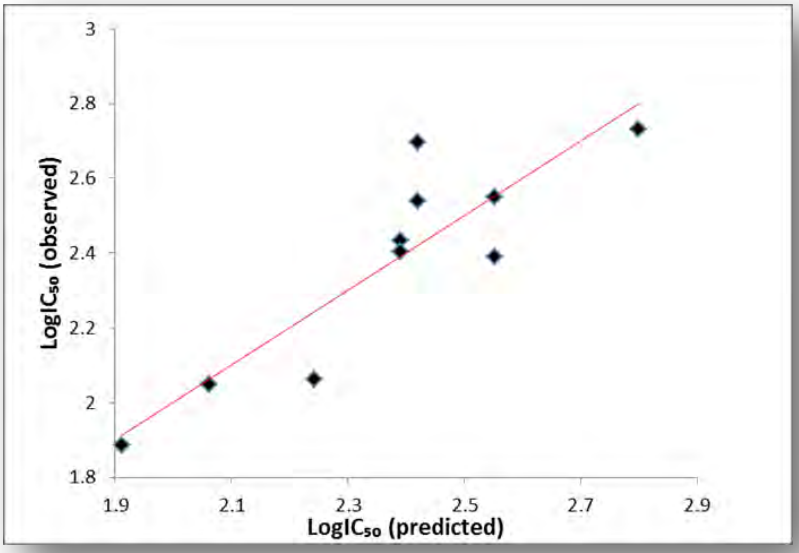

Figure 18: The positive linear regression plot of predicted versus observed LogIC_{50} values for β-haematin inhibition for the 4-aryl-1,4-DHP analogues.[98]

Observations from the equation show that the β-haematin inhibition activity increased with increasing lipophilicity of the C-4 substituent and increasing electron-deficient character. The maximum inhibition activity was seen with a hydrophobic C-4 phenyl disubstituted with electron-withdrawing groups at the *meta* and *para* positions. The trend in inhibition activity was supported by the Topliss decision tree. The best analogue was the 4-Cl-3-CF_3-phenyl-1,4-DHP (77 ± 17 µM) followed by 3,4-diCl-phenyl-1,4-DHP (115 ± 3.85 µM) as the second best. These results provided a starting point for the present study.[98]

At the beginning of the present project parasite testing on the series was performed and the results were rather disappointing. The initial thiophene hit compound together with its C-4 phenyl derivative were synthesised at the University of Cape Town by Mr F. L'bbatte and Ms N. Mvumvu (Hons students in 2012) respectively and were both found to be inactive against parasite growth as well as β-haematin formation. QSAR studies revealed no correlation between the $logIC_{50}$ with any of the free energy parameters, although the 3,4-dichlorophenyl-1,4-DHP (2.85 ± 0.03 μM) compound in Figure 19 was found to be the best analogue from the series and was therefore used as the hit for further development of this new antimalarial chemotype. [98]

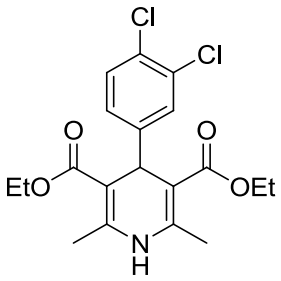

Figure 19: The hit 4-phenyl-1,4-DHP analogue used for the project**.**

This project thus investigated the synthesis of 1,4-DHP derivatives keeping the C-4 substituent fixed as the optimised 3,4-dichlorophenyl group and performing different positional substitutions on the rest of the molecule. In this regard, a key objective was to vary the ester component of the molecule in order to establish the effect on β-haematin formation as well as parasite growth inhibition, see Figure 20.

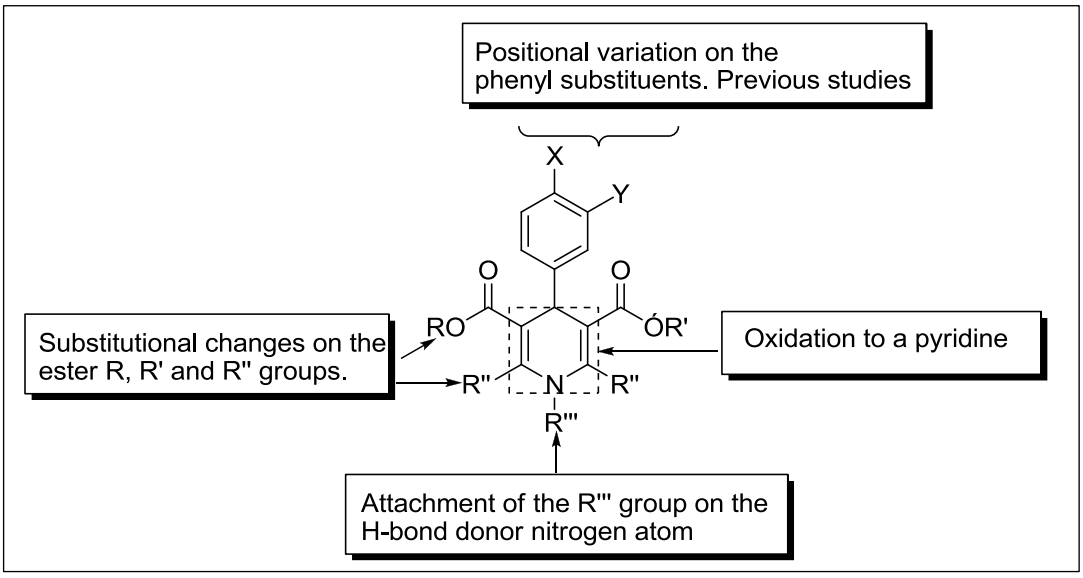

Figure 20: Structural alterations performed on the dihydropyridine template for the present project.

β-haematin inhibition was measured using a commercially available detergent-based (NP-40) 96-well plate assay that mimics the biological neutral lipid bodies formed *in vivo* in the parasite digestive food vacuole, while the in vitro antiplasmodial activity was measured against a chloroquine sensitive (NF54) strain and performed at the Pharmacology division, University of Cape Town Medical School.[90, 99]

1.8 Rational analogue design

1.8.1. Series 1: Variation of the ester groups.

Most of the studies reported in the literature focus on variations made at the C-4 position of a dihydropyridine molecule whist keeping the ester group constant as either the readily available methyl (Me) or ethyl (Et) ester. This is presumably due to the commercial availability of simple acetoacetate Me and Et esters and their reliability in the Hantzsch reaction. Rarely has the ester component of the molecule been changed. This study focused on synthesising a series of dihydropyridine analogues as β-haematin inhibitors and as potential antimalarial agents based on varying the ester group. These variations focused into two ester sub-groups: a symmetrical template and unsymmetrical template, as shown in Figure 21. The symmetrical products contained either a) an alkyl or substituted benzyl group or b) an *N*-heterocycle attached to an alkyl tether. The unsymmetrical products contained simple alkyl groups (**c** in Figure 21). A range of commercially unavailable

acetoacetate esters prepared from methyl acetoacetate and commercially available alcohols, or synthesised alcohols **1**-**4** to produce compounds **5**-**20** (see chapter **2** for synthetic method and structures of the reagents**)** together with commercially available acetoacetate esters, these were required for the successful synthesis of the dihydropyridine analogues.

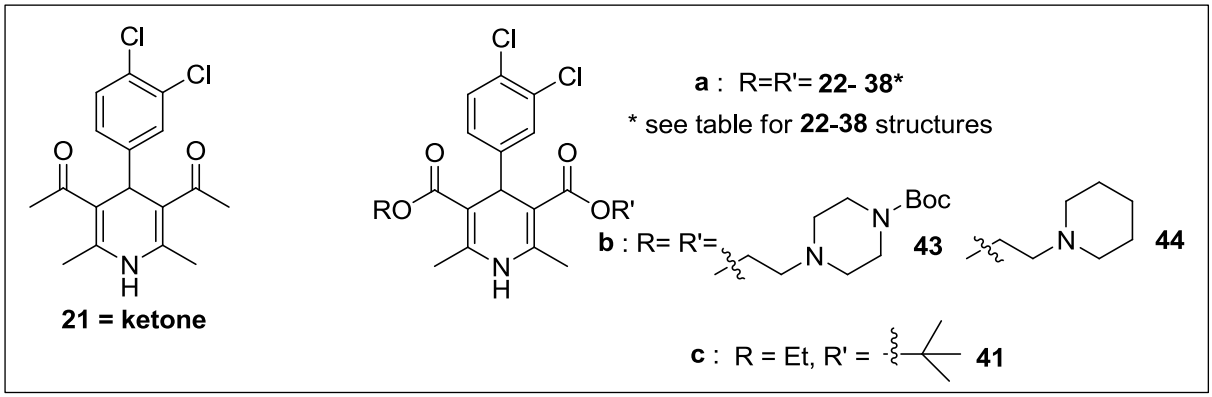

Figure 21: The 1,4-DHP ester analogues selected for the study.

a) Variations containing alkyl and benzyl substituents

Analogues selected were chosen with the aid of the Topliss decision tree, selecting groups from different branches. Table 1 shows the structures of chosen alkyl and benzyl analogues.

Table 1: Showing **21** and the alkyl and benzyl groups selected for ester modifications in the present study.

Analogue	R=R'	Product	R=R'
21	n/a	**30**	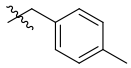
22		**31**	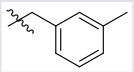
23		**32**	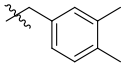
24	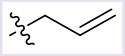	**33**	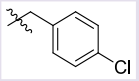
25		**34**	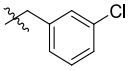
26		**35**	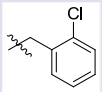
27		**36**	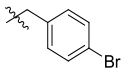
28		**37**	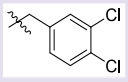
29	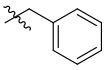	**38**	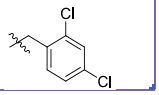

b) Analogues containing an N-heterocycle in the ester side chain

In an attempt to increase vacuolar accumulation of the drug, two analogues with basic amine side chains were identified for the study. This was based on the mode of action hypothesised for chloroquine regarding the understanding that in the acidic vacuole weak bases become protonated and membrane impermeable, resulting in pH trapping.[28, 73]

c) Effects on symmetry

Many of the known 1,4-dihydropyridine drugs, including the L-type calcium channel blockers, are unsymmetrical, and this sparked an interest into understanding the effect of chirality (or asymmetry) within the molecule on potential antimalarial activity. In this case the ester side groups were determined by the availability of reagents.

1.8.2 Series 2: Variations in the C-2 and C-6 (R'') groups

Four analogues were chosen for understanding the influence of the C-2 group on activity; these are shown in Figure 22.

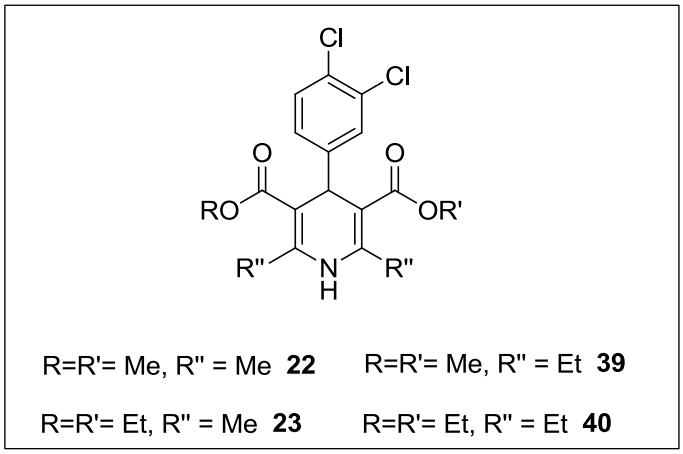

Figure 22: The analogues chosen for variation of the R'' group.

1.8.3 Series 3: The importance of the NH group on the dihydropyridine ring

Hydrogen bonds provide the most crucial non-covalent interactions in biological systems and an important force in molecular recognition of receptors by their substrates or guest molecules (such as drugs). Intermolecular hydrogen bonds between Fe(III)PPIX dimers are an important feature of haemozoin and suggest that H-bonds may also be important for inhibition of haemozoin formation. The propionate side chains (on Fe(III)PPIX) that form the intermolecular bonds are proposed to be significant during interactions of haem with various proton donor moieties.[67, 73, 75] The dihydropyridine molecule has one donor (the NH group in the ring) and three acceptor (the two carbonyl oxygens and the nitrogen in the ring) sites, respectively. Therefore, substitution of the hydrogen on the nitrogen ring would deny the possibility of hydrogen-bond donor character within the molecule. Hence a comparison of unsubstituted nitrogen (NH) with a substituted one needed to be undertaken. Figure 23 shows the variation identified.

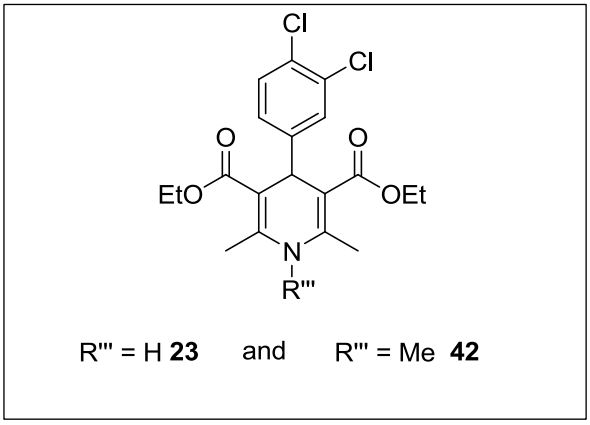

Figure 23: Analogues synthesised for evaluating H-bond donor influences on activity.

1.8.4 Series 4: Pyridine analogues

Studies performed by Schneider et al on the association energies of water-soluble porphyrin rings with small aromatic ring ligands revealed that increasing the number of π-electrons (thus increasing the aromatic rings) resulted in an increased strength of association.[100] Similar studies performed by Kuter et al also showed that the molecules with a greater number of conjugated π-electrons associated more strongly with haem.[101] For this reason it was decided that investigation of the oxidised product (pyridine) of the dihydropyridine derivative would be interesting. Oxidation increases the number of π-electrons in the molecule as well as making the ring flat. Part of the work thus involved oxidizing some of the 4-phenyl-1,4-dihydropyridine products synthesised previously at UCT, to their corresponding pyridine structures. This was aimed at investigating the effect on biological activity of changing from a non-planar, non-aromatic template to an aromatic and hence planar one, which it was hoped, would shed light on aspects of π-π stacking interactions with Fe (III) PPIX. Figure 24 shows the analogues chosen for the study.

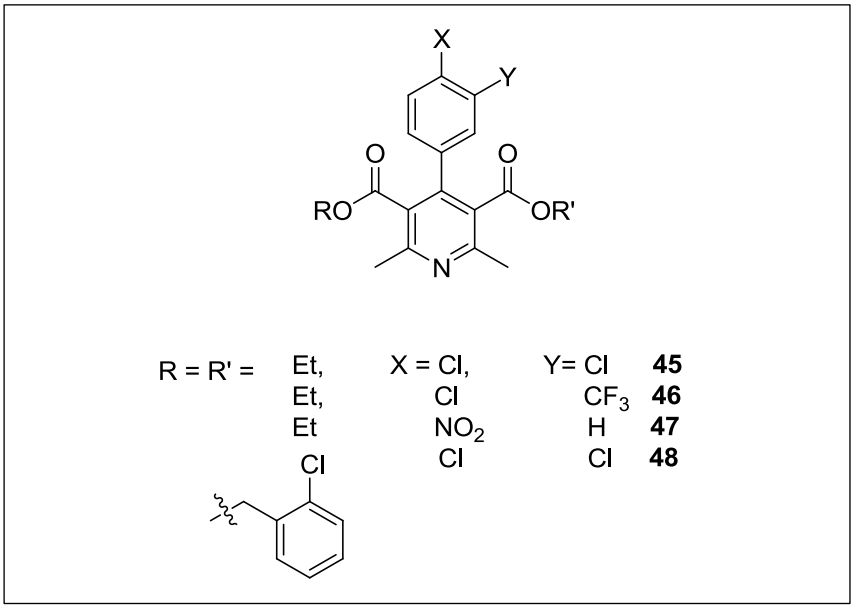

Figure 24: The oxidised derivatives selected for investigation.

1.9 Aim

The overall aim of the project was to develop a structure-activity profile for the 1,4-dihydropyridine lead against β-haematin formation and malarial parasite growth. This required synthesising analogues of the new C-4 phenyl molecule (Figure 20) using the Hantzsch pyridine reaction.

The study was designed to address the following aspects:

(i)Variation of the ester component of the molecule (R and R')

(ii) The effects of symmetry on activity

(iii) pH trapping and basicity of the compound.

(iv) The importance of having the NH on the dihydropyridine ring

(v) Extension of alkyl side chain of the R'' group

(vi) Oxidation of a dihydropyridine ring to a pyridine

The synthesised compounds were characterised using ^{1}H-NMR, ^{13}C NMR and IR spectroscopy, high-resolution mass spectrometry and melting points.

2. Organic Synthesis

2.1 An Overview and Mechanism of the Hantzsch pyridine reaction

The remarkable Hantzsch pyridine reaction is a one-pot, three component reaction involving the reaction of an aldehyde, acetoacetate (usually ethyl acetoacetate) and ammonium acetate (as the source of ammonia) to yield a 1,4-dihydropyridine intermediate. This intermediate can then be subsequently oxidised to form the corresponding pyridine molecule, Scheme 1.

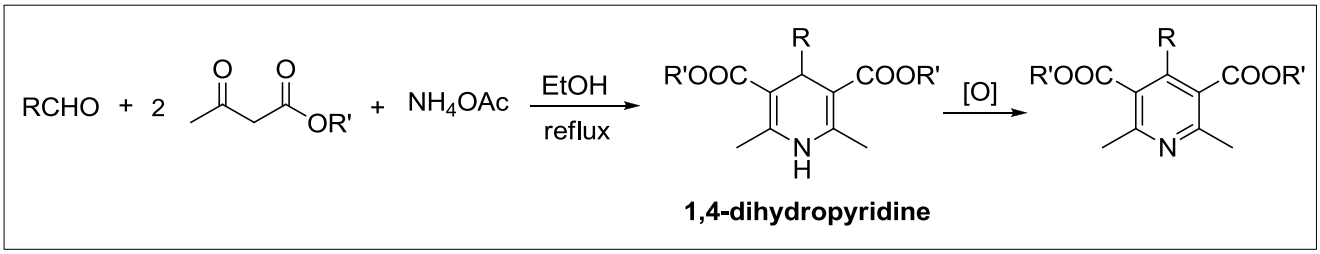

Scheme 1: General scheme for the Hantzsch synthesis via a 1,4-dihydropyridine intermediate

Formation of the 1,4-dihydropyridine intermediate involves the following steps: a Knoevenagel condensation between the aldehyde and the acetoacetate to form an enone intermediate, formation of an enamine intermediate from a second acetoacetate molecule, Michael addition of the enamine to the enone, tautomerism and cyclisation to afford the desired product. The Knoevenagel enone intermediate is formed via abstraction of an α-methylene proton of the acetoacetate by the acetate ion as a base and the ammonium ion as an acid, followed by addition and elimination (E1cB mechanism) reactions. Proton abstraction is regio-selective because protons at this position are more acidic than those on the methyl ketone due to the presence of two strongly electron-withdrawing groups that stabilise the resultant conjugate base by resonance stabilization. Scheme 2 shows the mechanism of the Knoevenagel condensation step to form the enone.

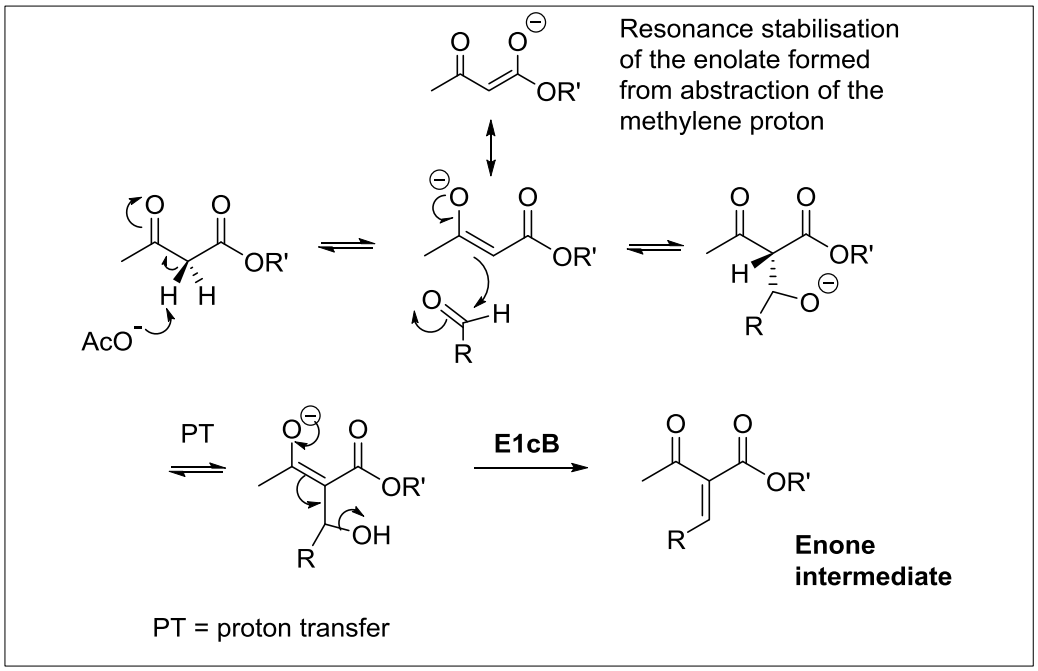

Scheme 2: The mechanism of the Knoevenagel step.[102]

Ammonium acetate then condenses with the second equivalent of acetoacetate to form an enamine intermediate. The two intermediates then undergo Michael (conjugate) addition which is believed to be the rate-determining step, followed by cyclisation to form a 1,4-dihydropyridine product. The removal of water from the reaction is the driving force for the formation of product. Scheme 3 shows the overall transformation.[95, 96, 102]

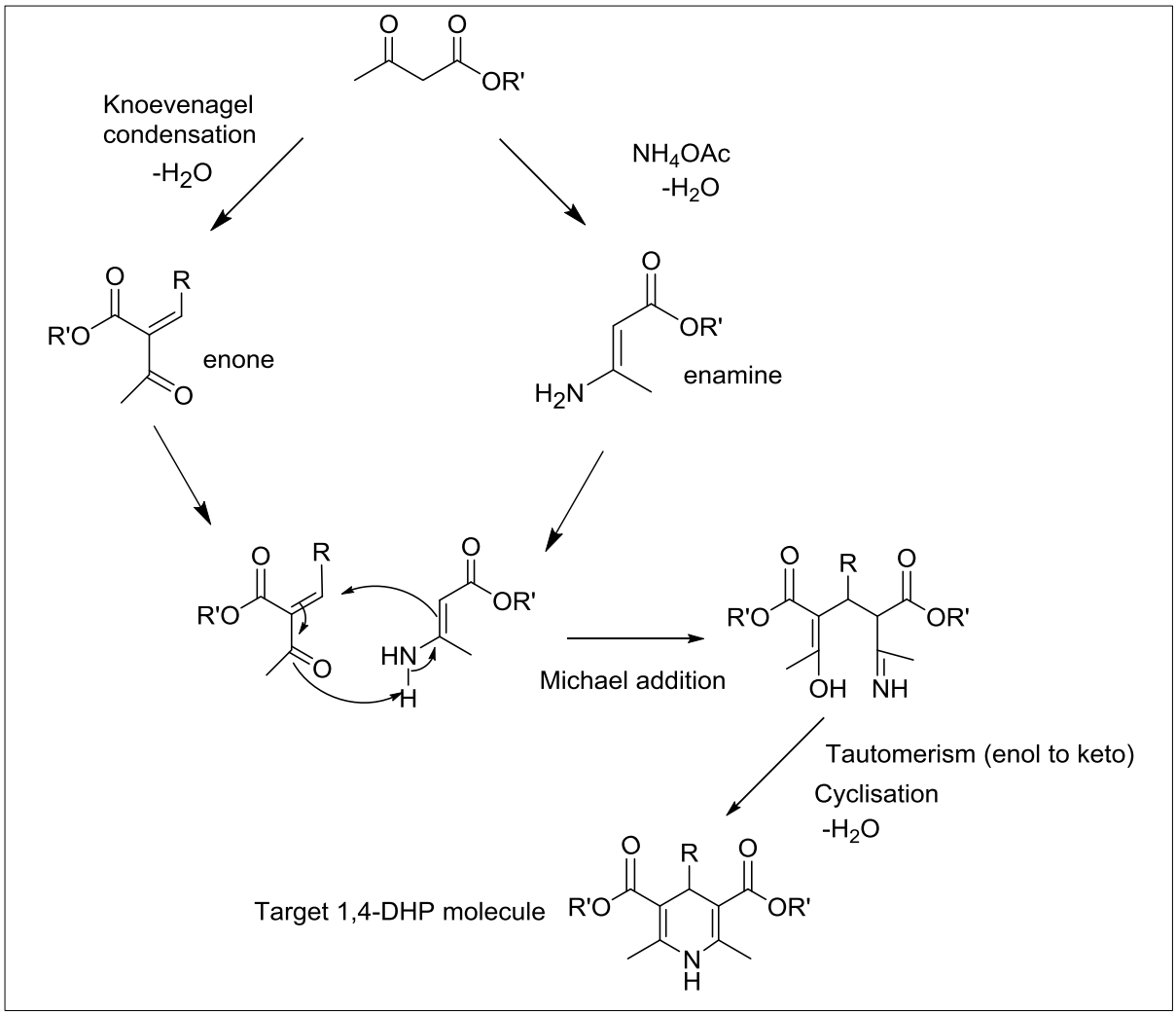

Scheme 3: An overview of the Hantzsch reaction.[102]

2.2 Review of the synthesis of 1,4-dihydropyridine esters.

A key objective in this project was to synthesize a library of Hantzsch 1,4-dihydropyridines varying the ester group while keeping the aldehyde component constant (see chapter 3), and for this a range of acetoacetate esters was required. Since most of the desired acetoacetate derivatives were unavailable commercially, methodology for their formation needed to bedeveloped. A number of methods for this are known in the literature and three of the main ones (including the one used in this project) will be described here as the Claisen condensation, the diketene approach, and the transesterification approach (used in the project).

i) The Claisen condensation

This is a carbon-carbon bond formation reaction involving an ester as the carbanion (instead of an aldehyde) in an aldol-type condensation. The enolate of the ester may be formed using a range of bases including the conjugate corresponding to the ester group (for simple self-condensations), and once formed undergoes a S_NAc reaction with another molecule of undeprotonated ester to form the acetoacetate derivative. This is then stabilised by deprotonation in view of the enhanced acidity of the protons at the methylene group between the two carbonyl groups, ensuring that the product doesn't undergo further Claisen reaction. The reaction may involve different esters (cross-Claisen) in which case a strong, non-nucleophilic base needs to be used in order to avoid scrambling, Figure 25.[102, 103]

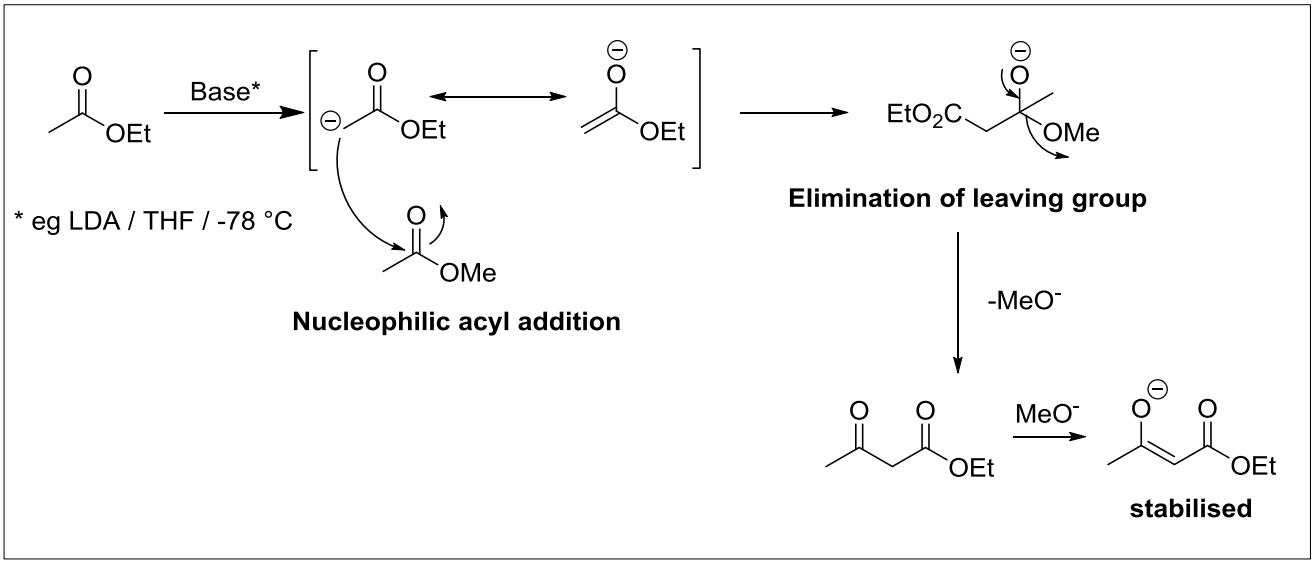

Figure 25: A cross-Claisen condensation.

Literature suggested that this methodology might be problematic for the range of acetoacetates required for this project.[104]

ii) The diketene approach

The acid- or base-catalysed addition of an alcohol to the four-membered lactone ring of diketene to yield a β-keto ester is a well-known reaction. The strained ring allows for nucleophilic attack of the alcohol on the carbonyl carbon resulting in ring opening of the molecule to afford the acetoacetate product. Figure 26 depicts the case for ethyl acetoacetate. A catalyst is required to enhance the poor nucleophilicity of the alcohol.

However, diketene is prone to hydrolysis and decarboxylation, and is quite toxic. Hence, this methodology was not seriously entertained either.[103, 105, 106]

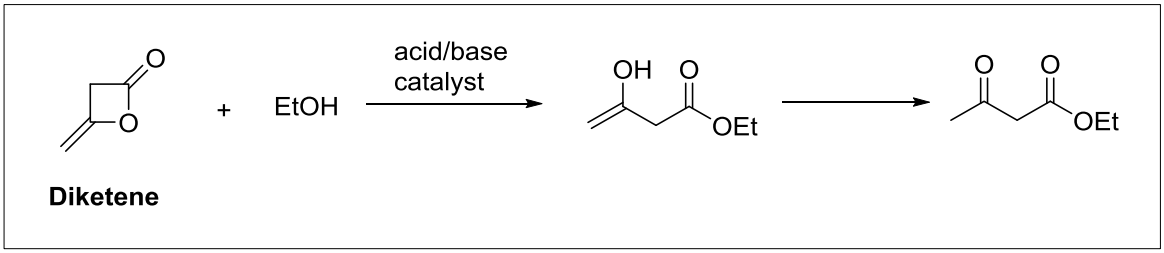

Figure 26: Addition of ethanol to diketene.

iii) Transesterification

The most efficient and straightforward approach for β-keto ester synthesis is via exchange of the ester group of a commercially available acetoacetate (methyl or ethyl) with an appropriate alcohol in a process termed transesterification. Such a process needs to be acid-catalysed (Bronsted or Lewis) in which an acid is required to enhance carbonyl electrophilicity towards the poorly nucleophilic alcohol.[103] Many catalysts have been used for this purpose such as zeolites, Lewis acids and bases, protic acids, solid acid, enzymes and transition-metal complexes. However, of these catalysts many are either expensive and / or, corrosive, or require synthesis.[107-110] Ultimately, the approach selected was the one reported by Chavan in view of its simplicity and facile product isolation, in which zinc iodide (produced *in situ* from zinc dust and iodine) is used as a mild Lewis acid catalyst.[111] Mechanistically the exchange is proposed to proceed via complexation of the zinc iodide to both carbonyl groups resulting in a six-membered chelate, activating the ester for nucleophilic addition leading to exchange in view of the presence of a leaving group. Methanol is removed from the reaction via a Dean-Stark apparatus, which drives the reaction equilibrium to the right.[104] The zinc iodide hydrolyses on work-up and is removed into the aqueous layer. Scheme 4 depicts a plausible ester-exchange mechanism for the transesterification.

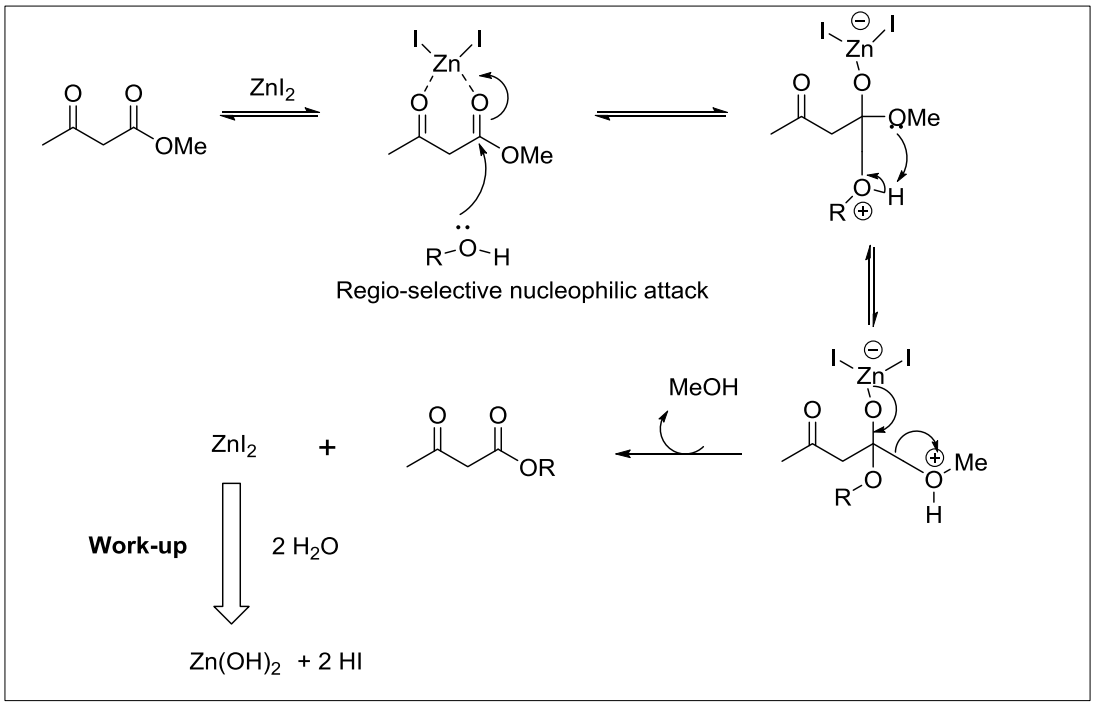

Scheme 4: The proposed reaction mechanism for acetoacetate transesterification using zinc iodide as catalyst.

2.3 Synthesis of the acetoacetate analogues

The analogues were selected in alignment with rational design aspects of the project, which were described in Chapter 1 (section 1.8, Topliss tree approach). The transesterification method used 2.0 mole equivalents of zinc, 1.2 mole equivalents of alcohol and 0.1 mole equivalents of iodine with respect to methyl acetoacetate in toluene at 110 °C and was applied to the synthesis of **6** (cyclohexyl) and **8** (benzyl) acetoacetate analogues, which were obtained in 80% and 85% yields respectively after work-up and chromatography. Owing to this success, the above conditions were applied to the other alcohols. Analogues **1**-**4** were prepared as pre-requisite substrates for further use in the reaction. Table 2 shows the percentage yield for each analogue synthesised.

Table 2: Percentage yields for the acetoacetate derivatives. a) The benzyl analogues and b) The alkyl side chains.

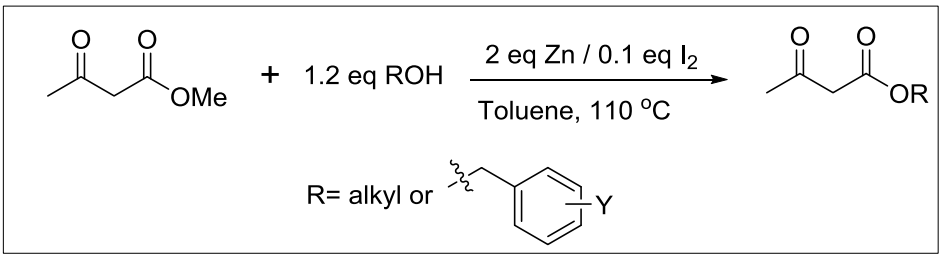

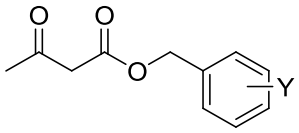

a

Product	8	9	10	11	12	13	14	15	16	17
Y	H	*o*-Cl	*p*-Cl	*m*-Cl	*p*-Br	*p*-Me	*m*-Me	3,4-Cl	2,4-Cl	3,4-Me
Yield	80	85	83	79	66	76	54	57	99	32

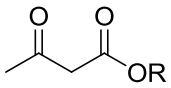

b

Product	R	Yield %
5		48
6	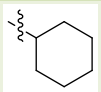	85
7		29
18	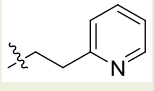	14
19	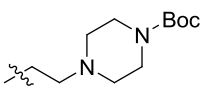	63
20	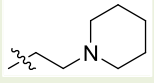	45

Yields for the exchange ranged from modest (~60%) to very good (~80%) except for products **7**, **17** and **18** where yields were disappointingly low (< 35%). Reasons for this were unclear although for analogue **18** it was hypothesised that the nitrogen atom in the pyridine ring co-ordinated with the catalyst forming a complex that competed with the six-membered chelate, Figure 27. In search of conditions that would overcome the competing complexation in the case of **18** where the yield was unacceptably low (14 %), a series of reactions were performed at 110 °C changing the molar equivalents of methyl acetoacetate involved in the reaction. Table 3 shows how yield increased with increasing molar equivalents of methyl acetoacetate used. Ultimately, 5 mole equivalents of methyl acetoacetate with 1 mole equivalent of 2-(2-pyridyl)ethanol in the presence of 2 mole and 0.1 mole equivalents of zinc dust and iodine respectively gave an acceptable yield of 70 % of the desired product.

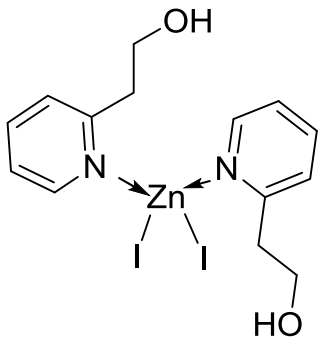

Figure 27: The proposed pyridine-ZnI_2 complex.

Table 3: Influence of reaction stoichiometry on the yield of **18**

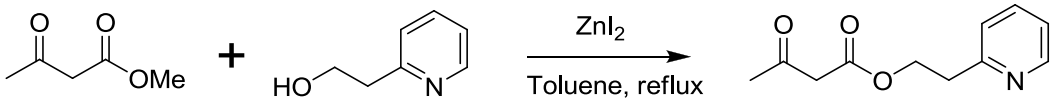

Methyl acetoacetate (mmol)	2-(2-pyridyl)ethanol (mmol)	Zinc (mmol)	Iodine (mmol)	Yield %
1	1.2	2	0.1	14
2	1	2	0.1	20
5	1	2	0.1	69
8	1	2	0.1	70

The NMR spectra of the acetoacetate products derived from the alkyl alcohols,revealed two core diagnostic singlets resulting from the ketone methyl group (H-1, range of 2.17-2.34 ppm) and the deshielded methylene group (H-3, range 3.26-3.46 ppm) in the ^{1}H spectra, together with two highly downfield carbonyl carbons and the signals for each ester R group in the ^{13}C spectra. These data strongly supported the existence of the keto form as the dominant tautomer based on the observation of the H-3 methylene singlet. Similarly, the ^{13}C NMR revealed four core resonances for carbonyl, methyl and methylene groups together with the relevant ester group signals. Figure 28 shows the ^{1}H NMR and ^{13}C NMR spectra of **6** as a representative case. The ^{13}C NMR spectrum suggests, possibly, that a small amount of enol is present by virtue of a peak at 90 ppm for the C-3 vinyl carbon. The existence of this tautomer might be due to its stabilisation by intramolecular hydrogen bonding, Figure 29.

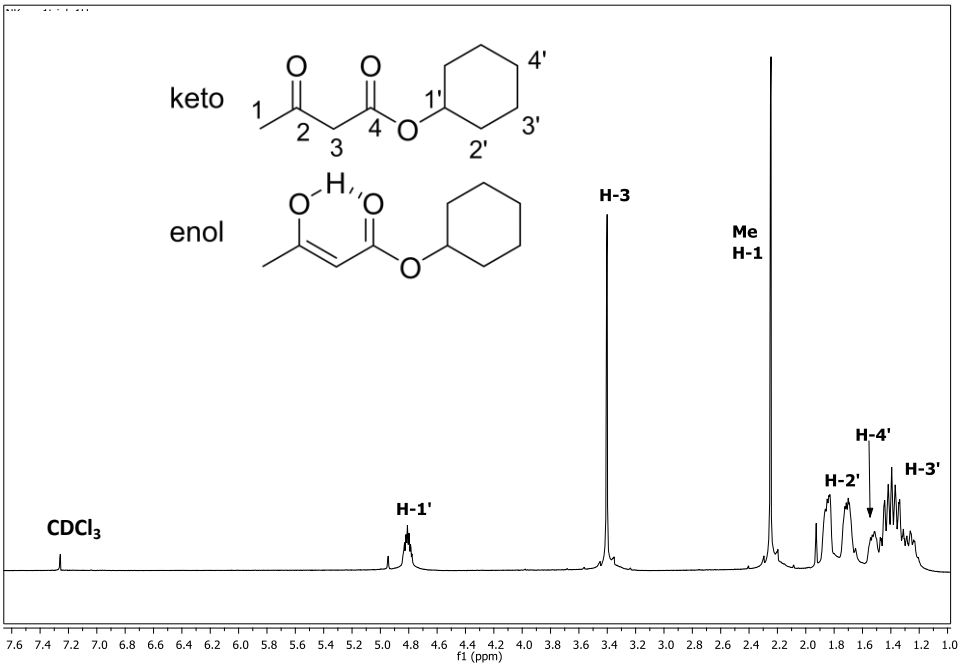

Figure 28a: The ^{1}H NMR spectrum of **6**.

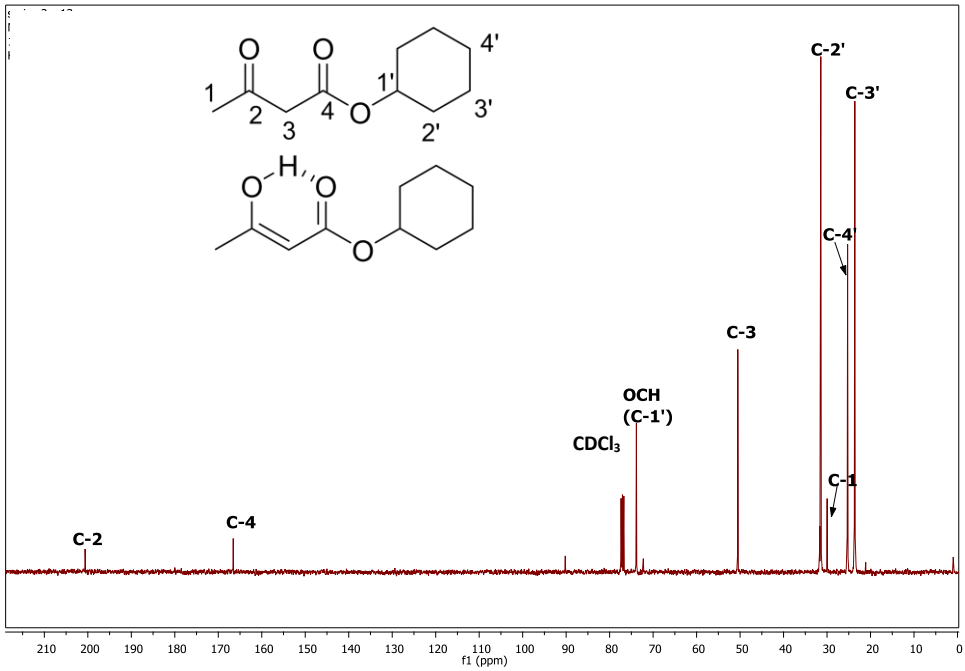

Figure 28b: The ^{13}C NMR spectrum for **6**.

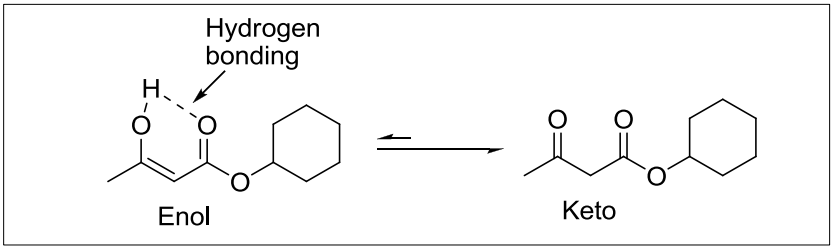

Figure 29: The diagram illustrating the keto-enol tautomerism for analogue **6**.

Another generic type in the project was based on using a substituted benzyl alcohol in the exchange. Here, in addition to the observed ^{1}H NMR signals for the acetoacetate core, a singlet was always observed at approximetely 5.0 ppm corresponding to the benzyloxy methylene protons. The analogues showed variation only in the aromatic region due to the substituents. Likewise, additional core signals for methylene and aromatic carbons were observed in the ^{13}C NMR spectra. The ^{1}H NMR and ^{13}C NMR spectra of analogue **8** demonstrate a typical profile, Figure 30.

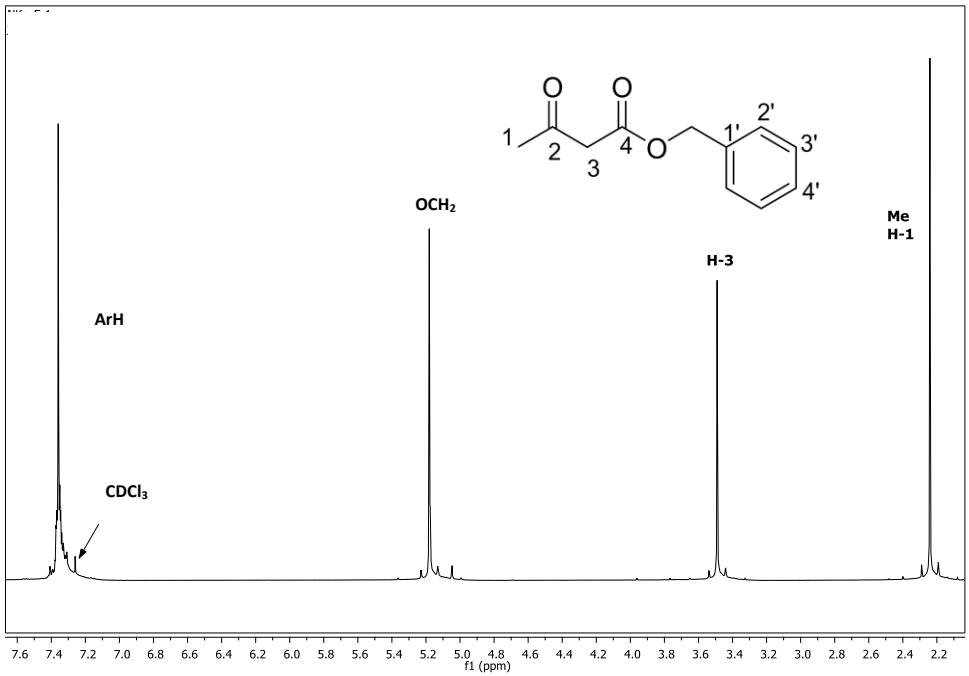

Figure 30a: The ^{1}H NMR spectrum of **8** as the prototype for benzyl acetoacetate analogues.

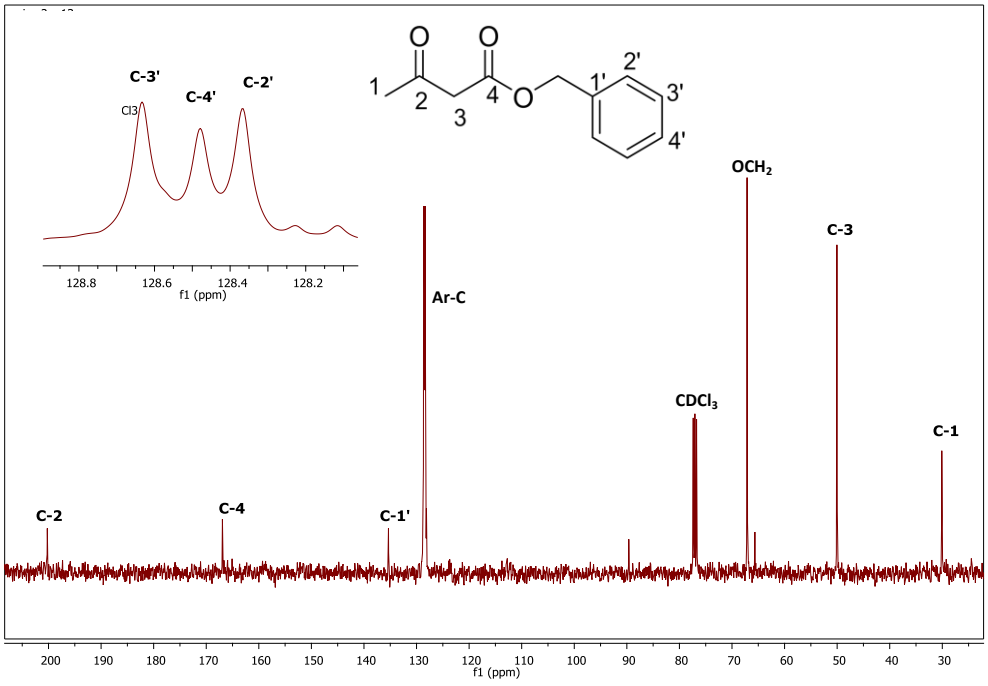

Figure 30b: ^{13}C NMR spectrum for analogue **8**. The expansion shows the aromatic carbons.

2.4 The library of Hantzsch-ester 1,4-DHP analogues

i) Synthesis and rationale:

Although the library synthesis in this study utilized 3,4-dichlorobenzaldehyde as the aldehyde component throughout, earlier optimization studies had used 4-

nitrobenzaldehyde with ethyl acetoacetate and ammonium acetate in ethanol. For the latter the best stoichiometry for optimal yield was found to be 5 mol equivalents of ammonium acetate with 20 mol equivalents of ethyl acetoacetate with respect to the aldehyde in ethanol at 60 °C using microwave irradiation. Figure 31 shows how the yield increased logarithmically with increasing mol equivalents of ethyl acetoacetate in the microwave reaction.[98] Therefore, for the synthesis of the library of derivatives in this project using 3,4-dichlorobenzaldehyde it was decided to use these same conditions on the basis that variation of thealdehyde should not have a significant effect. Fortunately, this turned out to be a valid assumption.

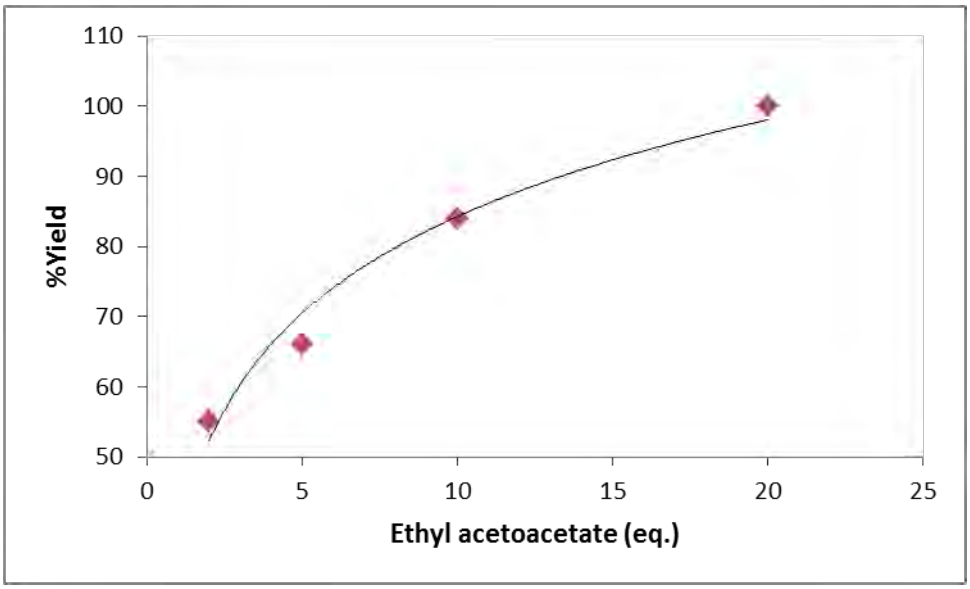

Figure 31: A plot depicting the increase in % yield with increasing mol equivalents of acetoacetate for Hantzsch synthesis with 4-nitrobenzaldehyde and ethyl acetoacetate.

Therefore, these one-pot, three-component, experimentally optimised Hantzsch reaction conditions were employed in the synthesis of the 1,4-DHP esters using the modified acetoacetate esters prepared. The reaction progress was monitored by TLC (hexane/ ethyl acetate 3:1) every 3 minutes for microwave (to avoid over-irradiation leading to degradation and low yield) or each hour for reactions conducted at reflux under N_2. Generally the reaction times ranged from 8 minutes to 26 minutes for the microwave and 2 hours to overnight for reactions conducted at reflux. Owing to unavailability of the microwave machine for a period of two months, conventional heatingat 80 °C was implemented for analogues (**22**, **24**, **26**, **27**, **28** and **29**) speculated to be prone to dehydrogenation. Owing to

formation of side products, after several attempts to synthesise the 1,4-DHP pyridine ester analogue from acetoacetate **18**, the synthesis was deemed unsuccessful. Upon completion of the reaction, products were isolated by column chromatography to give yields, ranging from moderate to excellent (51-96%) with greater than 95% purity as determined by HPLC. The same conditions were used for the synthesis of ketone **21**.Analogue Table 4 shows the results.

Table 4: The percentage yields for the 1,4-dihydropyridine ester series. * denotes ketone (Me) instead of ester (OR).

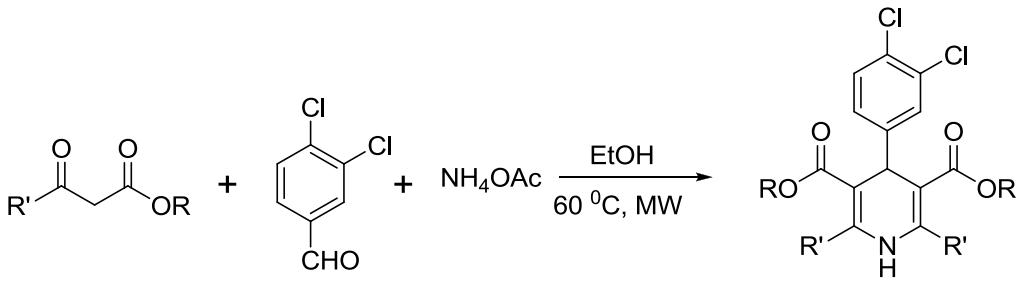

Product	R	R'	Yield %	Product	R	R'	Yield %
21	*	Me	88	**32**		Me	97
22		Me	66	**33**		Me	89
23		Me	94	**34**		Me	96
24		Me	72	**35**		Me	83
25		Me	91	**36**		Me	73
26		Me	51	**37**		Me	62
27		Me	82	**38**		Me	62
28		Me	80	**39**	Me	Et	93
29		Me	96	**40**	Et	Et	98
30		Me	87	**43**	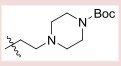	Me	62
31		Me	78	**44**		Me	83

*Denotes ketone

Characterisation of the products by the usual range of spectroscopic techniques (NMR, IR spectroscopy and Mass Spectrometry) was divided into two groups as 1,4-dihydropyridines with alkyl esters and those with benzyl esters.

1,4-dihydropyridines with alkyl esters (**21**-**28** and **39**-**40**):

The ^{1}H NMR spectra of the 1,4-dihydropyridines with alkyl esters differed only in the alkyl region due to the ester portion of the molecule, variation of which had little effect on the other signals. Variations in the substitution pattern in the alkyl region could also be discerned since either four signals were observed (for the isopropyl, ethyl and cyclopentyl analogues) or five signals for the more complicated allyl, *t*-butyl and cyclohexyl analogues. Each analogue revealed a core set of signals for the dihydropyridine moiety corresponding to: a singlet for H-4, a methyl singlet corresponding to the methyl groups at C-2 (for analogues **21**-**28**), and three aromatic signals (originating from the lead aldehyde used in the reaction (3,4-dichlorobenzaldehyde)) integrating for three protons and splitting as two doublets and a doublet of doublets. The latter signal, corresponding to H6', was due to coupling to H-5' and H-2' with typical ortho (~8 Hz) and meta (~2 Hz) coupling constants respectively. Similarly, the ^{13}C NMR spectra revealed the core signals for the dihydropyridine and phenyl moieties: five quaternary carbon signals (C-2, C-3, C-1', C-3', C-4'), one for the carbonyl carbons, one for the carbon at position 4 and one for the methyl group (except for analogues **39** and **40**, which had the C-2 methyl group replaced by an ethyl group).

^{1}H NMR spectrum for analogue **40**

The alkyl products contained mirror-plane symmetry and were thus achiral. However, products containing methylene groups bonded to the ester oxygen contained prochiral methylene carbons with diastereotopic hydrogens, which in some cases resulted in geminal coupling being observed between the two magnetically non-equivalent hydrogens. A case in point is the C-2 ethyl analogue **40** shown in Figure 32a in which the two methylene hydrogens appear as two independent doubled quartets due to geminal and vicinal coupling. The IR spectra generally displayed a broad NH peak at ~3500 cm^{-1}, a band at 1645 cm^{-1} for the C=C aromatic stretch, a band at 1695 cm^{-1} for the C=O group and the C-H

alkene/ alkane peaks were observed at ~3000 cm^{-1} and 2900 cm^{-1}, respectively. Spectroscopic analysis of **40** is shown below in Figure 32, where ethyl propionylacetate was used as the acetoacetate. Interestingly, both methylene groups show diastereotopic geminal hydrogen nuclei. High resolution mass spectrometry (Figure 32d) also gave substantial evidence in support of **40**. The high resolution mass spectrum shown in Figure 32d gave the dominant ion as $[M+H]^+$ with an observed molecular mass of 426.1243, which was within acceptable limits to the molecular mass expected of the $[M + H]^+$ ion equal to 426.1239. This ion contained two ^{35}Cl isotopes, ^{35}Cl being the major isotope.. The mass spectrum also showed the other dominant ion containing a combination of ^{35}Cl and ^{37}Cl isotopes, which appeared as a signal at 428.1218 due to the masses of the two different Cl ions. Other minor combinations were also revealed. Derivative **40** was also revealed to be 99 % pure by HPLC, Figure 32e.

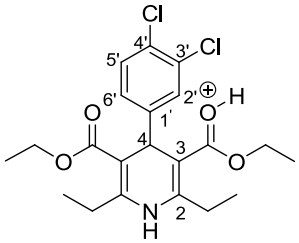

Chemical Formula: $C_{21}H_{26}Cl_2NO_4^+$
Exact Mass: 426.12
Molecular Weight: 427.34
m/z: 426.12 (100.0%), 428.12 (64.0%), 427.13 (23.2%), 429.12 (14.8%), 430.12 (10.3%), 428.13 (3.4%), 431.12 (2.4%), 430.13 (2.2%)

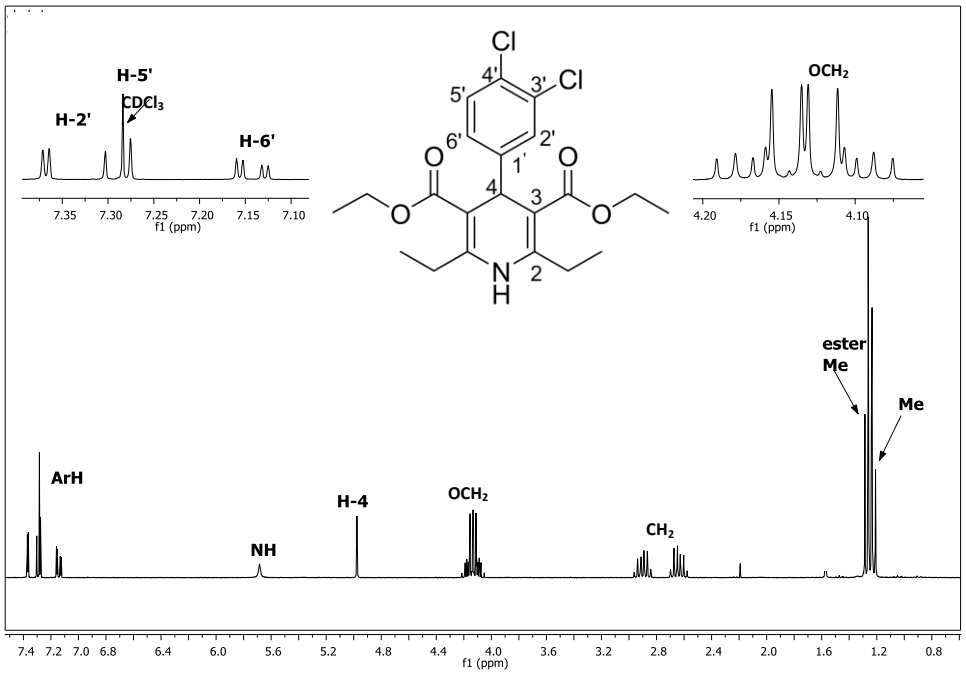

Figure 32a: The ^{1}H NMR of **40** in $CDCl_3$. H-6' couples to both H-5' and H-2' in the aromatic region.

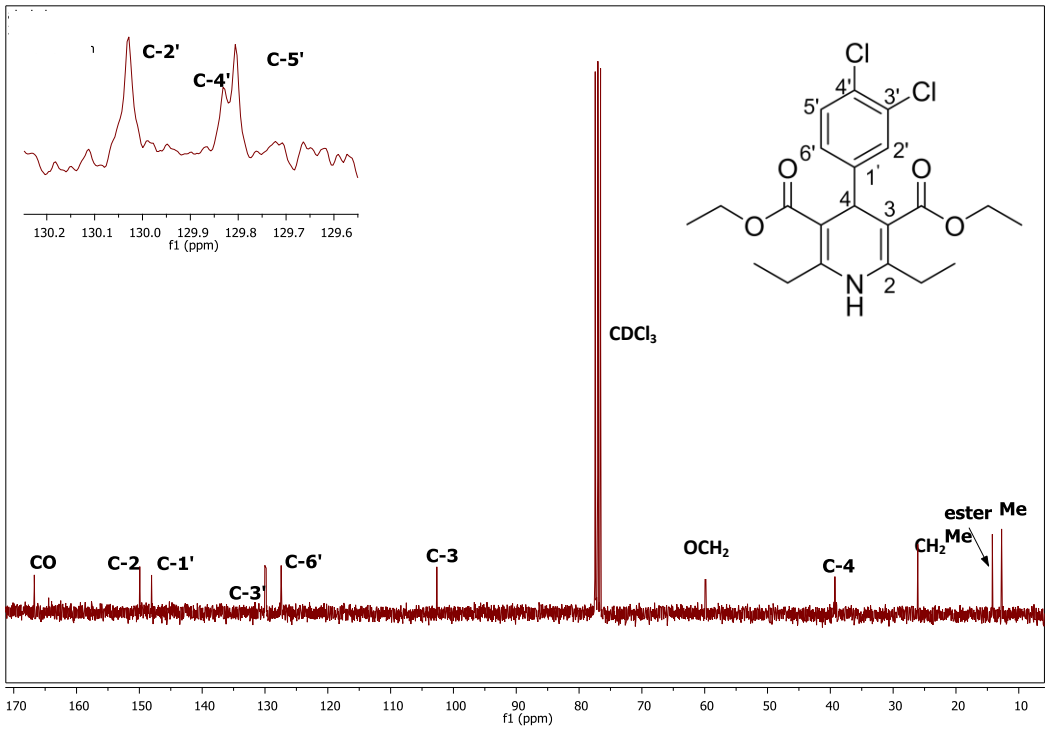

Figure 32b: The ^{13}C NMR spectrum for **40**.

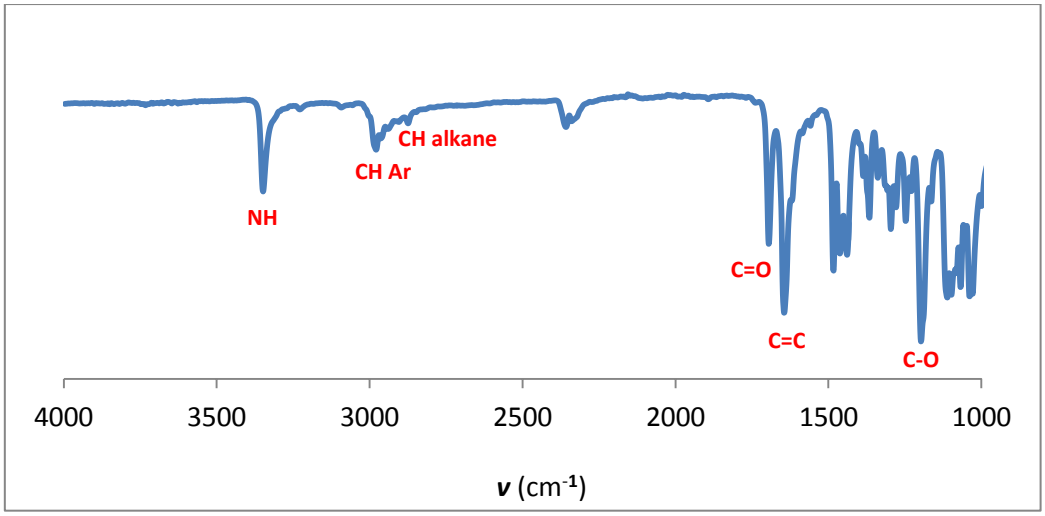

Figure 32c: The IR spectrum for analogue **40.**

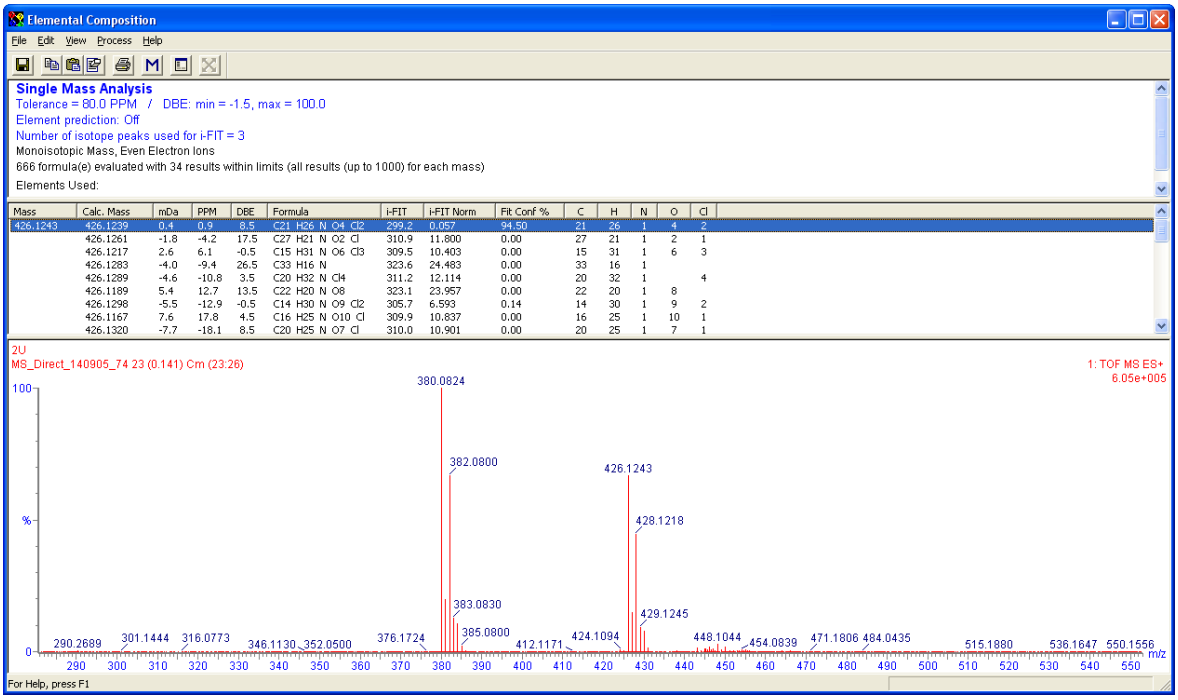

Figure 32d: The high-resolution mass spectrum of analogue **40**.

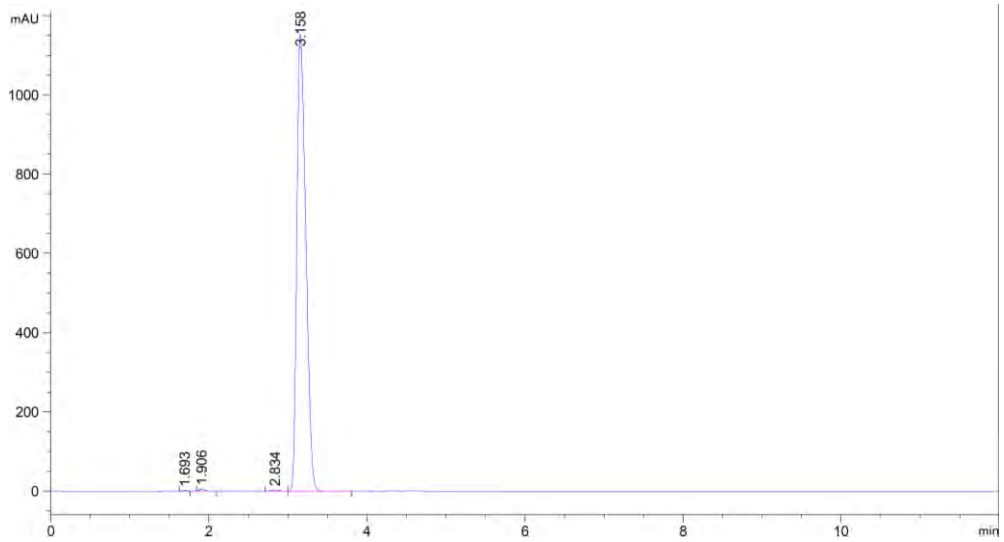

Figure 32e: The high-performance liquid chromatograph of analogue **40**.

Analogues containing an *N*-heterocycle in the tether **43** and **44**.

For the purposes of investigating the effect of pH-trapping on activity, synthesis of analogues having a second amine group in the molecule in order to increase basicity (protonation in the food-vacuole which promotes inhibitor accumulation) was implemented. This came in the form of either a piperazine (**43**) or piperidine (**44**) in the alkyl side chain. Piperazine derivative **43** is used for illustration purposes. As before, the ^{1}H NMR spectrum showed the presence of a diastereotopic quartet for the alkoxy methylene (OCH_2) protons at ~4.18 ppm. The methylene protons (NCH_2) in the piperazine ring revealed two downfield triplets with a coupling of *J*= 6.0 Hz, with H-3" being the more deshielded by virtue of the electron-withdrawing Boc group, which resonated as expected as a singlet, Figure 33. Similarly, the ^{13}C NMR spectrum of **43** showed the NCH_2 singlets at 56.5 (N**C**H_2CH_2O), 53.7 (H-3'') and 43.6 (H-2'') respectively. HRMS confirmed the structure (HRMS (EI): m/z 766.3346 [M+H^+], $C_{37}H_{54}Cl_2N_5O_8$ requires 766.3349).

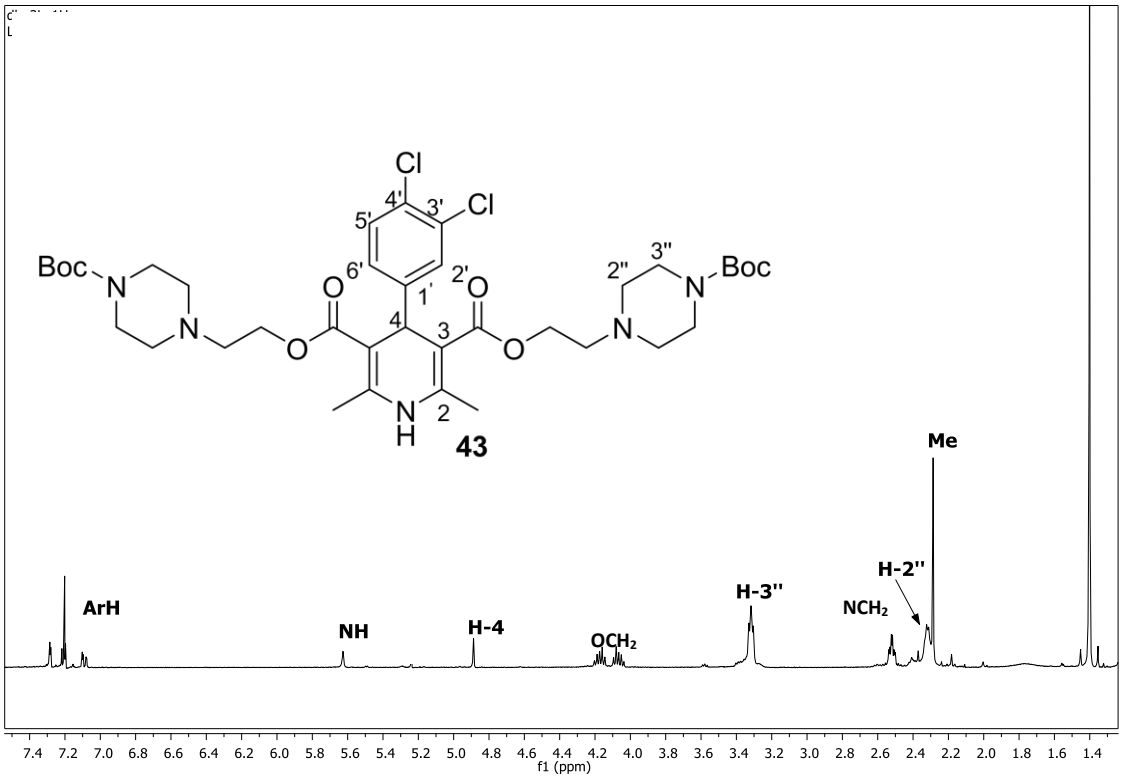

Figure 33a: The ^{1}H NMR of **43**.

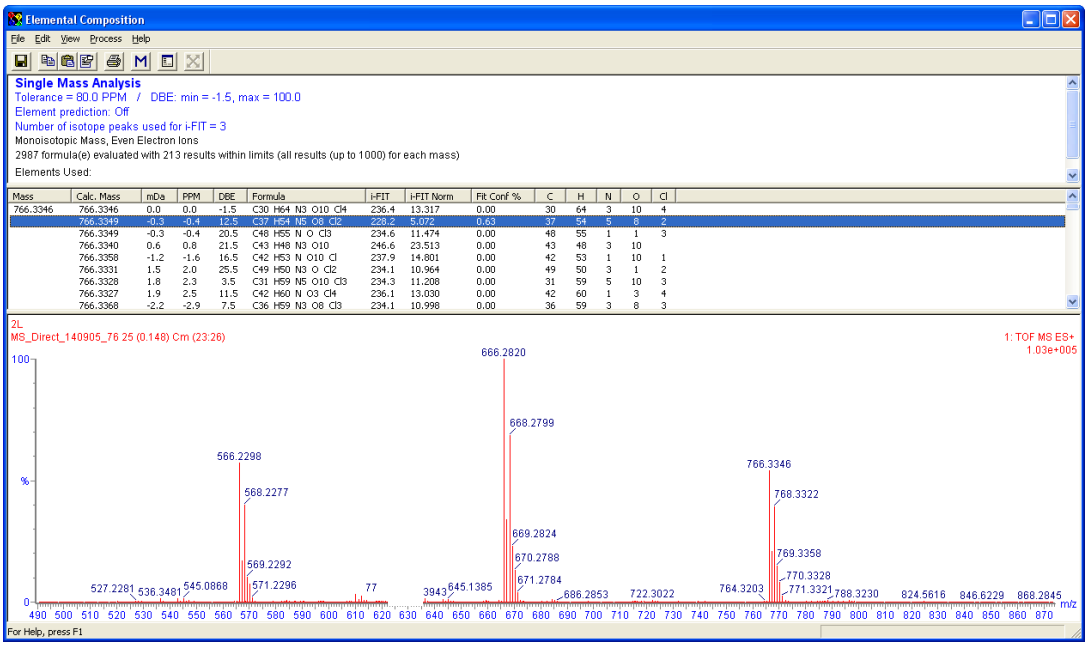

Figure 33b: The HRMS of **43**.

<u>Synthesis of *N*-methylated 1,4-DHP ester **42:**</u>

In order to address whether the NH group of the dihydropyridine moiety is essential for activity, we decided to mask this group with a simple methyl substituent. N-methylation of

23 was undertaken by taking advantage of the acidity of NH, which forms part of a vinylogous amide and thus could be removed by a strong base (NaH at 0 °C; weaker bases like NaOH failed to promote methylation). Dimethyl sulfate was used as the methylating agent at 0 °C, which produced the desired *N*-methyl derivative in 98% yield after work-up and chromatography. A mechanism for the reaction is depicted in Scheme 5 showing the resonance stabilisation of the anion. A regioselective methylation on nitrogen ensures that conjugation is preserved.

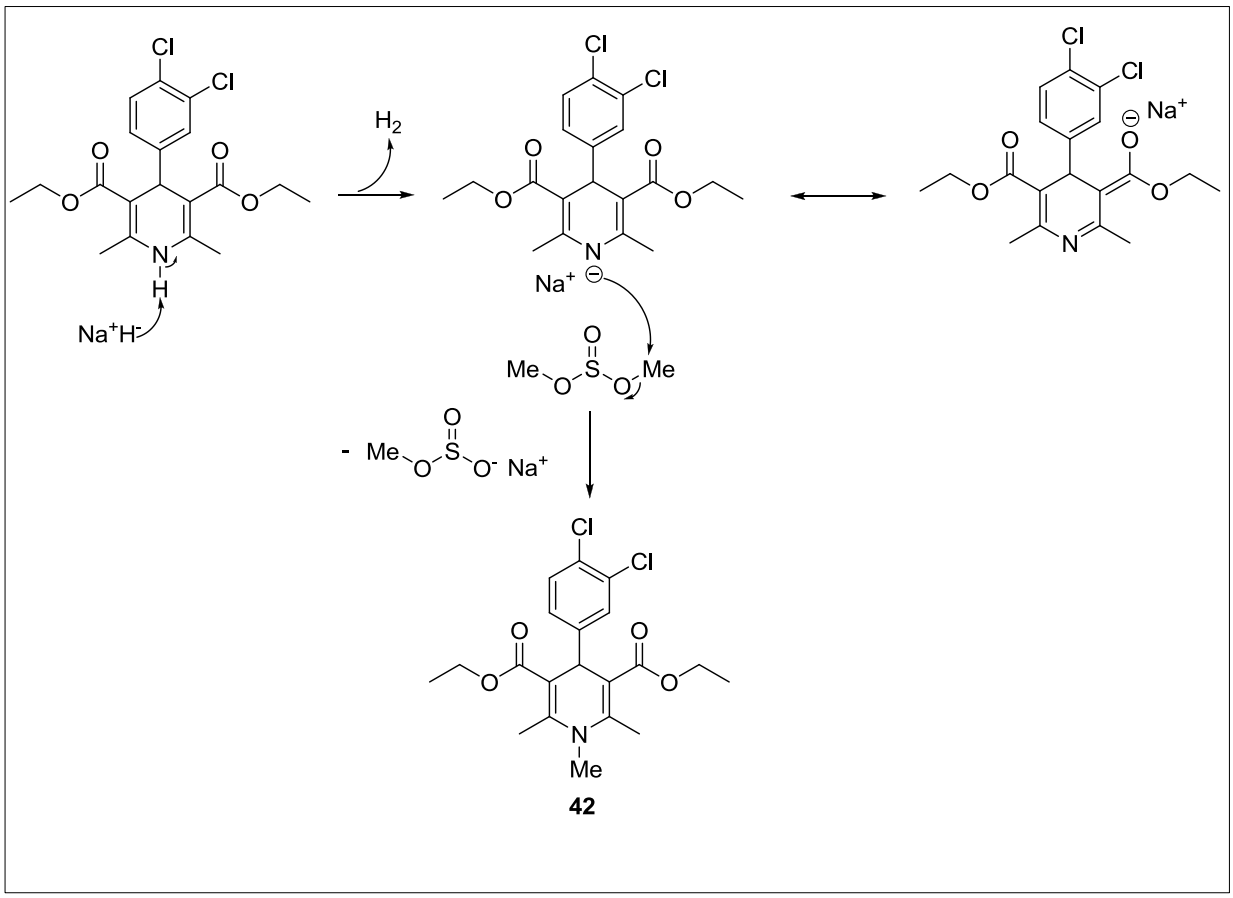

Scheme 5: The mechanistic scheme for the formation of **42**. A dihydropyridine resonance hybrid for the anion is also shown.

The spectra for the product were consistent with the proposed structure for **42** in that disappearance of the broad NH peak at ~5.50 ppm and that at ~3500 cm^{-1} in the ^{1}H NMR and IR spectra respectively was observed. In addition, a new singlet for the newly introduced N-methyl group was observed at 3.18 ppm in the ^{1}H NMR spectrum confirming the introduction of an *N*-methyl group, Figure 34c. Purity of analogue was 97%

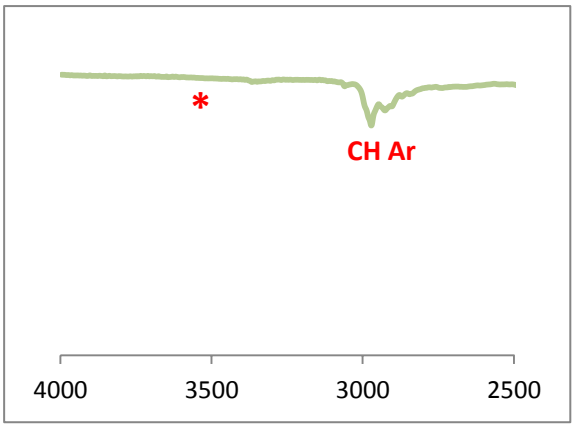

a

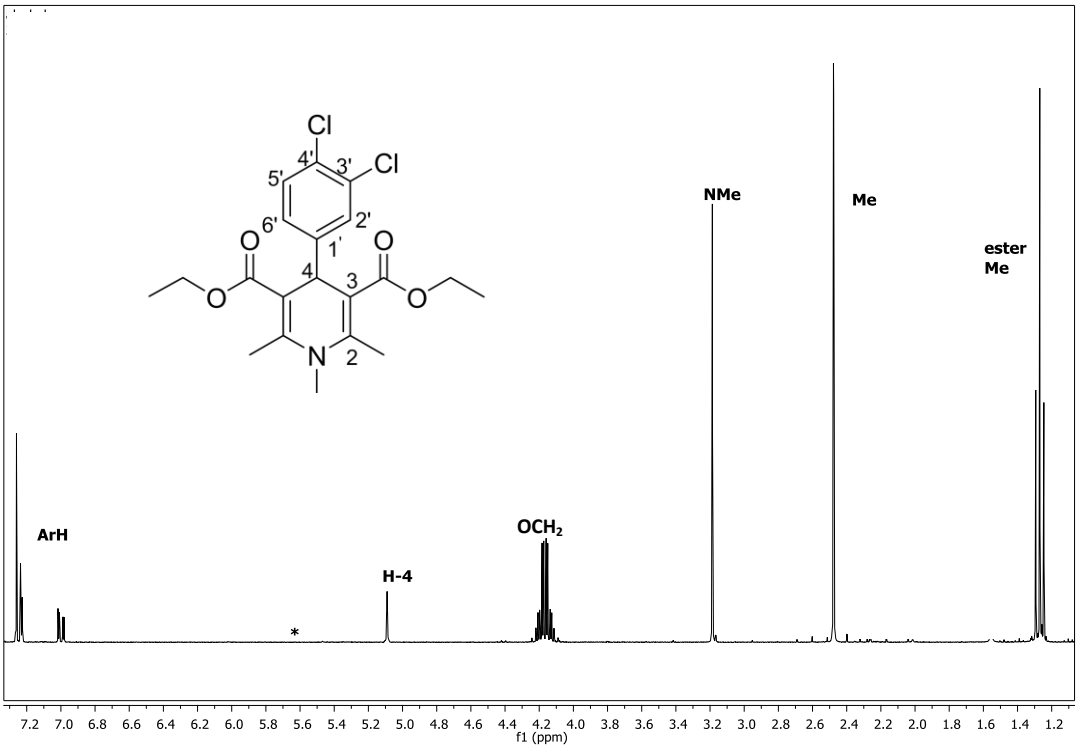

b

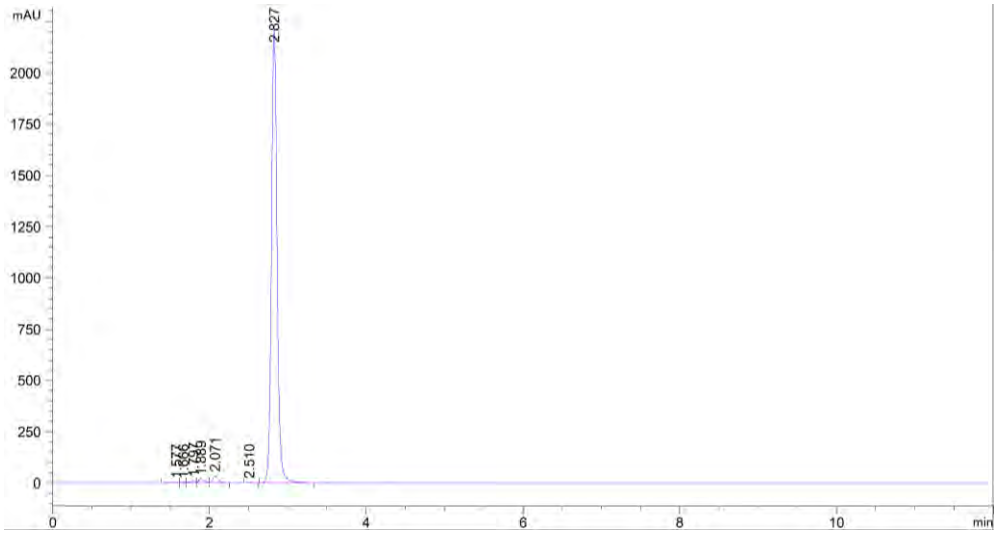

c

Figure 34: The a) IR, b)^{1}H NMR and c) the HPLC spectra for analogue **42**. The * illustrates the position of the NH peak in the starting material.

The 1,4-DHP benzyl esters (**29**-**38**)

The 1,4-DHP benzyl esters differed from alkyl counterparts only in the aromatic region of the spectra due to the additional, substituted phenyl group of the ester side chain in each case. As with the alkyl analogues each benzyl analogue revealed the same core set of NMR signals (^{1}H and ^{13}C) as described previously. The ^{1}H NMR spectra revealed an additional AB quartet for the diastereotopic benzyloxy methylene groups (OCH_2) also as a diagnostic part of the core signals as well as the relevant aromatic signals, depending on the substitution patterns introduced onto the aromatic ring. In the ^{13}C NMR spectra an additional core signal at 60.0 – 66.0 ppm for the benzyloxy methylene group (OCH_2) provided a marker for the successful synthesis of these analogues, and an additional four aromatic singlets were observed for the *para*-substituted analogues or six for the less symmetrical disubstituted rings. The ^{1}H NMR and ^{13}C NMR spectra for analogue **29** unsubstituted in the benzyloxy aromatic ring (X=H) in Figure 35 are shown to represent these features. Of note is the clear AB doublet pair for the diastereotopic benzyl hydrogens at around 5 ppm. The observed molecular mass of the dominant ion $[M+H]^+$ was found to be 522.1241, which was within acceptable limits of the molecular mass expected for the $[M+H]^+$ ion equal to 522.1239, Figure 35c.

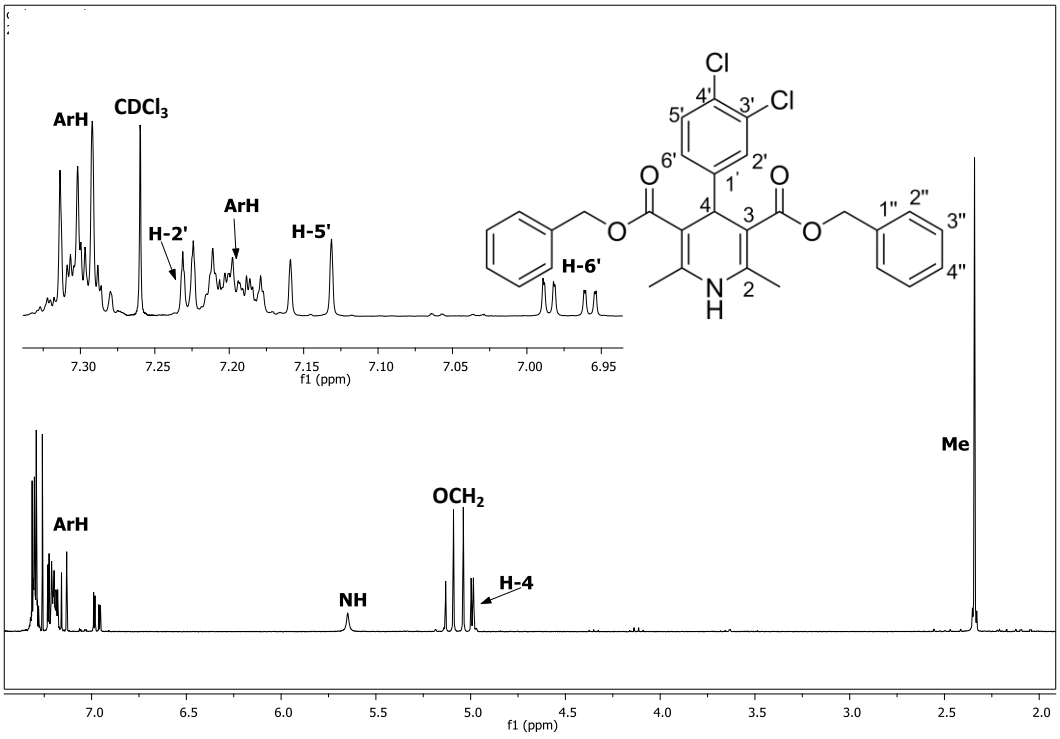

Figure 35a: The ^{1}H NMR spectrum of **29** in $CDCl_3$ as the prototype for the 1,4-DHP benzyl esters.

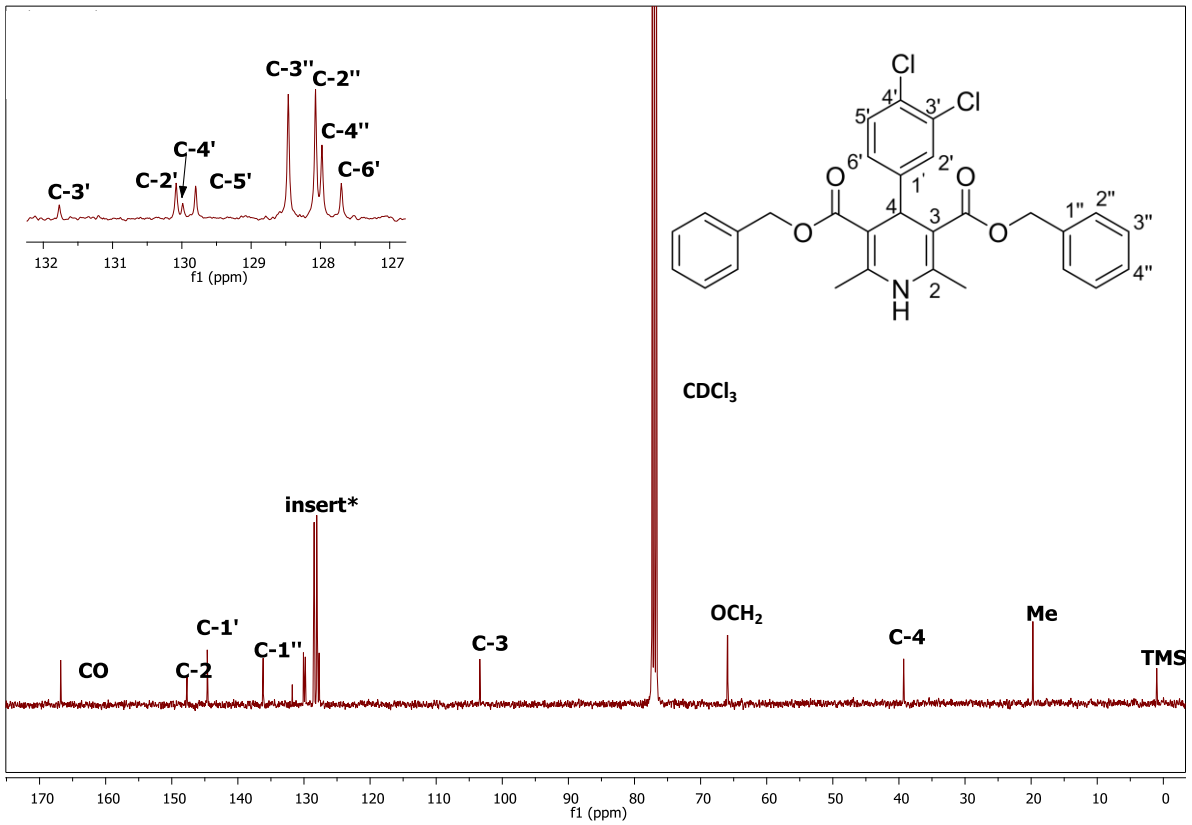

Figure 35b: The ^{13}C NMR for **29**.

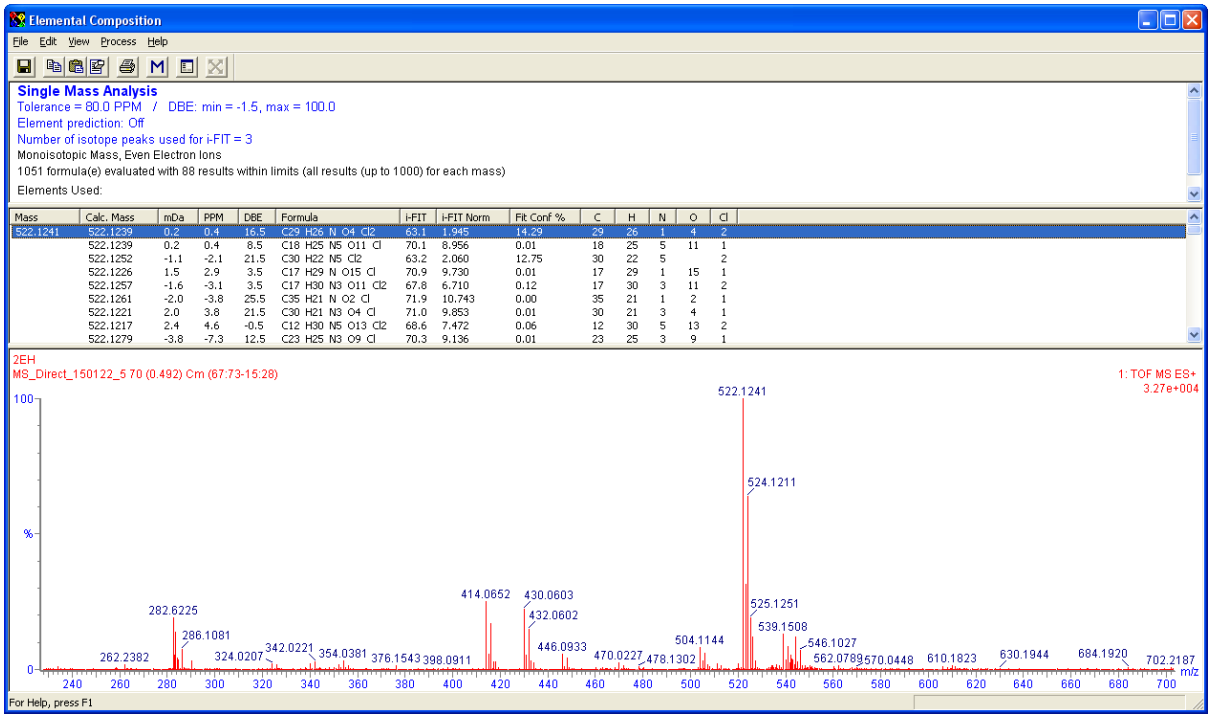

Figure 35c: The HRMS for **29**.

The unsymmetrical 1,4-DHP ester **41**

The use of an acetoacetate derivative in the multicomponent Hantzsch reaction results in a symmetrical product only. Differentiating the two esters of the dihydropyridine molecule disrupts C-2 symmetry resulting in the creation of a chiral centre at the C-4 methine carbon as a racemic product, and the effect of desymmetrizing the ring on biological activity was considered to be an interesting part of the study.

In order to access unsymmetrical derivatives two options were available. Either two different acetoacetates could be reacted (A and B, say), giving three different products as the two symmetrical derivatives (one from A and one from B) as well as the unsymmetrical derivative (A and B combined). Such a mixture would no doubt be difficult to separate into its components. Alternatively, one could do a targeted synthesis, which is more complicated but nevertheless is represented in the literature. Here, the two intermediates needed for the Michael addition would need to be synthesised in different flasks using each of the two acetoacetates, and thereafter condensed together to form the unsymmetrical product.[96, 112, 113] Ultimately, the latter option was adopted in which a mixture of *tert*-butyl acetoacetate, 3,4-dichlorobenzaldehyde and triethylamine (Et_3N) in ethanol was microwave irradiated for a minute in order to yield the enone intermediate, which resulted in a change in reaction colour from colourless to yellow and was observed as a yellow smudge on the TLC that was different in R_f to those of the starting materials. The product was not isolated as it was thought likely that the Knoevenagel condensation would occur. As usual a commercially available enamine (ethyl-3-aminocrotonate) together with a few drops of glacial acetic acid was then added to the reaction in order for the two intermediates to undergo Michael addition. Completion of the reaction as monitored by TLC occurred after 15 minutes, and the product was obtained in 36% yield after column chromatography. A blue fluorescence under Uv/vis (250 nm) typical of 1,4-dihydropyridines was visible on TLC. Scheme 6 below shows the overall reaction.

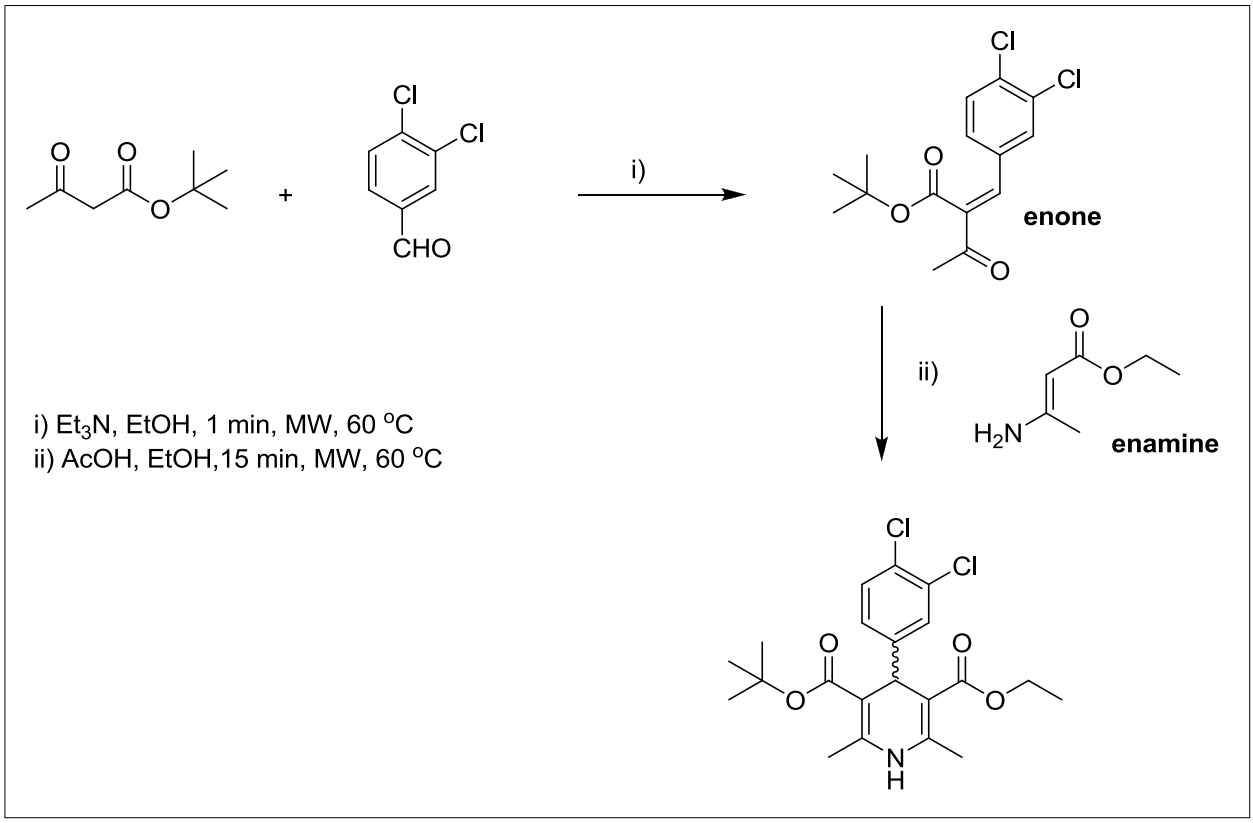

Scheme 6: The schematic diagram for the overall reaction for analogue **41**.

The asymmetric nature of the product now led to differences in the core signals in the NMR spectra compared to those of the symmetrical cases. Thus, the two methyl groups on the dihydropyridine ring appeared as two singlets rather than one in both ^{1}H and ^{13}C NMR spectra (2.32 ppm and 19.6 ppm for Me-6 as well as 2.30 ppm and 19.5 ppm for Me-2 respectively). Likewise, the ^{13}C NMR spectrum revealed the two ester carbonyl groups as different at 167 ppm ($CO_{t\text{-butyl}}$) and 166.5 ppm (CO_{ethyl}). The identity of the peaks was resolved using HSQC and COSY NMR spectra. Figure 36 shows the ^{1}H and ^{13}C NMR spectra for **41**. The molecule is now chiral (although racemic) but this cannot be ascertained directly from the NMR (NMR doesn't distinguish enantiomers), and as before diastereotopic methylene hydrogens were observed for the ethyl ester fragment.

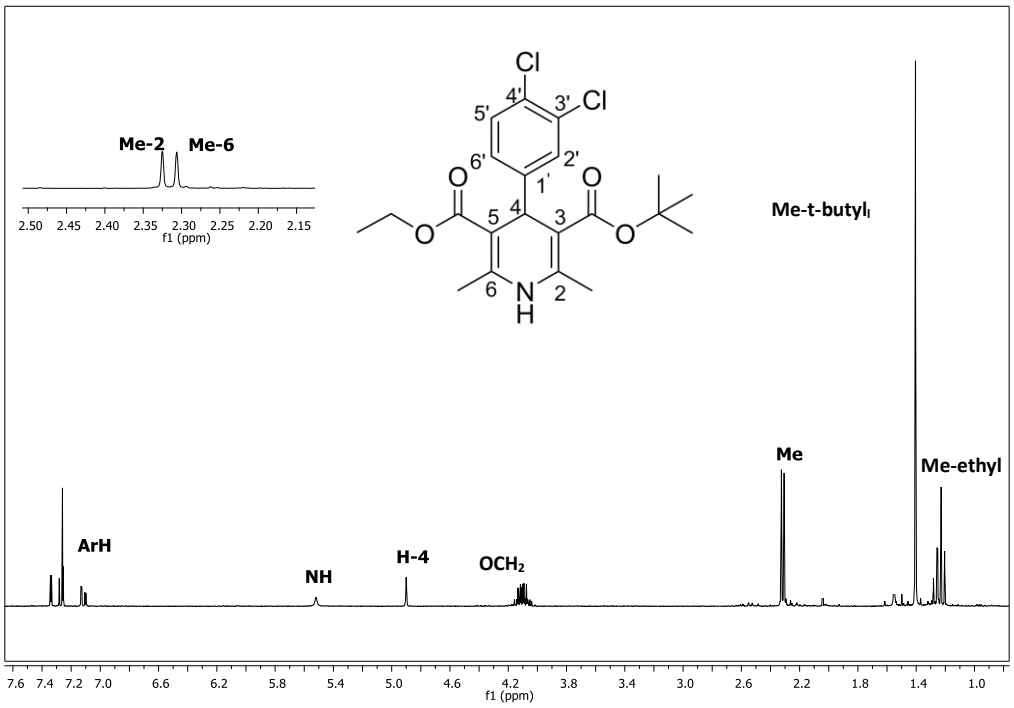

Figure 36a: The ^{1}H NMR for analogue **41**.

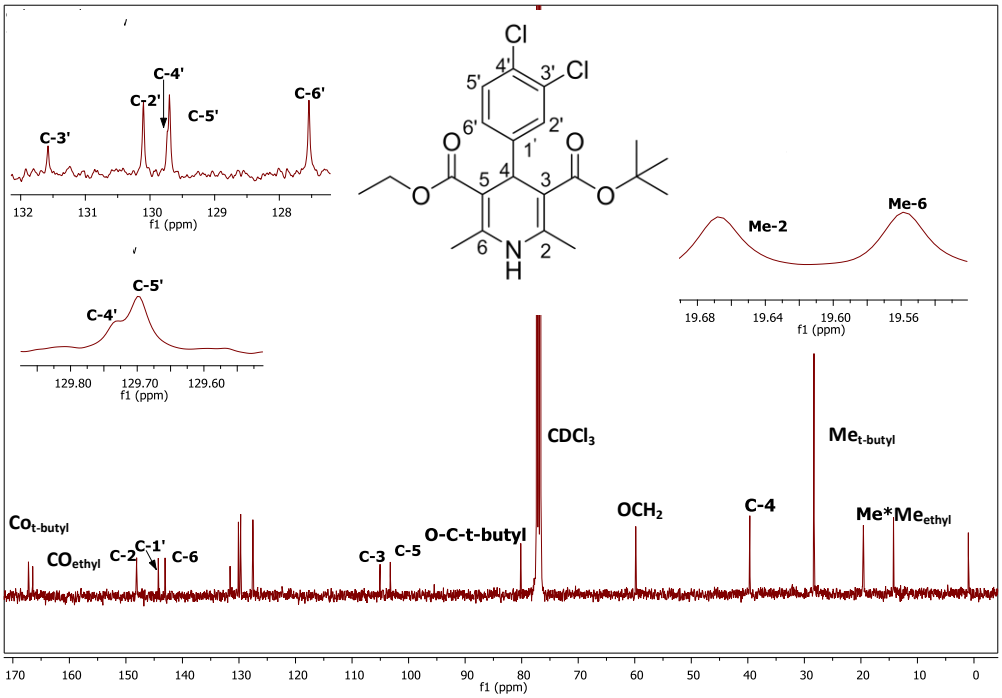

Figure 36b: The ^{13}C NMR spectra for analogue **41** * denotes the two methyl peaks.

Literature has revealed that a symmetrical dihydropyridine is one of the products (by-products) formed during the synthesis of an unsymmetrical dihydropyridine derived from preformed coupling partners (enone and enamine), themselves derived from different acetoacetate substrates.[94, 96, 113] Studies have proposed this to be due to a retro-Michael

addition involving an iminium ion in equilibrium with the enamine intermediate. This was observed in the synthesis of unsymmetrical dihydropyridine **41** (3-*tert*-butyl-5-ethyl-4-(3,4-dichlorophenyl))-2,6-dimethyl-1,4-dihydropyridine-3,5-dicarboxylate), in which the symmetrical dihydropyridine derivative **23** was also formed as a major by-product in 30% yield. Scheme 7 shows the mechanism for these two reactions involving the same intermediate.

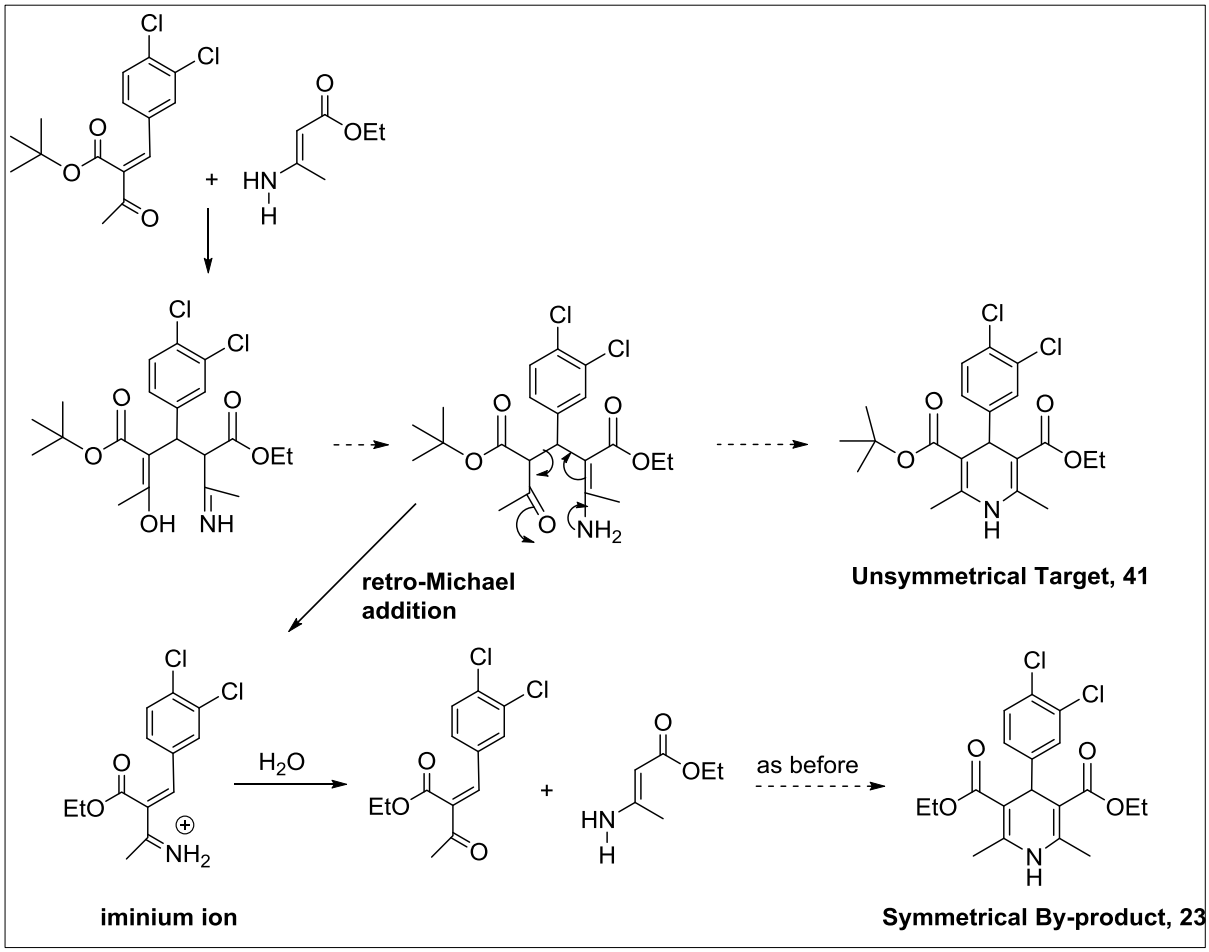

Scheme 7: The two mechanisms illustrating the formation of unsymmetrical and symmetrical 1,4-DHPs respectively during the modified Hantzsch synthesis of the unsymmetrical 1,4-DHP **41**.

2.5 Aromatization of the 1,4-DHP ring

As stated in Chapter 1 previously, one of the aims was to investigate the effect on biological activity of oxidising the Hantzsch 1,4-dihydropyridine intermediate to its corresponding pyridine derivative. Derivatives **A45**-**A48** were subjected to oxidation under heterogeneous conditions (chosen because of their experimental simplicity, their cost-effective, and environmentally safe nature as well as the availability of reagents). The reagent chosen,

developed by Zolfogol *et al*., involved using the inorganic oxidant oxone® (K_2SO_4. $KHSO_4$. $2KHSO_5$) in conjunction with sodium nitrite ($NaNO_2$). The latter acts as a strong electron acceptor, and is adsorbed onto wet silica (SiO_2 (50% *w*/*w*), which acts as a phase transfer catalyst and heterogeneous *in situ* surface area (for the generation of $NOKSO_5^-$).[114, 115]

Yields were moderately good (63-70%) the reactions proceeded relatively fast (1–2 hours), and the products could be separated easily by column chromatography, followed by recrystallisation to afford pure products. Table 5 illustrates the results.

Table 5: Oxidation of 1,4-dihydropyridines

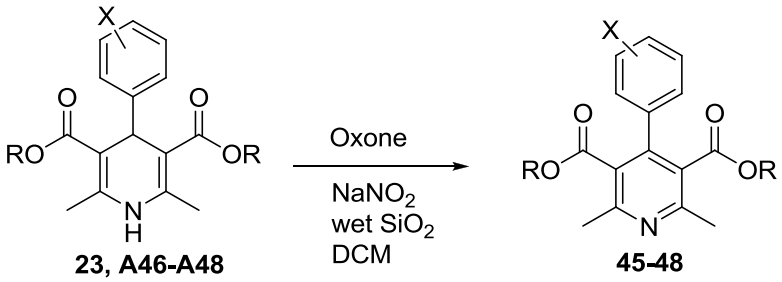

23, A46-A48 → **45-48**

Compound	R	X	Yield%
45	Et	3,4-Cl	70
46	Et	4-Cl-3-CF_3	66
47	Et	4-NO_2	69
48	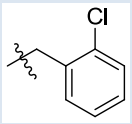	3,4-Cl	63

In addition, pyridine analogue **49** was inadvertently obtained under microwave conditions that were used during the target synthesis of Hantzsch analogue **29** (benzyl group) based on the disappearance of the NH and H-4 methine protons in the ^{1}H NMR spectrum of **29** at 5.50 ppm and 4.18 ppm. The cause of oxidation was not fully understood. The appearance of an N=C stretch at ~1500 cm^{-1} together with the absence of the NH peak at ~3500 cm^{-1} in the IR spectrum lent further support for the formation of the pyridine analogue. The appearance of three extra aromatic resonances for the pyridine ring in the ^{13}C NMR spectrum (notably, C-3 of **29** shifted from the alkene region (~103.0 ppm) into the aromatic region at 126.0

ppm to give seven aromatic quaternary carbon signals in total, one for the benzyl phenyl) provided confirmation that oxidation to the pyridine had taken place, Figure 37.

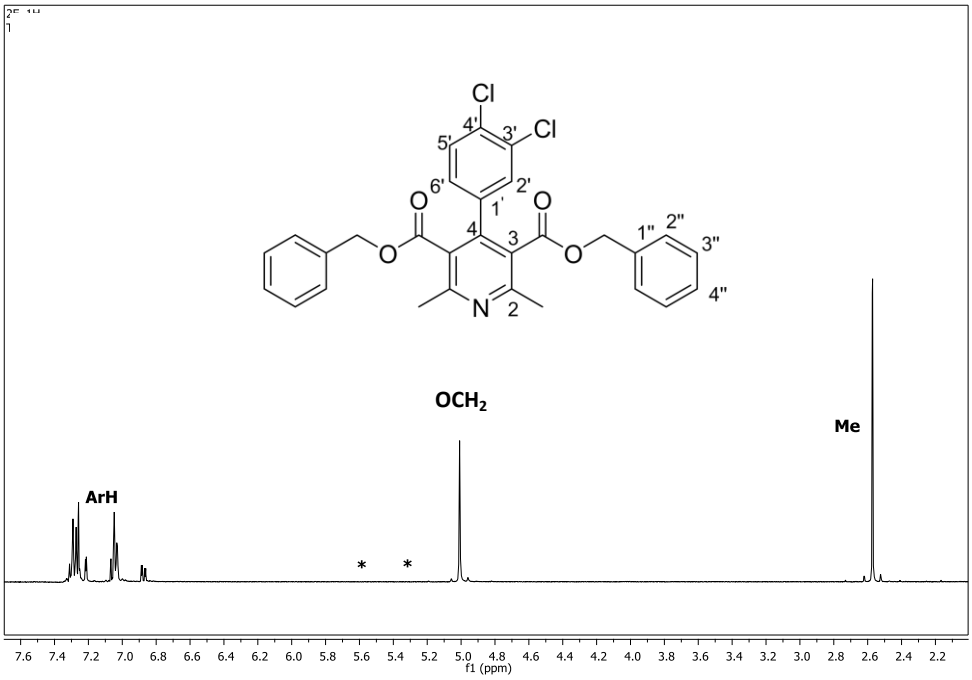

Figure 37a: The ^{1}H NMR spectrum of **49** as the oxidised product of **29**.*illustrates the position of the NH and H-4 peaks in the starting material.

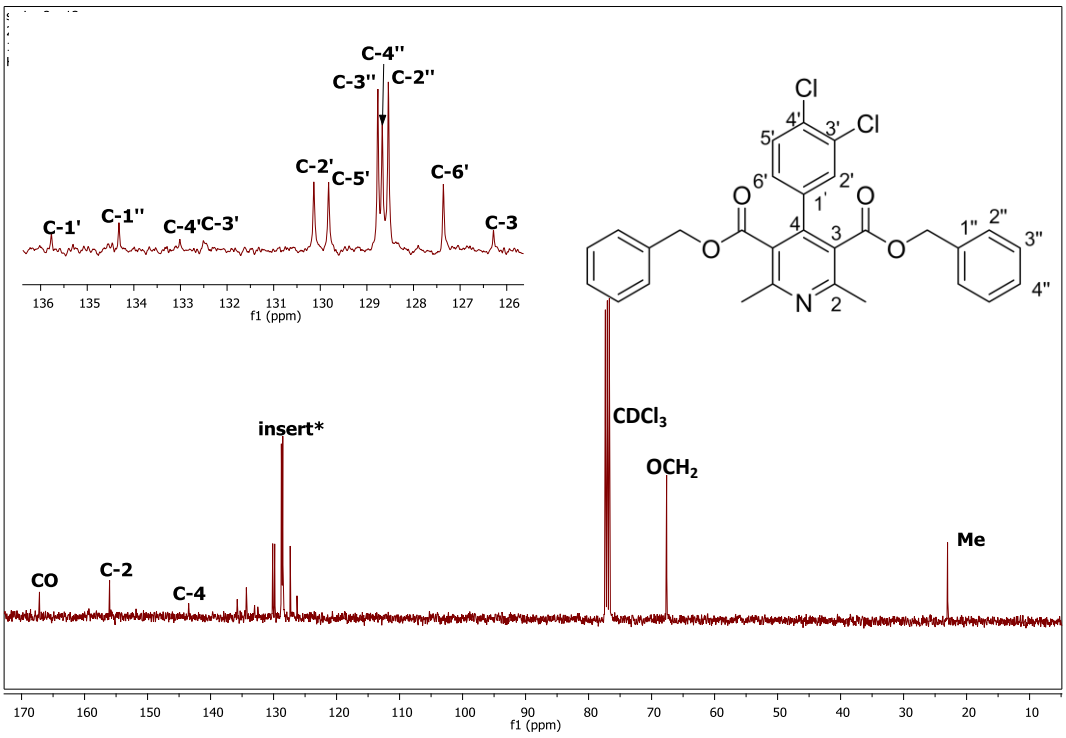

Figure 37b: The ^{13}C NMR spectrum of **49** in $CDCl_3$. Expanded **insert** spectrum showing the aromatic carbons including five of the seven quaternary carbon signals.

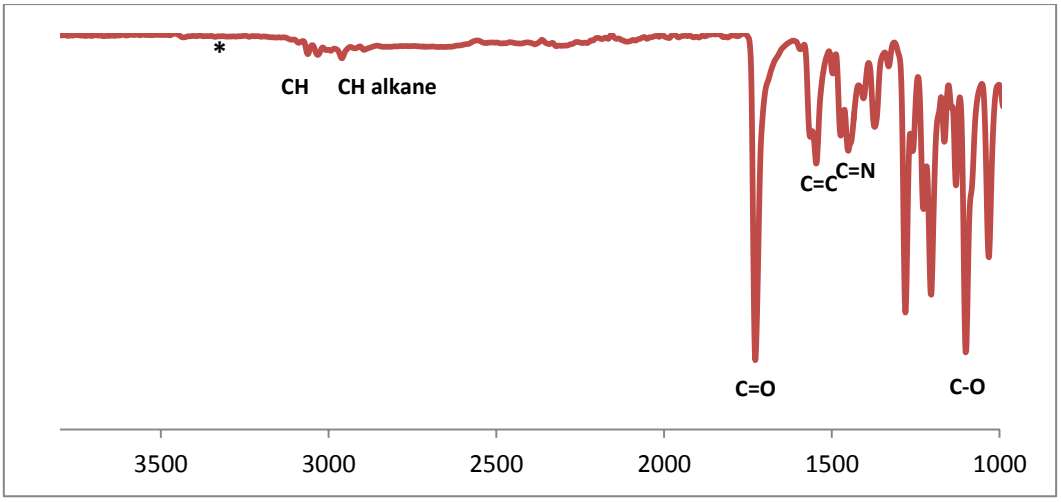

Figure 37c: The IR spectrum of 4**9** as an example of a pyridine analogue. * denotes the absence of the NH peak.

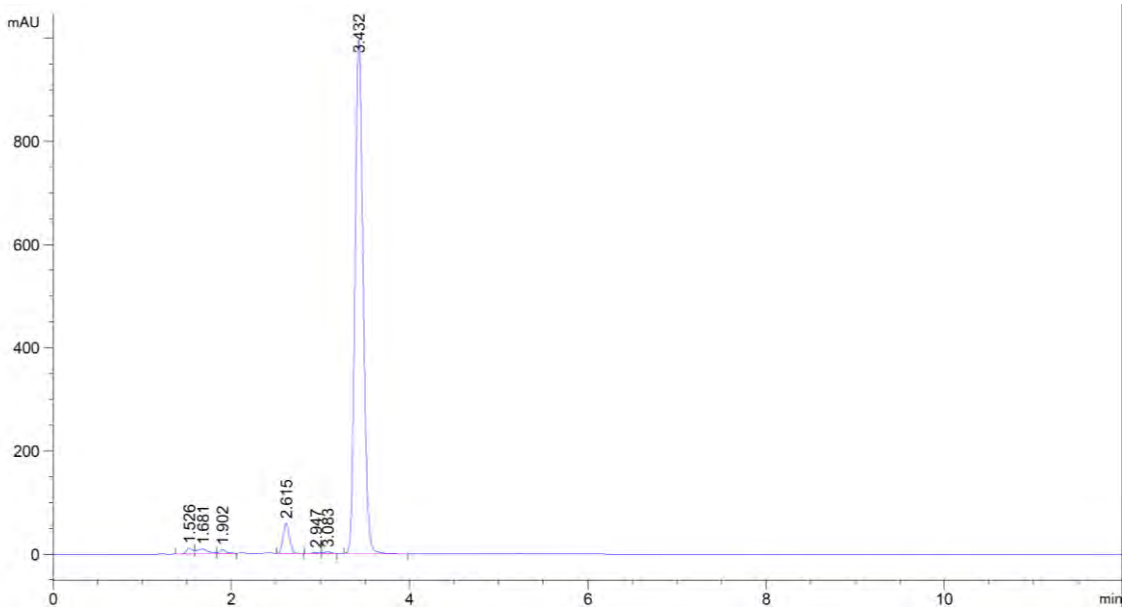

Figure 37d: The HPLC trace of analogue **49**. 95% purity

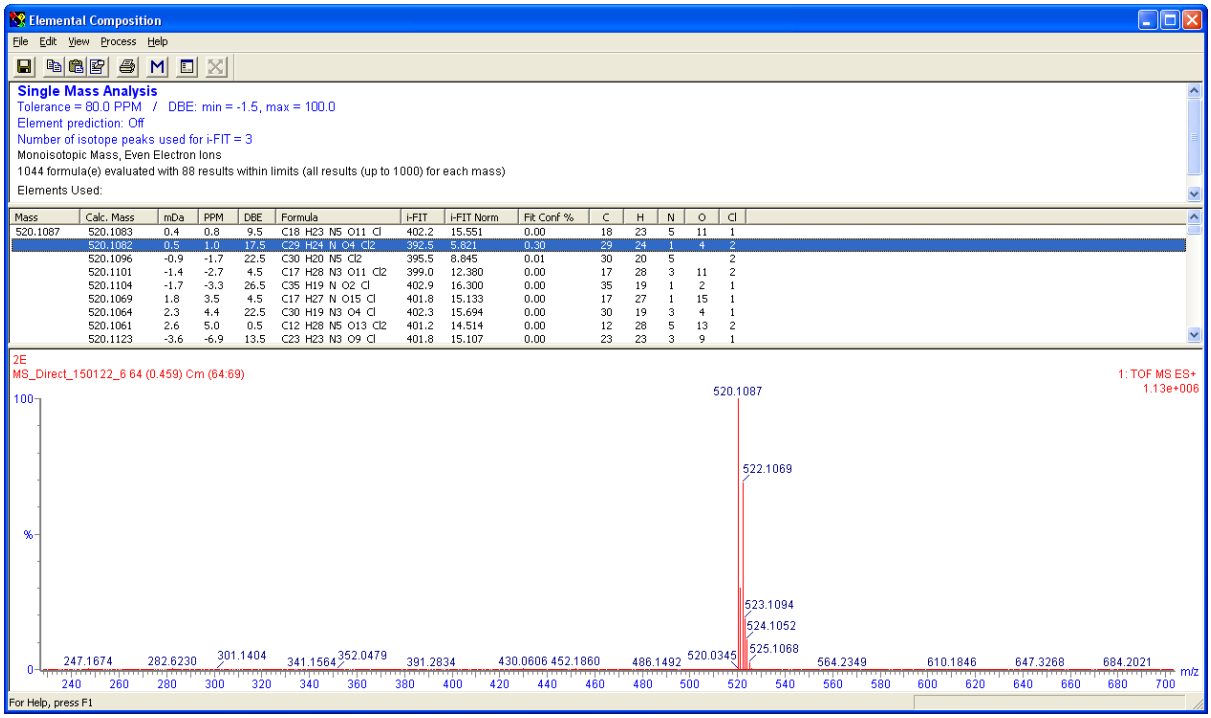

Figure 37e: The high-res mass spectrum of **49.** Expected m/z: $[M+H]^+$ 520.1082, observed$[M+H]^+$ 520.1087

In conclusion, the Hantzsch reaction was successfully used in the synthesis of a small library of 1,4-dihydropyridines containing novel ester side-chains. Microwave conditions gave the best results in which yields ranged from 51-98 % and in which a level of correlation between the type of ester and the yield could be identified. The acetoacetate esters were synthesized via transesterification of methyl acetoacetate with various alcohols using zinc iodide as catalyst. This expands on the type of ester grouping in the Hantzsch repertoire. The exception was in the synthesis of derivative **29** which oxidised to the pyridine **49**, although the Hantzsch derivative **29** could be obtained using a conventional heating. Oxidation to the pyridine derivative, though also of interest for biological evaluation, could be achieved routinely using oxidation with oxone on silica-gel. Following recrystallisation in triplicate, the Hantzsch products were analysed by HPLC and found to be >95% pure and thus of an acceptable purity for biological evaluation.

3. Inhibition of β-haematin formation and Parasite growth

3.1 Introduction

The emergence of parasite resistance to quinoline-based antimalarial drugs such as chloroquine has led to a need for new and effective drugs. For identification and development of these new scaffolds, the structure-activity model for chloroquine is a useful exemplar used for selection and synthesis of various analogues of other templates in order to explore structure activity relationships and to further develop them into potential haemozoin/β-haematin inhibitors.

Structure-activity relationships (SARs) attempt to find the structural features responsible for physico-chemical factors that contribute to the activity of a compound, for example, biological activity of a drug. A good SAR model helps in narrowing down the route leading to the most active analogue specific to a certain target. SAR can be qualitative as well as quantitative (QSAR). For the latter, certain free energy molecular descriptors such as Hammett constants, quantum mechanical and structural descriptors (for example polarizability of a compound, molar refractivity, Van der Waals volume, HOMO/LUMO energy) as well as other 2D descriptors such as molecular weight and logP are used to look for correlations with the IC_{50} values of a series of compounds.[86, 116] Thus analysis of such correlations yields a model which gives insight to the influences these factors have on activity. Correlation analyses between the IC_{50} values of the analogues synthesised in this work and molecular descriptors (calculated using MarvinSketch ChemAxon version 6.3.1)[117] described below were found to be significant:

i) Fraction of saturated (sp^3 hybridised) carbon atoms (Fsp^3):this describes the degree of saturation of the molecule by calculating the ratio of number of saturated carbon atoms in the molecule over the total number of carbon atoms. This is closely associated with solubility of the molecule.[118, 119]

ii) Molecular polarizability: this is a measure of the ability of a non-polar neutral molecule to be distorted after induction by a charged particle. It provides information about the drug-receptor interactions such as dispersion forces.[120, 121]

iii) Molecular refractivity: this describes the size and volume of the molecule.[121]

iv) Van der Waals volume: the actual volume of a molecule. It is important for understanding the biological compatibility of the compound which includes its ability to be absorbed and penetrate through membrane barriers and is closely associated with molecular refractivity.[122]

v) Molecular weight: the mass of the molecule. Likewise this is related to the ability of a molecule to diffuse through membranes to its target (or receptor) site.

vi) Logarithm of the partition coefficient (logP): a measure of lipophilicity of a molecule. This indicates the relative solubility of a drug in a lipid membrane. Positive values of this constant indicate that the substance is hydrophobic while negative values indicate hydrophilicity of the molecule.

3.2 Measurement of β-haematin formation

The *in vitro* β-haematin inhibition assay was performed in 96-well plates using the method described by Carter et al.[99] The method makes use of a non-ionic lipophilic detergent known as Nonidet P-40 (NP-40) to mimick the role of neutral lipid bodies inside the parasite digestive food vacoule associated with promoting haemozoin formation. The use of neutral lipid droplets in high-throughput screening is time consuming and requires expensive materials hence their use is unfeasible. The detergent is believed to have the ability of aligning free haem at the micelle-water interface. Its hydrophobic side chain facilitates an ordered packing, assisting in π-stacking of haem porphryin groups, hence promoting β-haematin formation. The detergent assay significantly reduces the analysis time to about 5 hours, whilst also being user-friendly and requiring less expensive materials. The structure of NP-40 is shown in Figure 38 below. Modifications and validation of the method previously used in high-throughput screening has been reported previously.[90]

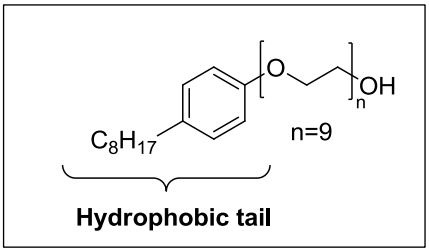

Figure 38: The structure of the NP-40 detergent showing the hydrophobic tail that is believed to assist in π-stacking with haem vinyl groups therefore promoting crystallisation to β-haematin. [91]

Addition of acetate buffer (pH 4.8 ± 0.1) initiates the β-haematin crystallisation process. Assay analysis was achieved using the colourimetric pyridine-ferrichrome method developed by Ncokazi and Egan.[123] The method determines the IC_{50} value of the inhibitor by measuring the percentage of free haematin in the haematin/ β-haematin mixture. It involves detecting non-crystallised haematin by selectively coordinating it with pyridine present in a 5% (v/v) pyridine solution (pH 7.4). The strong field pyridine ligand displaces the axial water ligands coordinated to the iron (Fe(III)) centre of free haematin, forming a monomeric low-spin, bis-pyridine complex (pyridine$_2$-Fe(III)PPIX) with haematin without affecting β-haematin, Figure 39. The complex has an intense orange colour.

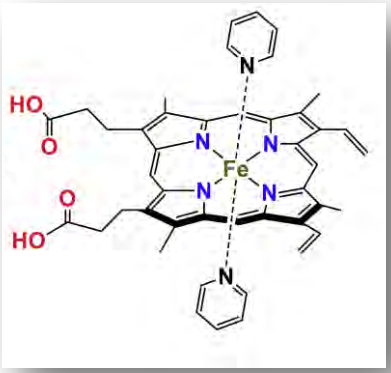

Figure 39: The low-spin pyridine$_2$-Fe(III)PPIX complex.[91] Reprinted from International Journal for Parasitology-Drugs and Drug Resistance, Vol 4, Sandlin, Rebecca D. Fong, Kim Y. Wicht, Kathryn J. Carrell, Holly M. Egan, Timothy J. Wright, David W., The role of antimalarial treatment in the elimination of malaria, 316-325., Copyright (2014), with permission from Elsevier

The intense absorption peak at 405 nm is used to produce a concentration dependent inhibition curve which is then fitted to a sigmoidal dose response equation using non-linear least squares fitting in Graph Prism v3.02.[124] This is in the form of a plot of absorbance at

405 nm against the log of the inhibitor concentration. The IC_{50} value for the analogue is then found. Figure 40 shows a dose-response curve of analogue **23** as a typical example.

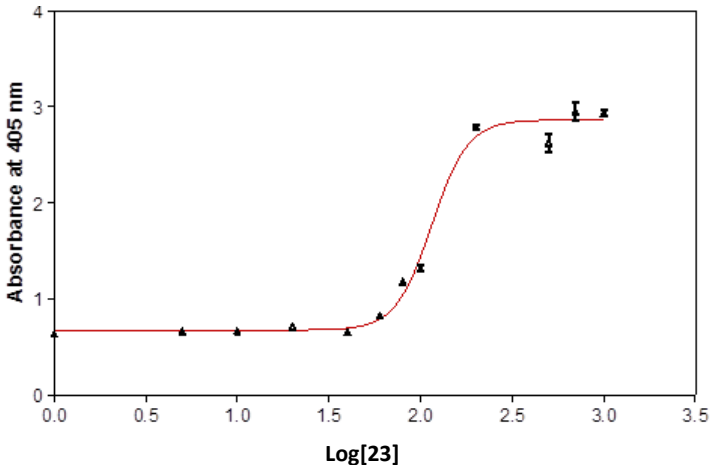

Figure 40: The sigmoidal dose response curve for analogue **23**

The β-haematin formation inhibitor amodiaquine, was used as a positive control to validate the use of the NP-40 detergent assay for screening of compounds. The IC_{50} for the drug was found to be 18 µM in good agreement with the IC_{50} of 21.0 µM obtained using the same positive control in a 384-well plate reported by Sandlin et.al.[90] Following validation, serial dilutions of different analogues in 96-well plates were then performed in order to determine their IC_{50}s. These data were then used in structure activity relationship studies.

3.3 Structure activity relationships for β-haematin inhibition

3.3.1 Series 1: Variation of the ester component (R and R').

Series 1 consisted of twenty-one compounds in which the side chains of the ester (or in one case a ketone) groups were varied, Figure 41.

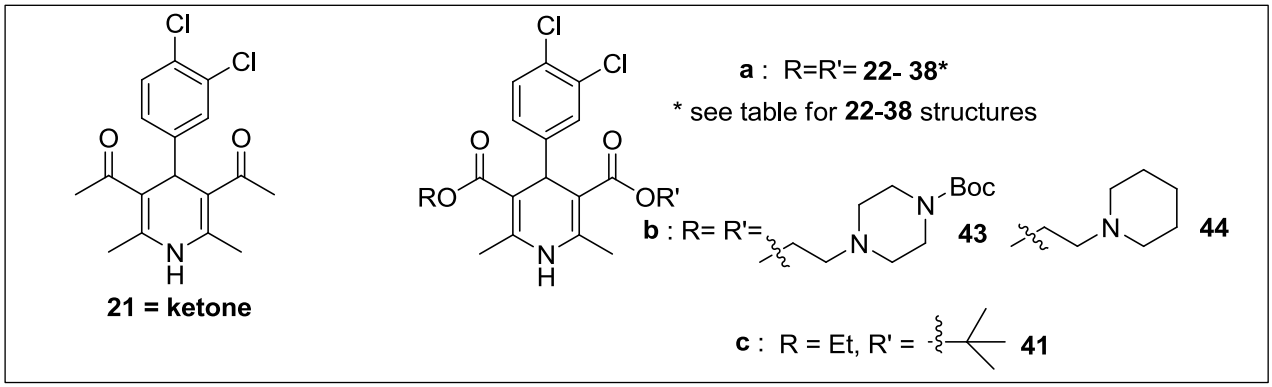

Figure 41: 1,4-dihydropyridine ester (or ketone) compounds tested.

a) Compound **21** and the alkyl and benzyl substituents

The IC_{50} values for the β-haematin inhibition assay for **21** and the alkyl analogues are shown in Table 7 below.

Table 7: The β-haematin inhibition IC_{50} values for the alkyl derivatives

Analogue	R=R'	IC_{50} (µM)	logIC_{50} (µM)
21	**N/A**	>2000	inactive
22		350±14	2.54±0.04
23		115±3.9	2.06±0.01
24	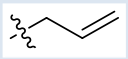	66±6.2	1.82±0.04
25		38±2	1.56±0.03
26		59±5.1	1.77±0.04
27		82±4	1.91±0.02
28		70±5	1.85±0.03

The derivatives showed no direct correlation between the logIC_{50} for inhibition of β-haematin formation (LogβIC_{50}) and any of the free energy parameters. However it was observed that a shift to larger alkyl groups increased the activity of the compound probably indicating the influence of hydrophobicity (log P) on activity. The isopropyl analogue exhibited the best activity, see table 8.

Table 8: The β-haematin inhibition activity of alkyl analogues in an ascending order.

Structure		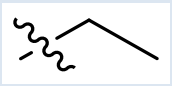	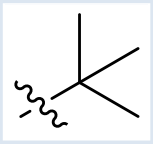	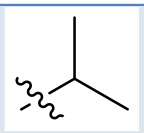
Analogue	**22**	**23**	**26**	**25**
IC_{50} (µM)	350±14	115±3.9	59±5	38±2
LogP	3.08	3.8	5.19	4.63

For the benzyl series multiple correlation analysis revealed a statistically significant correlation at the 95% confidence level between LogβIC_{50} and Log P together with one of several constants (Table 10). In all cases it was observed that increasing the hydrophobicity of the compound resulted in a decrease in IC_{50} thus leading to a more active analogue. The presence of groups that have more saturated (sp^3) carbon atoms and lower molecular weight also contributed positively to the activity against β-haematin formation of the 1,4-dihydropyridine benzyl esters. Table 9 shows the IC_{50} values for this series.

Table 9: The β-haematin inhibition IC_{50} values for the benzyl series.

Analogue	**R=R'**	**IC_{50} (µM)**	**logIC_{50} (µM)**	**Analogue**	**R=R'**	**IC_{50} (µM)**	**logIC_{50} (µM)**
29	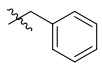	80954	4.91	**34**	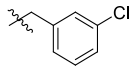	54±4.6	1.73±0.04
30	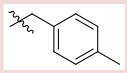	76±5.3	1.88±0.03	**35**		25±2	1.40±0.04
31	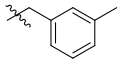	57±2.7	1.76±0.02	**36**	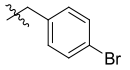	51±4.5	1.71±0.04
32	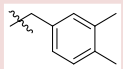	30±2.8	1.48±0.04	**37**	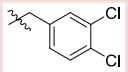	62±3.9	1.79±0.03
33	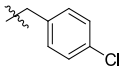	57±3.1	1.76±0.02	**38**	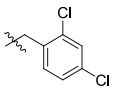	58±3.0	1.76±0.02

Table 10: Summary of multiple correlation results for the benzyl derivatives

QSAR model	Parameter	Coefficient	Log P coefficient	R-squared	F-value	F-critical at 95% interval
1	Fsp^3	-5.39	-1.12	0.64	6.13	4.74
2	Mr	0.00674	-1.53	0.64	6.31	4.74
3	Van der vaals volume (Å³)	0.00355	-1.22	0.6	5.2	4.74

In spite of the statistical significance on these correlations (Table 10), a two-tailed t-test on each individual parameter revealed that only Log P correlated with the IC_{50} at the 90 % confidence level. The other parameters correlated only at the 80 and 75 % levels (Table 11). Other parameters such as the Fsp^3, molecular weight and van der Waals volume, might also contribute to the activity although this is even less certain based on statistical confidence levels. Table 11 shows a summary for the t-test results.

Table 11: Summary of t-test results.

QSAR model	Parameter	t-test value	Log P t-test value	t-critical and confidence level for parameter	t-critical and confidence level Log P
1	Fsp^3	0.85	3.36	0.711 (75%)	3.00 (99%)
2	Mr	0.933	2.81	0.896 (80%)	2.37 (98%)
3	Van der vaals volume (Å³)	0.127	1.57	insignificant	1.45 (90%)

An attempt to combine the two ester groups for QSAR analysis was unsuccessful, since no correlations could be found.

b) Analogues containing an N-heterocycle in the ester side chain

Table 12 shows the β-haematin inhibition results for analogues **43** and **44** selected to study the possible effect of pH trapping. Unfortunately attachment of a N-heterocyclic group on the molecule abolished β-haematin inhibition activity.

Table 12: β-haematin inhibition IC_{50} values for N-heterocycle analogues.

Compound	IC_{50} (µM)
43	>2000
44	>2000

c) Effect of removing symmetry

In order to test the effect if any of changing from achiral to chiral analogues on β-haematin formation, the asymmetrical analogue **41** was compared to the two symmetrical compounds (**23** and **26**) possessing the two esters found in **41**. The results are in the table 13 below

Table 13: Results for analogue **41**

Compound	IC_{50} (µM)
23	115±3.9
26	59±5.1
41	74±4

The results showed some improvement in activity for **41** compared to **23** and reduction with respect to **26** indicating little or no obvious influence of chirality on inhibition of β-haematin formation.

3.3.2 Series 2: Variations on the R'' group

The results for the four analogues selected to study functional group influences at the 2 and 6 positions (R'') on the dihydropyridine are shown in Table 14.

Table 14: The SAR study for the 1,4-DHP analogues in which R'' was varied

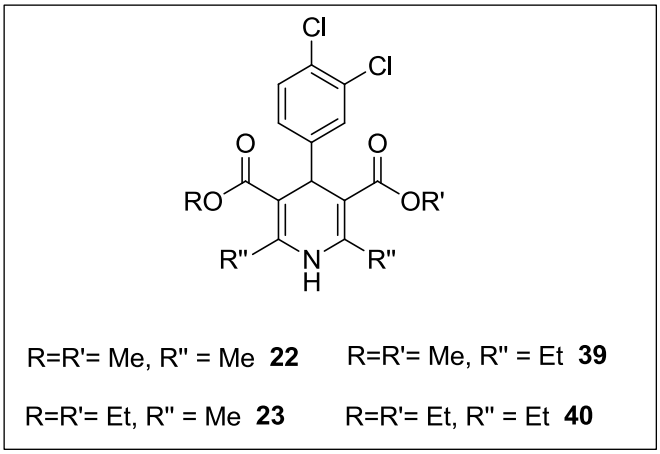

Compound	IC_{50} (μM)
22	350±14
23	115±3.9
39	87±6.8
40	74±3.1

The presence of the ethyl group at R'' position decreases the IC_{50} value in analogues **39** and **40** improving activity of these analogues relative to their methyl analogues **22** and **23**. This also fits with the idea that increasing logP improves activity.

3.3.3 Series 3: The importance of the NH group on the dihydropyridine ring

In contrast to **23**, **42** was found to be inactive (Table 15) indicating that hydrogen bond donor ability of the nitrogen atom is probably crucial to β-haematin inhibition activity. Loss of this interaction by attachment of the methyl group is most likely the cause of loss of β-haematin formation inhibition inactivity of the analogue. A steric effect cannot, however, be excluded.

Table 15: β-haematin inhibition IC_{50} results for evaluating possible H-bond donor influences on activity.

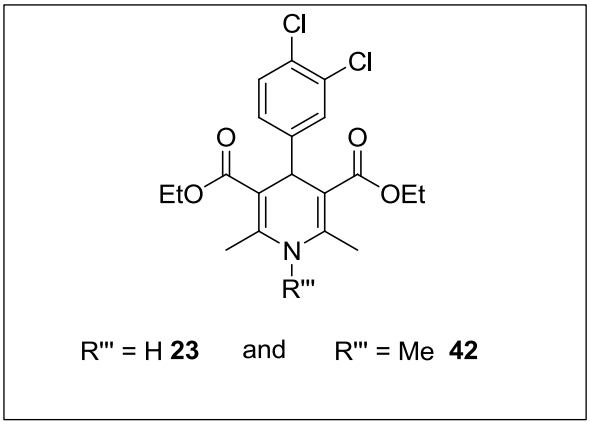

Compound	IC_{50} (µM)
23	115±3.9
42	>2000

3.3.4 Series 4: Effect of oxidation to a pyridine

It was hypothesised that moving from a dihydropyrdine to the aromatic pyridine ring will increase π-π stacking interactions and thus improve activity. However, the β-haematin inhibition results rather displayed the opposite trend. All five oxidised analogues (Figure 42) exhibited >800 µM IC_{50} values thus indicating no potency against β-haematin formation. These results support the hypothesis that hydrogen bonding of the NH group is crucial for activity. Loss of the hydrogen atom by oxidation removes H-bond donor ability of the compound.

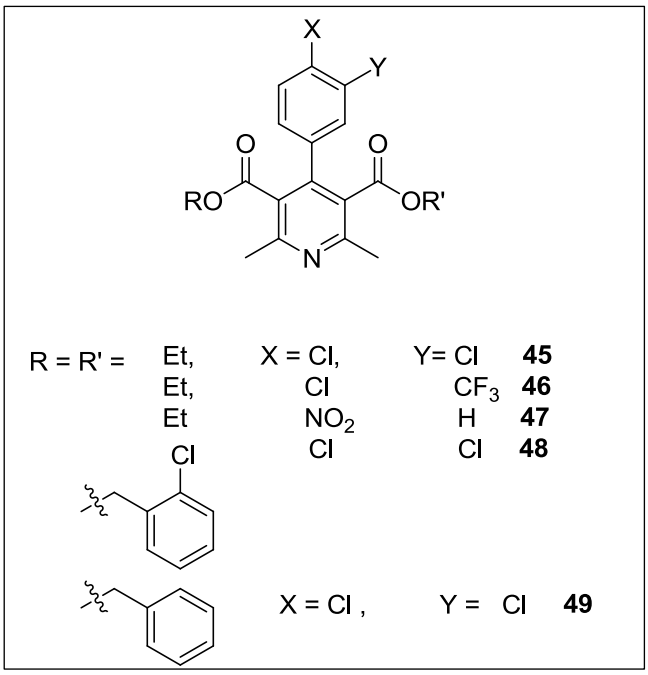

Figure 42: The 1,4-pyridine compounds tested against β-haematin formation. All were inactive.

3.4 Measurement of parasite growth inhibition

The *in vitro* antiplasmodial activity testing for the 1,4-DHP series was performed by the University of Cape Town Health Sciences Faculty, Division of Pharmacology, using a method previously reported by Zishiri et al.[125] The method used to test the compounds against the asexual RBC stages of a *P. falciparum* chloroquine sensitive strain (NF54).[126] The lactate dehydrogenase assay of Makler et al. was used for quantitative assessment of the antiplasmodial activity of each inhibitor.[127] The antimalarial drugs chloroquine and artesunate were used as controls for the experiments.

3.5 Structure activity relationships for *in vitro* antimalarial activity

3.5.1 Series 1: Variation in the ester group.

a) Compound **21** and the alkyl and benzyl series

The antiplasmodium IC_{50} values for **21** and the alkyl compounds are reported in Table 16.

Table 16: The results of the *in vitro* antimalarial assay for **21** and the 1,4-DHP alkyl esters.

Analogue	R=R'	IC_{50} (µM)	$logIC_{50}$ (µM)
21	**N/A**	5.2±1.7	0.7±0.1
22		2.8±0.5	0.45±0.08
23		2.8*	0.45
24	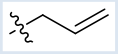	2.0±0.5	0.3±0.1
25		0.5±0.1	(-0.30)±0.09
26		1.7±0.1	0.23±0.09
27		3.9±0.9	0.6±0.1
28		1.0±0.4	0.02±0.17

*Denotes single determination

It was hypothesised that activity might correlate with logP, but the correlation was poor (Figure 43a). However, **21**, **25** and **27** looked like they may represent outliers and when omitted a good correlation was obtained (Figure 43b) and conformed to equation **3.4.1**.

Using single linear correlation analysis, $logIC_{50}$ was found to correlate with logP (r^2 = 0.94). The correlation yielded an empirical equation **3.4.1**

$$LogIC_{50}= -7.91\mathbf{logP} + 7.11\ldots\ldots \text{ eq}(\mathbf{3.4.1})$$

The analysis revealed that parasite growth inhibition activity increases with an increase in hydrophobicity of the compound. Hydrophobicity allows for membrane solubility and also promotes interaction with haem, which is also hydrophobic.[101, 128-130]

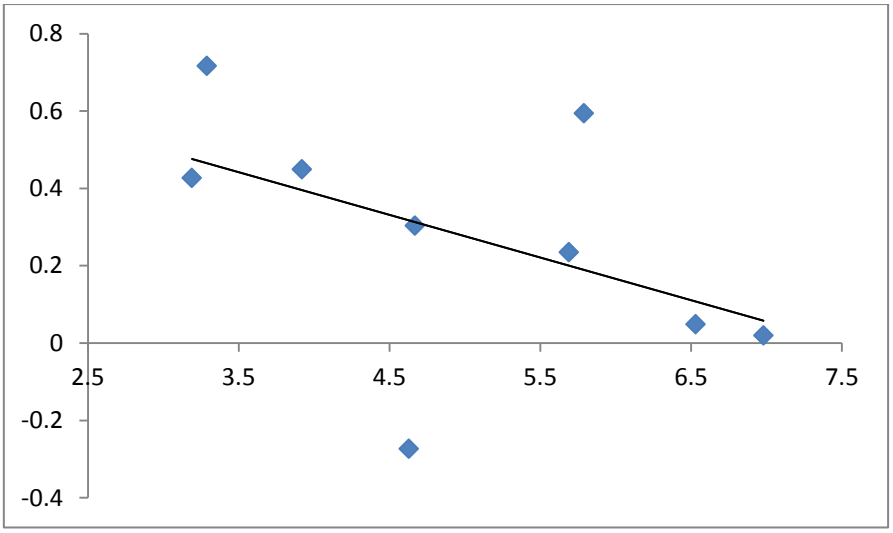

Figure 43a: The linear regression plot of $logIC_{50}$ vs logP for 1,4-DHP alkyl esters (including **21**, **25** and **27**). Empirical equation: $LogIC_{50}$= -0.110**logP** + 0.828 (r^2 = 0.24)

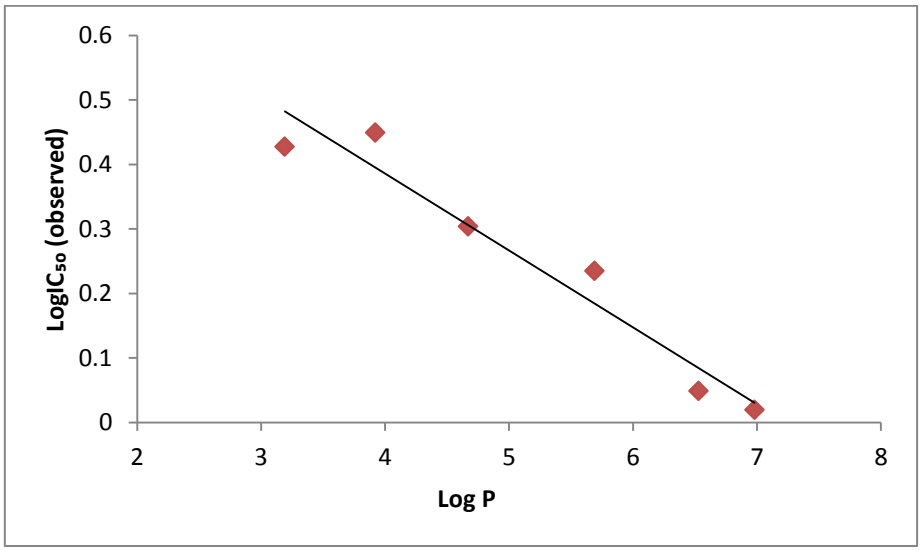

Figure 43b: The linear regression plot of $logIC_{50}$ vs logP for 1,4-DHP alkyl esters (excluding **21**, **25** and **27**). LogP is inversely proportional to antiplasmodium activity.

At the 95% confidence level, multiple linear regression analysis for the benzyl substituents (see Table 17 for the IC_{50} values) revealed a correlation between the $logIC_{50}$ value of the compound with Fsp^3 and molecular weight of the analogues (r^2= 0.64)

Empirical equation: Log IC_{50} = 0.0065**Mr** + 8.07**Fsp^3**- 4.78 …..eq (**3.4.2**)

The observations suggested that analogues with high molecular weight and possessing more saturated carbon atoms possess increased IC_{50} values leading to a decrease in activity of the analogues. Small molecules tend to be more drug-like than large molecules due to their

small surface areas required for diffusion through membranes to access their specific target sites. This has been seen for many haemozoin formation inhibiting antimalarial drugs.[128, 130-132] The empirical equation (**3.5.2**) which was determined using the overall $F_{2,7}$ distribution with the critical *F*-value of 4.74 (F= 6.38 > $F_{2,7}$ = 4.74), is statistically significant at the 95% confidence level. Looking at the coefficient values in the equation, it is observed that degree of saturation of analogues has more influence on activity than molecular weight, signifying that π-stacking interactions may be of greater importance. Molecules that are unsaturated have a greater number of conjugated electrons (π-electrons) therefore increasing strength of association between the inhibitor and the haem porphyrin ring which promotes inhibition of haemozoin formation. [101] A two-tailed t-test done on individual parameters (t = 3.22 (**Mr**), 2.78 (**Fsp^3**) > t_{crit} = 2.45) showed that both Mr and Fsp^3 correlated significantly with logIC_{50} at the 98% confidence level. Figure 44 is a multiple linear regression plot of predicted against observed IC_{50} of the 1,4-dihydropyridine benzyl ester analogues.

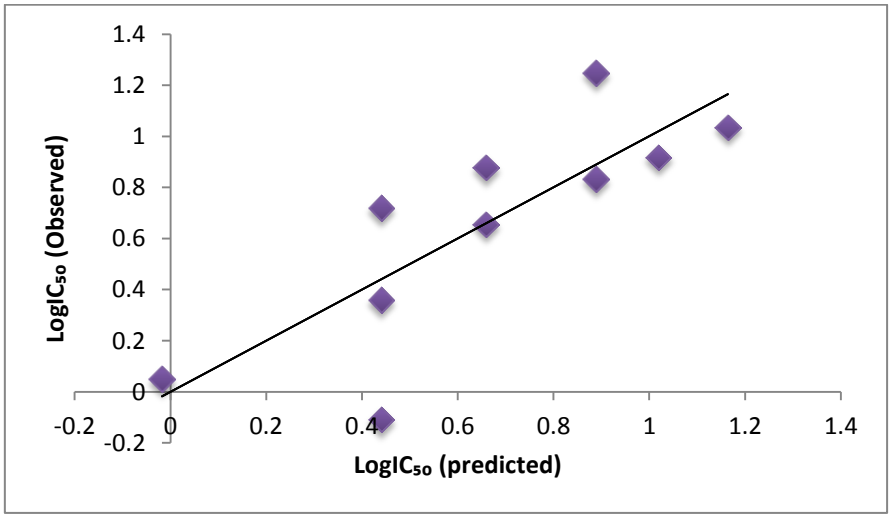

Figure 44: The linear regression plot of observed vs predicted logIC_{50} for antiplasmodium activity of 1,4-DHP benzyl ester compounds. The plot displays a positive linear correlation of parasite growth inhibition (logIC_{50}) with **Mr** and **Fsp^3** (r^2 = 0.64).

Table 17: The results of the *in vitro* antimalarial assay for the 1,4-DHP benzyl esters.

Analogue	R=R'	IC_{50} (μM)	$logIC_{50}$ (μM)	Analogue	R=R'	IC_{50} (μM)	$logIC_{50}$ (μM)
29	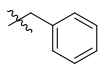	1.1±0.1	0.05±0.04	**34**	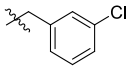	2.3±0.3	0.36±0.06
30	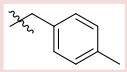	7.5±2.6	0.88±0.2	**35**		0.8±0.2	(-0.1)±0.1
31	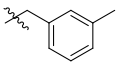	4.5±0.5	0.65±0.05	**36**	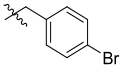	8.3±0.8	0.92±0.04
32	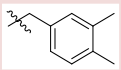	11±0.7	1.04±0.03	**37**	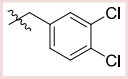	18±4.9	1.3±0.1
33	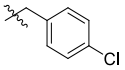	5.2±0.9	0.72±0.08	**38**	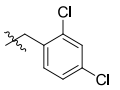	6.8±0.6	0.83±0.04

The antiplasmodium activity of a compound appears to be greatly reduced when it is a disubstituted benzyl analogue. For mono substituted analogues, a greater reduction of activity occurs for *para* substituents than the *ortho* and *meta* cases. Except for **37** electron-withdrawing substituents led to greater activity. This is in agreement with the hypothesis that electron-releasing substituents increase electron density in the aromatic ring weakening the π-π stacking interactions of the compound with the haem macrocycle.

b) Analogues containing an N-heterocycle in the ester side chain

It was hypothesised that introducing a second amine group on the 1,4-DHP molecule would increase basicity of the molecule therefore resulting in pH trapping inside the parasite digestive vacuole. The presence of a tertiary amine in the molecule can permit penetration across the cell membrane into the acidic food vacuole where it is protonated resulting in accumulation of charged species and consequent inhibition of the haem detoxifiction pathway. The results for the two analogues selected for studying this phenomenon are shown in Table 18 below.

Table 18: Parasite growth inhibition results for compounds **43** and **44.**

Compound	IC_{50} (µM)	VAR	LAR	Log P
43	0.680±0.01	17783	2.43	4.62
44	3.9±0.6	2.83	4.58	4.82

Compound **43** showed fairly strong activity while **44** showed only very weak activity. The weak antiplasmodium activity of compound **44** may be primary because of the lack of β-haematin inhibiting activity. It may also be caused by the absence of the second nitrogen atom of the piperazine ring which increases its lipophilicity. This also increases its solubilty in membranes more than in aqueous solution leading to poor accumulation in the digestive vacuole as seen by the vacuolar accumulation ratio (VAR). The ratio is predicted using the Henderson-Hasselbalch equation which uses the distribution coefficient (logD) to calculate the lipophilicity of an ionised compound at various pH values assuming that drug diffuses across membranes without assistance of transporters (see experimental section for the equation of both VAR and lipid accumulation ratio (LAR)).[131, 133-135] Calculations predicted that **43** would accumulate in the food vacuole 125 times more than **44.** Although this compound exhibited very poor β-haematin inhibition activity, its activity could possibly still be attributed to weak β-haematin inhibition combined with the great digestive vacuole accumulation resulting in inhibition of haemozoin at higher concentrations compared to **44**. However, since both analogues exhibited no β-haematin inhibition at the highest concentration that could be tested, this could not be confirmed and their activity may also be ascribed to a different mechanism of action (which nonetheless involves pH trapping), or alternatively the NP-40 assay does not adequately mimic the effect of lipids in the case of these specific derivatives.

c) Effects of removal of symmetry

Stereoisomerism plays an important role in biological molecular recognition of drugs by their receptors. A chiral molecule has greater three dimensional spatial complexities which increases its receptor affinity and recognition of functional groups by its potential target

molecule.[136, 137] It is clear from Table 19 that the chirality possessed by **41** has a significant effect on the biological activity. Since this has no effect on β-haematin inhibition, it either also points to another mechanism of action or a role for transporters in uptake of these compounds which discriminates between them.

Table 19: The SAR results for the effect of symmetry study.

Compound	IC_{50} (μM)
22	2.7±0.5
23	2.81*
41	0.600±0.007

* single determination

3.5.2 Series 2: Variations on the R'' group

Lengthening the alkyl group at positions 2 and 6 on the dihydropyridine ring appears to be well tolerated and influences activity to some extent as seen in Table 20 below. The effect seems to parallel β-haematin inhibition.

Table 20: IC_{50} values for R'' position analogues

Compound	IC_{50} (μM)
22	2.7±0.5
23	2.8*
39	1.6±0.2
40	1.4±0.6

* single determination

3.5.3 Series 3: The role of the NH group in the dihydropyridine ring

The results of the *in vitro* antimalarial assay for the alkylated derivative at the NH group were similar to those found for β-haematin inhibition with the alkylated derivative showing reduced activity. However, the reduction in activity was less marked. Table 21 shows the IC_{50} values for the analogues.

Table 21: Parasite growth inhibition IC_{50} results for evaluating H-bond donor influences on activity.

Compound	IC_{50} (μM)
23	2.8*
42	3.8±0.1

* single determination

3.5.4 Series 4: Oxidation to pyridines

Although the pyridine molecule provides the electron cloud system with more π-electrons which can π-stack with the hydrophobic haem macrocycle whilst having an electron deficient nitrogen atom, the lack of β-haematin inhibition described previously seems to result in poor parasite growth inhibition activity. This outweighs any advantages conferred by the rigidity of the molecule (sp^2 hybridised carbons). Oxidation to the pyridine of the 1,4-dihydropyridine nucleus resulted in weak or no antiplasmodium activity, table 22.

Table 22: The IC_{50}'s for the oxidised derivatives.

Compound	IC_{50} (μM)
45	>19.9
46	4.9±1.4
47	>26.9
48	>17.0
49	3.8±1.3

3.6 Relationship between activity against parasite growth and β-haematin formation

Although a direct correlation between the $\log IC_{50}$ for parasite inhibition with that for β-haematin inhibition for the 1,4-DHP series could not be established, a direct comparison

revealed that the two inhibition activities did generally parallel each other with the exception of analogue **43** which showed no or very weak activity against β-haematin formation with good biological activity. Possible reasons for the lack of a direct correlation may be that the detergent assay did not adequately mimic the role of lipids for these compounds or that their access across the digestive vacuole membrane is limited.

The expected 1000 fold parasite digestive vacuole accumulation of **43** suggests two possible reasons for its activity:

i) Compound accumulation to levels where it can inhibit haemozoin at high concentrations

ii) It may exert its antimalarial potency via a different mechanism of action (example inhibition of a digestive vacuole channel or transporter or protease inhibition within the digestive vacuole) to inhibit parasite growth.

In case of 1,4-DHP esters, the activity against parasite growth and β-haematin formation increased with increasing hydrophobicity of the analogue. A statistically significant trend was found for parasite activity when analogues **27**, **25** and **21** were omitted from the data. This indicated that other factors also played a role in activity of compounds. The inactivity of **21** against both β-haematin formation and parasite growth can most likely be attributed to the absence of an ester group in this ketone derivative which may be essential for activity.

The β-haematin inhibition activity for benzyl derivatives showed a more complex dependency on several factors such as log P, size and saturation of molecules. However for inhibition of parasite growth a quantitative correlation revealed that increasing molecular weight and number of saturated carbon atoms in the molecule decrease the activity of a compound. Apart from **29** which exhibited a non-existent activity against β-haematin formation, the activity of the benzyl series showed parallel behaviour between parasite and β-haematin inhibition.

Alkylation on the nitrogen abolishes or weakens activity of the molecule suggesting importance of hydrogen-bonding. For compounds **39** and **40**, activity slightly increased

suggesting limited influence of substituents at 2 and 6 positions on both antiplasmodium and β-haematin activities.

3.7 Conclusions

Based on the results found in the present study, a structure-activity relationship model using molecular descriptors for antimalarial activity of a 1,4-DHP molecule was deduced. These structural factors are as follows:

i) Introduction of chirality appears to have an influence on antiplasmodial activity with little or no effect on β-haematin formation.

ii) Loss of hydrogen bond donor attributes of the nitrogen atom in the dihydropyridine ring results in elimination of activity.

iii) The 1,4-DHP nucleus is essential for maintaining activity. Upon oxidation of the ring to a pyridine group, activity is either obliterated or substantially decreased.

iv) Changes to a larger alkyl group at the 2 and 6 (R'') position are well tolerated, slightly increasing activity.

v) Vacuolar accumulation is probably enhanced by presence of a lipophilic N-heterocycle, but to the detriment of haemozoin inhibition.

vi) For the alkyl esters, larger hydrophobic groups greatly increase activity of the compound.

vii) Saturation and increased molecular weight of the molecule has a negative effect on parasite activity for 1,4-DHP benzyl esters.

Overall, the shape of a 1,4-DHP molecule is of importance for specific recognition and interaction with haem (haemozoin) influencing its activity. Figure 45 shows the SAR model predicted for the antimalarial activity of 1,4-dihydropyridines.

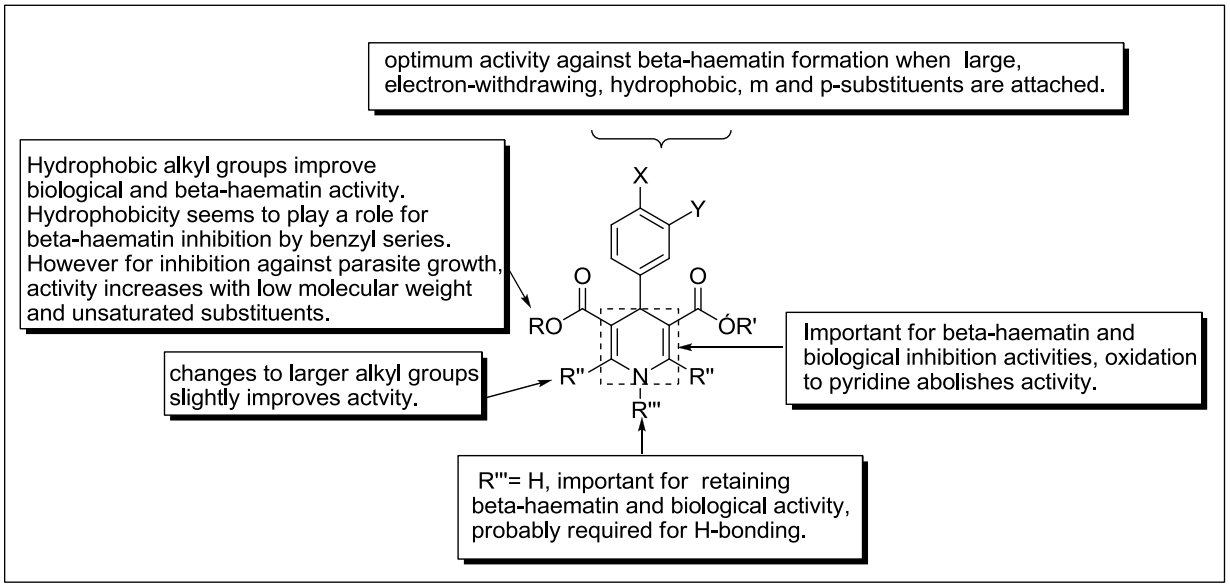

Figure 45: The proposed SAR model in the 1,4-DHP template for antimalarial activity for the current project based on 40 1,4-DHP compounds (inclusive of the 12 analogues from a previous study described in section 1.8).

4. Conclusions and Future-Work

4.1 General Conclusions

The key objective of the project was to synthesise analogues of the 1,4-DHP molecule by performing various positional structural alterations and thereafter explore structure activity relationships and using statistical correlation analysis to also investigate quantitative structure activity relationships influencing both inhibition of β-haematin formation and parasite growth. The one pot experimentally convenient Hantzsch pyridine reaction was successfully used for the synthesis and testing of forty 1,4-DHP compounds (including 12 compounds from previous work) selected to cover a range of activity space guided by the Topliss scheme. In agreement with literature, microwave irradiation was used to accelerate the reaction whilst obtaining high product yields. A transesterification process for the synthesis of a range of acetoacetate substrates required for Hantzsch reaction was carried out using a Dean stark apparatus to drive formation of products. This proved efficient for the synthesis of many derivatives with varied groups.

Studies revealed three analogues (Figure 46) that showed promising antimalarial potency. These were: the chiral analogue **41** (βIC_{50} = 74±4 and parasite IC_{50} = 0.600±0.007 μM); the symmetrical benzyl ester **35** (βIC_{50} = 25±2 and parasite IC_{50} = 0.8±0.2 μM); and the symmetrical alkyl ester **25** (βIC_{50} = 38±2 and parasite IC_{50} = 0.5±0.1 μM.

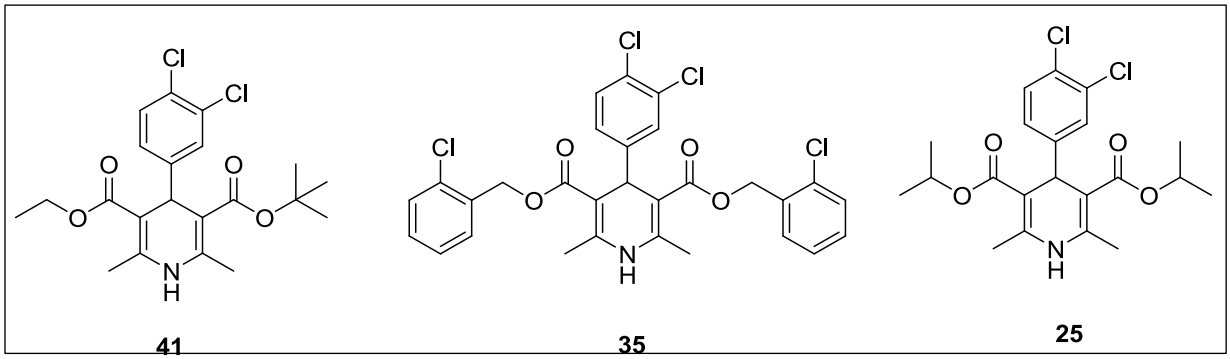

Figure 46: The structures of 1,4-DHP analogues showing promising antimalarial activity.

The parasite activity of **41** may reflect the complexity of biological targets or transporters which frequently display preferences for a stereospecific molecule. Although this may be

true, the remarkable activity of **25** suggests that antimalarial activity of the 1,4-DHP scaffold may be more complicated than speculated, hence a more in depth analysis is required. Correlation studies for 1,4-DHP benzyl esters revealed that low molecular weight and low degree of saturation correlated well with activity of the compound. Since only a relatively small number of derivatives were synthesised for physico-chemical studies, correlation of more than two parameters with log IC_{50} at once is not statistically valid owing to over determination. This may have hindered discovery of more complex underlying SARs.

With respect to the various analogues modified at the ester groups, quantitative correlation results provided a useful structure-activity model which may be a powerful tool for predicting the activity of the 1,4-dihydropyridine template as a chemotype against the malaria parasite.

4.2 Future-Work

The structure-activity relationship model presented in this project mainly focused on structural influences possessed by the ester component of the 1,4-DHP molecule. As a result, only a few analogues with modifications on the R'' and R''' positions were synthesised. Hence for validation purposes, a quantitative study involving more extensive exploration at these positions would be worthwhile. Similarly, introduction of further modifications on the 4-phenyl ring may prove a fruitful avenue of investigation. Conformational analysis using molecular mechanics modelling could be of interest for insight into intermolecular forces and structural differences between the inactive pyridine analogues and the active 1,4-dihydropyidines.

The ability of the compounds to inhibit haemozoin in the parasite has not yet been investigated. This will be required. Indeed, the good activity of **43** against the parasite despite poor activity against β-haematin formation indicates that at least some of these analogues may have other mechanisms of action which need to be explored.

Finally, investigation of the absorption, distribution, metabolism, excretion and toxicity properties of the compounds would need to be investigated to establish their potential for further drug development.

Chapter 5: Experimental Section

5.1 Organic Synthesis

Materials and techniques:

Reagents were purchased from Sigma Aldrich and were used without further purification. Thin layer Chromatography (TLC) was used to monitor reaction progression and was done on precoated silica gel 60 F_{254} plates purchased from Merck. Microwave reactions were done on a CEM Discover microwave machine using 0.0 bar of pressure and 250 W of power.

Reaction progression on TLC plates were visualised by staining (anisaldehyde:sulphuric acid (50:50))and by ultraviolet light.

Melting points are uncorrected and were measured on a Riechert-Jung Thermovar hot-stage microscope. ^{1}H NMR and ^{13}C NMR spectra were obtained on either 400 MHz or 300 MHz Bruker spectrometers or on a 300 MHz Varian Mercury Unity spectrometer. Chemical shifts (δ) are presented in parts per million (ppm) and coupling constants (*J*) in Hertz (Hz). Signal multiplicity are represented by: s for singlet, bs for broad singlet, d for doublet, dd for doublet of doublet, ddd for doublet of doublet of doublet, ddt for doublet of doublet of triplet, t for triplet and m for a multiplet. The reference chemical shifts for $CDCl_3$ are 7.26 ppm in the ^{1}H NMR and 77.16 ppm in the ^{13}C NMR spectra.

Infrared spectra were recorded using A225/Q platinum ATR diamond infrared spectrum machine. The high resolution mass spectrometry was recorded on a Waters Synapt G2 HRMS instrument at the Central Analytical Facilities, University of Stellenbosch. High Pressure liquid chromatography was recorded on an Agilent technologies 1220 Infinity LC HPLC machine as a solvent system 9:1 acetonitrile/water.

General Procedure for synthesis of the benzyl alcohols.[138]

The relevant aldehyde (17.0 mmol) was dissolved in ethanol (10.0 ml) at 0°C followed by portion-wise addition of sodium borohydride (25.0 mmol, 1.50 eq). The reaction was then stirred at room temperature under N_2 for five minutes before being quenched with aqueous ammonium chloride. Thin layer chromatography (TLC) revealed a spot-to-spot conversion. Ethanol was removed under reduced pressure and cold water (15.0 mL) was added and the solution extracted using ethyl acetate (3 x 30.0 mL). The ethyl acetate extracts were dried over magnesium sulfate ($MgSO_4$), the solvent removed under reduced pressure and the product dried under vacuum. The product was used in the subsequent step without further purification.

4-Methylbenzyl alcohol (1)[139]

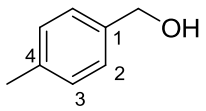

Compound **1** (1.90 g, 94%) was obtained as colourless solid; ^{1}H NMR (400 MHz, $CDCl_3$) δ 7.27 (2H, d, *J* = 8.1 Hz, H-3), 7.17 (2H, d, *J* = 8.1 Hz, H-2), 4.92 (1H, bs, OH) 4.65 (2H, s, $ArCH_2$), 2.35 (3H, s, Ar_{Me}); ^{13}C NMR (100 MHz, $CDCl_3$) δ 137.9 (C-1), 137.5 (C-4), 129.4 (C-3), 127.2 (C-2), 65.3 ($ArCH_2$), 21.2 (Ar_{Me}).

3-Methylbenzyl alcohol (2)[140]

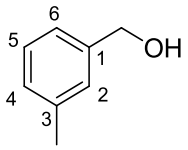

Compound **2** (1.88 g, 91%) was obtained as a yellow liquid. ^{1}H NMR (400 MHz, $CDCl_3$) δ 7.28 (1H, d, *J* = 7.2 Hz, H-6), 7.24 (1H, d, *J* = 8.1 Hz, H-4), 7.16 (1H, m, H-5), 7.12 (1H, d, *J* = 2.6 Hz, H-2), 4.98 (1H, bs, OH), 4.65 (2H, s, $ArCH_2$), 2.37 (3H, s, Ar_{Me}); ^{13}C NMR (100 MHz, $CDCl_3$) δ 140.9 (C-1), 138.3 (C-3), 128.5 (C-6), 128.4 (C-2), 127.8 (C-5), 124.1 (C-4), 65.4 ($ArCH_2$), 21.5 (Ar_{Me}).

3,4-Dichlorobenzyl alcohol (3)

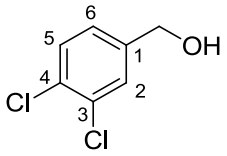

Compound **3** (2.86, 95%) was obtained as a colourless solid; ^{1}H NMR (400 MHz, $CDCl_3$) δ 7.47 (1H, d, *J* = 2.1 Hz, H-2), 7.43 (1H, d, *J* = 8.1 Hz, H-5), 7.19 (1H, dd, *J* = 8.1, 2.1 Hz, H-6), 4.88 (1H, bs, O<u>H</u>), 4.67 (2H, s, $ArCH_2$); ^{13}C NMR (100 MHz, $CDCl_3$) δ 143.2 (C-1), 134.9 (C-4), 133.7 (C-3), 132.8 (C-5), 131.0 (C-2), 128.0 (C-6), 66.2 ($ArCH_2$)

2,4-Dichlorobenzyl alcohol (4)[141]

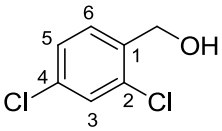

Compound **4** (2.88 g, 95%) was obtained as a colourless solid; ^{1}H NMR (400 MHz, $CDCl_3$) δ 7.43 (1H, d, *J* = 8.2 Hz, H-6), 7.38 (1H, d, *J* = 2.1 Hz, H-3), 7.26 (1H, dd, *J* = 8.2, 2.0 Hz, H-5), 4.75 (2H, s, $ArCH_2$), 2.00 (1H,s, O<u>H</u>). ^{13}C NMR (100 MHz, $CDCl_3$) δ 136.7 (C-1), 133.9 (C-4), 133.2 (C-2), 129.4 (C-6), 129.2 (C-3), 127.3 (C-5), 62.2 ($ArCH_2$).

<u>General Procedure for synthesis of acetoacetate ester analogues:</u> [111]

Zinc (1.31 g, 20.0 mmol) was dissolved in anhydrous toluene (20.0 mL) at 110 °C, methyl acetoacetate (1.13 ml, 10.0 mmol) was then added. Addition of the alcohol (12.0 mmol) and a catalytic amount of iodine (254 mg, 1.00 mmol) respectively was then performed. The mixture was subsequently refluxed under N_2 and methanol removed by distillation. TLC using a solvent system of hexane/ ethyl acetate (3:1) was used to monitor the reaction progress, but generally reaction times were in the order of 3 hours to overnight. De-ionised water was used to quench the reaction, and the mixture filtered through Celite and washed with cold toluene (3 x 15.0 ml). Removal of the toluene was done under vacuum. Ice-cold water (10.0 ml) followed by brine (25.0 mL) were added to the residue and extraction performed using DCM (3 x 20.0 mL). The organic extracts were dried with $MgSO_4$ and the solvent evaporated under reduced pressure. Column chromatography was performed using hexane/ ethyl acetate (3:1) as eluent.

Isopropyl acetoacetate (5)[142]

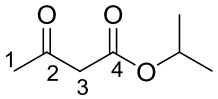

The reaction yielded compound **5** (696 mg, 48%) as a colourless liquid. ^{1}H NMR (400 MHz, $CDCl_3$) δ 5.06 (1H, sep, OCH), 3.40 (2H, s, H-3), 2.25 (3H, s, H-1), 1.25 (6H, d, *J* = 6.3 Hz, $Me_{isopropyl}$); ^{13}C NMR (100 MHz, $CDCl_3$) δ 200.6 (C-2), 166.6 (C-4), 69.0 (OCH), 50.5 (C-3), 30.0 (C-1), 21.7 ($Me_{isopropyl}$).

Cyclohexyl acetoacetate (6)[142]

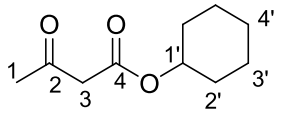

The reaction yielded compound **6** (1.57 g, 85%) as a colourless liquid. ^{1}H NMR (400 MHz, $CDCl_3$) δ 4.84-4.80 (1H, m, OCH (1')), 3.41 (2H, s, H-3), 2.26 (3H, s, H-1), 1.85, 1.73 (4H, m, H-2'), 1.53 (2H, m, H-4'), 1.35 (4H, m, H-3'); ^{13}C NMR (100 MHz, $CDCl_3$) δ 200.6 (C-2), 166.6 (C-4), 73.8 (OCH), 50.5 (C-3), 31.4 (C-2'), 29.9 (C-1), 25.2 (C-4'), 23.6 (C-3').

Cyclopentyl acetoacetate (7) [142]

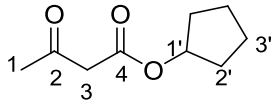

The reaction yielded compound **7** (494 mg, 29%) as a colourless liquid. ^{1}H NMR (400 MHz, $CDCl_3$) δ 5.20-5.12 (1H, m, OCH (1')), 3.20 (2H, s, H-3), 2.17 (3H, s, H-1), 1.80-1.65 (4H, m, H-2'), 1.63, 1.52 (4H, m, H-3'); ^{13}C NMR (100 MHz, $CDCl_3$) δ 200.6 (C-2), 166.9 (C-4), 78.3 (OCH), 50.4 (C-3), 32.6 (C-2'), 30.0 (C-1), 23.7 (C-3').

Benzyl acetoacetate (8) [142]

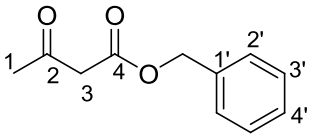

The reaction yielded compound **8** (1.54 g, 80%) as a colourless liquid. ^{1}H NMR (400 MHz, $CDCl_3$) δ 7.30-7.20 (5H, m, Ar-H), 5.10 (2H, s, OCH_2), 3.42 (2H, s, H-3), 2.17 (3H, s, H-1). ^{13}C

NMR (100 MHz, $CDCl_3$) δ 200.2 (C-2), 166.9 (C-4), 135.3 (C-1'), 128.6 (C-3'), 128.4 (C-4'), 128.3 (C-2'), 67.1 (OCH_2), 50.0 (C-3), 30.1 (C-1).

2-Chlorobenzyl acetoacetate (9)[143]

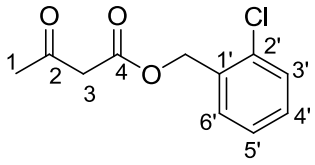

The reaction mixture was refluxed overnight yielding compound **9** (1.92 g, 85%) as colourless crystals. ^{1}H NMR (400 MHz, $CDCl_3$) δ 7.42-7.12 (4H, m, Ar-H), 5.30 (2H, s, OCH_2), 3.56 (2H,s, H-3), 2.30 (3H, s, H-1); ^{13}C NMR (100 MHz, $CDCl_3$) δ 200.5 (C-2), 166.8 (C-4), 138.2 (C-1'), 130.2 (C-2'), 129.4 (C-6'), 128.9 (C-3'), 128.8 (C-4'), 127.0 (C-5'), 62.9 (OCH_2), 50.0 (C-3), 30.2 (C-1).

4-Chlorobenzyl acetoacetate (10)[144]

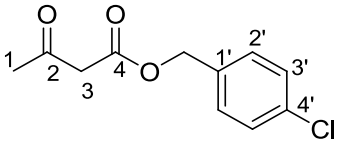

The reaction yielded compound **10** (1.87 g, 83%) as a pale-yellow liquid. ^{1}H NMR (400 MHz, $CDCl_3$) δ 7.26 (2H, d, *J* = 8.8 Hz, H-3'), 7.22 (2H, d, *J* = 8.8 Hz, H-2') 5.06 (2H, s, OCH_2), 3.42 (2H, s, H-3), 2.17 (3H, s, H-1); ^{13}C NMR (100 MHz, $CDCl_3$) δ 200.0 (C-2), 166.8 (C-4), 134.5 (C-1'), 133.9 (C-4'), 129.8 (C-3'), 128.8 (C-2'), 66.3 (OCH_2), 50.0 (C-3), 30.2 (C-1).

3-Chlorobenzyl acetoacetate (11)[145]

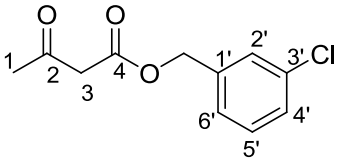

The reaction yielded compound **11** (1.80 g, 79%) as a colourless liquid. ^{1}H NMR (400 MHz, $CDCl_3$) δ 7.40-7.35 (1H, m, H-5'), 7.33-7.30 (3H, m, H-2', H-4' and H-6'), 5.17 (2H, s, OCH_2), 3.54 (2H, s, H-3), 2.29 (3H, s, H-1); ^{13}C NMR (100 MHz, $CDCl_3$) δ 200.2 (C-2), 166.8 (C-4), 137.3 (C-1'), 134.5 (C-3'), 130.0 (C-5'), 128.6 (C-4'), 128.3 (C-6'), 126.3 (C-2'), 66.2 (OCH_2), 49.9 (C-3), 30.2 (C-1).

4-Bromobenzyl acetoacetate (12)[143]

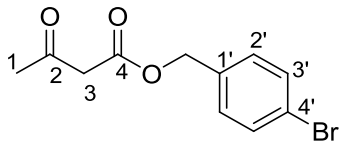

The reaction yielded compound **12** (1.78 g, 66%) as a colourless solid. ^{1}H NMR (400 MHz, $CDCl_3$) δ 7.50 (2H, d, *J* = 6.8 Hz, H-3'), 7.24 (2H, d, *J* = 6.8 Hz, H-2'), 5.11 (2H, s, OCH_2), 3.49 (2H, s, H-3), 2.24 (3H, s, H-1); ^{13}C NMR (100 MHz, $CDCl_3$) δ 200.2 (C-2), 166.8 (C-4), 134.3 (C-1'), 131.8 (C-3'), 130.0 (C-2'), 122.5 (C-4'), 66.3 (OCH_2), 49.9 (C-3), 30.2 (C-1).

4-Methylbenzyl acetoacetate (13)[144]

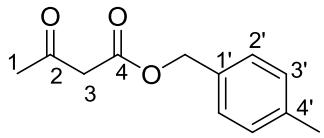

The reaction yielded compound **13** (1.56 g, 76%) as a colourless liquid. ^{1}H NMR (400 MHz, $CDCl_3$) δ 7.26 (2H, d, *J* = 8.0 Hz, H-2'), 7.18 (2H, d, *J* = 8.0 Hz, H-3'), 5.14 (2H, s, OCH_2), 3.48 (2H, s, H-3), 2.36 (3H, s, Ar_{Me}), 2.24 (3H, s, H-1); ^{13}C NMR (100 MHz, $CDCl_3$) δ 200.5 (C-2), 167.0 (C-4), 138.5 (C-1'), 132.3 (C-4'), 129.3 (C-2'), 128.6 (C-3'), 67.2 (OCH_2), 50.1 (C-3), 30.2 (C-1), 21.2 (Ar_{Me}).

3-Methylbenzyl acetoacetate (14)

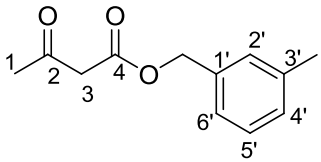

The reaction yielded compound **14** (1.11 g, 54%) as a yellow liquid; ^{1}H NMR (400 MHz, $CDCl_3$) δ 7.29-7.13 (4H, m, Ar-H), 5.15 (2H, s, OCH_2), 3.50 (2H, s, H-3), 2.37 (3H, s, Ar_{Me}), 2.25 (3H, s, H-1); ^{13}C NMR (100 MHz, $CDCl_3$) δ 200.3 (C-2), 166.9 (C-4), 138.5 (C-3'), 135.2 (C-1'), 129.2 (C-6'), 129.1 (C-2'), 128.6 (C-5'), 125.4 (C-4'), 67.3 (OCH_2), 50.1 (C-3), 30.1 (C-1), 21.3 (Ar_{Me}).

3,4-Dichlorobenzyl acetoacetate (15)[145]

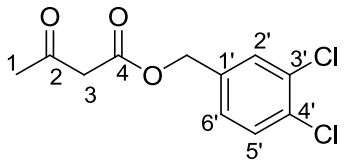

The reaction yielded compound **15** (1.50, 57%) as a pale-yellow liquid. ^{1}H NMR (400 MHz, $CDCl_3$) δ 7.46 (1H, d, *J* = 2.1 Hz, H-2'), 7.43 (1H, d, *J* = 8.2 Hz, H-5'), 7.20 (1H, dd, *J* = 8.2, 2.1 Hz, H-6'), 5.11 (2H, s, OCH_2), 3.52 (2H, s, H-3), 2.26 (3H, s, H-1); ^{13}C NMR (100 MHz, $CDCl_3$) δ 200.1 (C-2), 166.7 (C-4), 135.5 (C-1'), 132.8 (C-4'), 132.6 (C-3'), 130.7 (C-5'), 130.2 (C-2'), 127.5 (C-6'), 65.5 (OCH_2), 49.9 (C-3), 30.3 (C-1).

2,4-Dichlorobenzyl acetoacetate (16)[146]

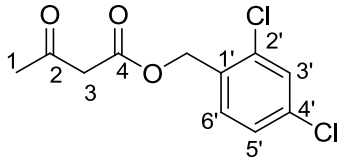

The reaction yielded compound **16** (2.58 g, 99%) as a colourless solid; ^{1}H NMR (400 MHz, $CDCl_3$) δ 7.42 (1H, d, *J* = 8.4 Hz, H-6'), 7.36 (1H, d, *J* = 2.1 Hz, H-3'), 7.25 (1H, dd, *J* = 8.4, 2.1 Hz, H-5'), 5.24 (2H, s, OCH_2), 3.53 (2H, s, H-3), 2.27 (3H, s, H-1); ^{13}C NMR (100 MHz, $CDCl_3$) δ 200.1 (C-2), 166.6 (C-4), 135.0 (C-1'), 134.5 (C-4'), 131.2 (C-2'), 131.0 (C-6'), 129.5 (C-3'), 127.3 (C-5'), 63.7 (OCH_2), 49.9 (C-3), 30.1 (C-1).

3,4-Dimethylbenzyl acetoacetate (17)

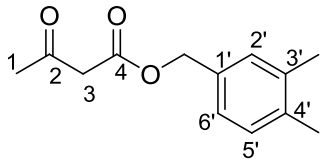

The reaction yielded compound **17** (0.696 g, 32%) as a colourless liquid. ^{1}H NMR (400 MHz, $CDCl_3$) δ 7.13 (1H, d, *J* = 8.0 Hz, H-5'), 7.34 (1H, bs, H-2'), 7.09 (1H, dd, *J* = 8.0, 2.0 Hz, H-6'), 5.11 (2H, s, OCH_2), 3.48 (2H, s, H-3), 2.28-2.26 (6H, m, Ar_{Me}), 2.25 (3H, s, H-1); ^{13}C NMR (100 MHz, $CDCl_3$) δ 200.5 (C-2), 167.0 (C-4), 137.2 (C-3'), 136.9 (C-4'), 132.6 (C-1'), 129.9 (C-5'), 129.8 (C-2'), 126.1 (C-6'), 67.3 (OCH_2), 50.2 (C-3), 30.2 (C-1), 19.8 (Ar_{me}), 19.6 (Ar_{me}).

2-Pyridylethyl acetoacetate (18)[147]

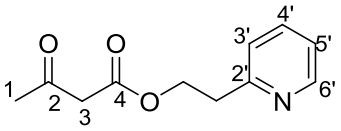

The reaction was done using methyl acetoacetate (80.0 mmol) and 2-(2-pyridyl)ethanol (10.0 mmol). The reaction yielded compound **18** (1.47 g, 70%) as a yellow liquid. ^{1}H NMR (400 MHz, $CDCl_3$) δ 8.50 (1H, d, *J* = 6.0 Hz , H-6'), 7.60-7.56 (1H, m, H-4'), 7.14 (1H, d, *J* = 8.0 Hz, H-3'), 7.11 (1H, m, H-5'), 4.52 (2H, m, OCH_2), 3.37 (2H, s, H-3), 3.10 (2H, t, *J* = 6.8 Hz, $OCH_2C\underline{H}_2$), 2.15 (3H, s, H-1).

***tert*-butyl 4-(2-(3-oxobutanoyloxy)ethyl)piperazine-1-carboxylate)**[148]

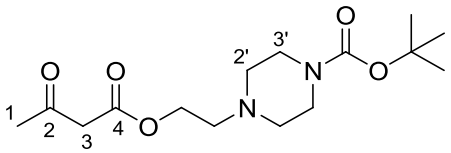

The reaction yielded compound **19** (1.97 g, 63%) as a pale-yellow liquid. ^{1}H NMR (400 MHz, $CDCl_3$) δ 4.26 (2H, t, *J* = 5.8 Hz, OCH_2), 3.45 (2H, s, H-3), 3.40 (4H, t, *J* = 5.2 Hz, H-2'), 2.64 (2H, t, *J* = 5.8 Hz, NCH_2), 2.43 (4H, t, *J* = 5.2 Hz, H-3'), 2.27 (3H, s, H-1), 1.45 (9H, s, $Me_{t\text{-butyl}}$); ^{13}C NMR (100 MHz, $CDCl_3$) δ 200.3 (C-2), 166.9 (C-4), 154.7 (NCO), 79.7 (OC-*t*-butyl), 62.3 (OCH_2), 56.5 (C-2'), 53.7 (NCH_2), 50.1 (C-3), 43.6 (C-3'), 30.1 (C-1), 28.4 ($Me_{t\text{-butyl}}$).

2-(piperidin-1-yl)ethyl acetoacetate (20)[149]

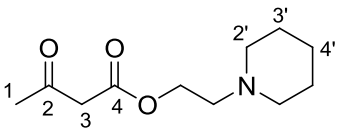

The reaction yielded compound **20** (957 mg, 45%) as a colourless liquid. ^{1}H NMR (400 MHz, $CDCl_3$) δ 4.28 (2H, t, *J* = 6.0 Hz, OCH_2), 3.47 (2H, s, H-3), 2.64 (2H, t, *J* = 6.0 Hz, NCH_2), 2.45 (4H, t, *J* = 5.4 Hz, H-2'), 2.29 (3H, s, H-1), 1.64-1.59 (4H, m, H-3'), 1.47-1.43 (2H, m, H-4'); ^{13}C NMR (100 MHz, $CDCl_3$) δ 200.5 (C-2), 167.0 (C-4), 62.7 (OCH_2), 57.2 (NCH_2), 54.8 (C-2'), 50.2 (C-3), 30.1 (C-1), 25.9 (C-3') 24.2 (C-4').

Representative procedure for synthesis of the 1,4-dihydropyridine analogues:

Ammonium acetate (1.40 mmol, 5.00 eq), 3,4-dichlorobenzaldehyde (0.280 mmol, 1.00 eq) and the relevant acetoacetate (5.60 mmol, 20.0 eq) were dissolved in ethanol (2.00 ml). The reaction mixture was microwave irradiated at 60 °C, 250 W until completion (8-26 minutes) followed by the removal of ethanol. Water (5.00 mL) was then added to the resultant residue, which was extracted using ethyl acetate (3x 15.0 mL), the organic extracts dried with $MgSO_4$ and the solvent removed under reduced pressure. Column chromatography was performed and the product obtained (solid) recrystallized from DCM/hexane to yield the product.

To the best of our knowledge all the compounds are novel compounds except for **22** and **23** which were reported by Pedemonte *et al.*. with no physical data to support the successful synthesis of the analogues**.**

1,1'-(4-(3,4-dichlorophenyl)-2,6-dimethyl-1,4-dihydropyridine-3,5-diyl)bis(ethan-1-one) (21)

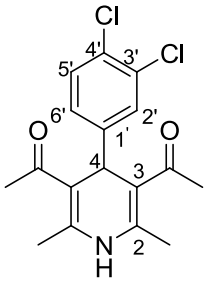

The reaction yielded compound **21** (84 mg, 88%) as pale-yellow crystals; m.p. 179-180 °C; HPLC: 99%; HRMS (EI): m/z 338.0715 $[M+H]^+$, $C_{17}H_{18}Cl_2NO_2$ requires 338.0715; ^{1}H NMR (400 MHz, CDCl3) δ 7.30 (1H, d, *J* = 1.6 Hz, H-2'), 7.28 (1H, d, *J* = 8.4 Hz, H-5'), 7.10 (1H, dd, *J* = 8.4 , 2.1, Hz, H-6'), 5.81 (1H, bs, NH), 5.15 (1H, s, H-4), 2.34 (6H, s, Me_{ketone}), 2.26 (6H, s, Me); ^{13}C NMR (100 MHz, $CDCl_3$) δ 197.1 (CO), 146.0 (C-2), 143.2 (C-1'), 132.4 (C-3'), 130.5 (C-4'), 130.3 (C-2'), 129.4 (C-5'), 127.1 (C-6'), 113.5 (C-3), 39.1 (C-4), 30.2 (Me_{ketone}), 20.5 (Me); IR. v_{max}/ cm^{-1} 3330 (N-H), 3254 (C-H aromatic), 1710 (C=O), 1652 (C=C aromatic).

Dimethyl-4-(3,4-dichlorophenyl)-2,6-dimethyl-1,4-dihydropyridine-3,5-dicarboxylate (22)[150]

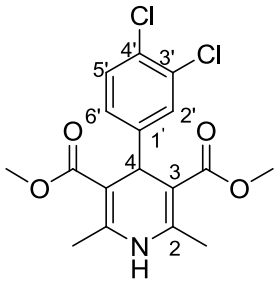

The reaction was performed on a 0.853 mmol scale of aldehyde. The mixture was refluxed under N_2 yielding compound **22** (242 mg, 66%) as a colourless powder; m.p. 176-177 °C; HPLC: 98 %; HRMS (EI): m/z 370.0598 $[M+H]^+$, $C_{17}H_{18}Cl_2NO_4$ requires 370.0613; ^{1}H NMR (400 MHz, $CDCl_3$) δ 7.31 (1H, d, *J* = 2.0 Hz, H-2'), 7.28 (1H, d, *J* = 8.2 Hz, H-5'), 7.11 (1H, dd, *J* = 8.2, 2.0 Hz, H-6'), 5.64 (1H, bs, NH), 4.97 (1H, s, H-4), 3.66 (6H, s, OMe), 2.35 (6H, s, Me). ^{13}C NMR (100 MHz, $CDCl_3$) δ 167.4 (CO), 147.5 (C-2), 144.4 (C-1'), 131.7 (C-3'), 129.9 (C-4'), 129.7 (C-2'), 129.5 (C-5'), 127.1 (C-6'), 103.5 (C-3), 50.9 (OMe), 38.8 (C-4), 19.5 (Me); v_{max}/ cm^{-1} 3352 (N-H), 3255 (C-H aromatic), 2957 (C-H alkane), 1710 (C=O), 1652 (C=C aromatic), 1122 (C-O ester).

Diethyl-4-(3,4-dichlorophenyl)-2,6-dimethyl-1,4-dihydropyridine-3,5-dicarboxylate (23)[150]

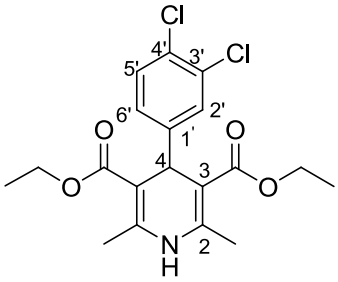

The reaction was performed on a 0.332 mmol scale. The reaction yielded compound **23** (126 mg, 96%) as pale yellow crystals; m.p. 131-133 °C; HPLC: 97 %; HRMS (EI): m/z 398.0923 $[M+H]^+$, $C_{19}H_{22}Cl_2NO_4$ requires 398.0926; ^{1}H NMR (400 MHz, $CDCl_3$) δ 7.36 (1H, d, *J* = 2.1 Hz, H-2'), 7.27 (1H, d, *J* = 8.3 Hz, H-5'), 7.15 (1H, dd, *J* = 8.3 Hz, 2.1 Hz, H-6'), 5.64 (1H, bs, NH), 4.98 (1H, s, H-4), 4.19 – 4.07 (4H, m, OCH_2), 2.37 (6H, s, Me), 1.25 (6H, t, *J* = 7.2 Hz, Me_{ester}); ^{13}C NMR (100 MHz, $CDCl_3$) δ 169.1 (CO), 149.0 (C-2), 144.2 (C-1'), 132.2 (C-3'), 130.1 (C-2'),129.9 (C-4'), 129.7 (C-5'), 127.6 (C-6'), 103.8 (C-3), 59.9 (OCH_2), 39.4 (C-4), 19.6 (Me),

14.2 (Me_{ester}); v_{max}/ cm^{-1} 3353 (N-H), 3254 (C-H aromatic), 2956 (C-H alkane), 1713 (C=O), 1652 (C=C aromatic), 1124 (C-O ester)

Diallyl 4-(3,4-dichlorophenyl)-2,6-dimethyl-1,4-dihydropyridine-3,5-dicarboxylate (24)

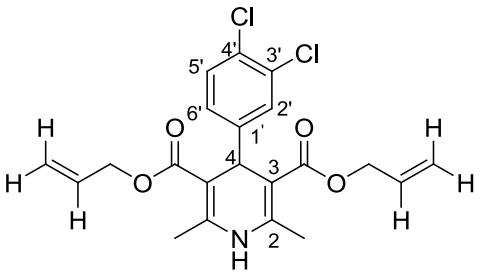

The reaction was performed on a 0.853 mmol scale. The mixture was refluxed under N_2 yielding compound **24** (260 mg, 72%) as a colourless powder; m.p. 149-152 °C; HPLC purity: 97%; HRMS (EI): m/z 422.0925 $[M+H]^+$, $C_{21}H_{22}Cl_2NO_4$ requires 422.0926; ^{1}H NMR (400 MHz, $CDCl_3$) δ 7.33 (1H, d, *J* = 2.2 Hz, H-2'), 7.26 (1H, d, *J* = 8.3 Hz, H-5'), 7.12 (1H, dd, *J* = 8.3, 2.1 Hz, H-6'), 5.92-5.88 (2H, m, CH_{vinyl}) 5.65 (1H, bs, N<u>H</u>), 5.25-5.22 (4H, m, CH_{2vinyl}), 5.01 (1H, s, H-4), 4.90-4.88 (4H, m, OCH_2) 2.35 (6H, s, Me); ^{13}C NMR (100 MHz, $CDCl_3$) δ 166.8 (CO), 147.7 (C-2), 144.6 (C-1'), 132.5 (<u>C</u>H_{vinyl}), 131.8 (C-3'), 130.0 (C-2'), 129.9 (C-4'), 129.7 (C-5'), 127.6 (C-6'), 117.9 (<u>C</u>$H_{2\ vinyl}$), 103.3 (C-3), 64.8 (OCH_2), 39.2 (C-4), 19.7 (Me); v_{max}/ cm^{-1} 3317 (N-H), 3246 (C-H aromatic), 3105 (C-H alkene), 2952 (C-H alkane), 1695 (C=O), 1654 (C=C aromatic), 1120 (C-O ester), 922 (C-H alkene bend).

Diisopropyl-4-(3,4-dichlorophenyl)-2,6-dimethyl-1,4-dihydropyridine-3,5-dicarboxylate (25)

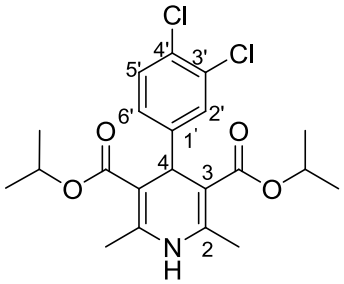

The reaction yielded compound **25** (108 mg, 91%) as colourless crystals; m.p. 167-169 °C; HRMS (EI): m/z 426.1236 $[M+H]^+$, $C_{21}H_{26}Cl_2NO_4$ requires 426.1239; ^{1}H NMR (400 MHz, $CDCl_3$) δ 7.34 (1H, d, *J* = 2.1 Hz, H-2'), 7.27 (1H, d, *J* = 8.3 Hz, H-5'), 7.12 (1H, dd, *J* = 8.3, 2.0 Hz, H-6'), 5.55 (1H, bs, NH), 4.96 (2H, sep, *J* = 6.30 Hz, OCH), 4.92 (1H, s, H-4), 2.33 (6H, s,

Me), 1.20 (12H, 2xd, *J* = 6.2 Hz, $Me_{isopropyl}$); ^{13}C NMR (100 MHz, $CDCl_3$) δ 167.7 (CO), 148.1 (C-2), 143.9 (C-1'), 130.3 (C-3'), 130.1 (C-4'), 129.7 (C-2'), 129.6 (C-5'), 127.7 (C-6'), 103.8 (C-3), 66.9 (OCH), 39.4 (C-4), 21.8 ($Me_{isopropyl}$), 19.4 (Me); v_{max}/ cm^{-1} 3315 (N-H), 3118 (C-H aromatic), 2972 (C-H alkane), 1670 (C=O), 1645 (C=C aromatic), 1101 (C-O ester).

Di-tert-butyl-4-(3,4-dichlorophenyl)-2,6-dimethyl-1,4-dihydropyridine-3,5-dicarboxylate (26)

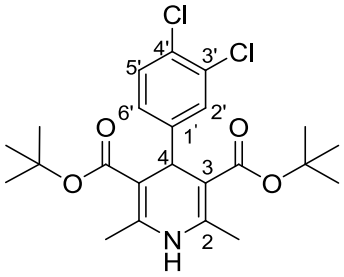

The reaction was performed on a 0.853 mmol scale. The mixture was refluxed under N_2 yielding compound **26** (197 mg, 51%) as yellow crystals; m.p. 149-151 °C; HPLC: 98%; HRMS (EI): m/z 454.1552 $[M+H]^+$, $C_{23}H_{30}Cl_2NO_4$ requires 454.1552; ^{1}H NMR (400 MHz, $CDCl_3$) δ 7.35 (1H, d, *J* = 2.0 Hz, H-2'), 7.27 (1H, d, *J* = 8.3 Hz, H-5'), 7.12 (1H, dd, *J* = 8.3, 2.1 Hz, H-6'), 5.36 (1H, bs, N<u>H</u>), 4.80 (1H, s, H-4), 2.23 (6H, s, Me), 1.34 (18H, s, $Me_{t\text{-butyl}}$); ^{13}C NMR (100 MHz, $CDCl_3$) δ 166.6 (CO), 148.4 (C-2), 143.4 (C-1'), 131.7 (C-3'), 130.2 (C-4'), 129.8 (C-2'), 129.6 (C-5'), 127.7 (C-6'), 103.8 (C-3), 66.9 (OC-*t*-butyl), 39.4 (C-4), 21.8 ($Me_{t\text{-butyl}}$), 19.4 (Me); v_{max}/ cm^{-1} 3329 (N-H), 3126 (C-H aromatic), 2977 (C-H alkane), 1701 (C=O), 1645 (C=C aromatic), 1109 (C-O ester).

Dicyclopentyl-4-(3,4-dichlorophenyl)-2,6-dimethyl-1,4-dihydropyridine-3,5-dicarboxylate (27)

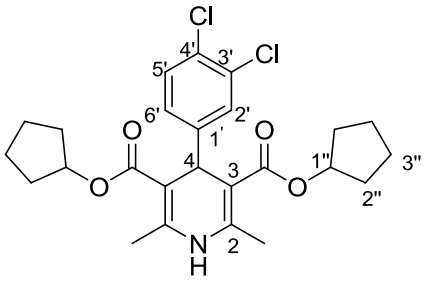

The reaction was performed on a 0.568 mmol scale. The reaction mixture was refluxed under N_2 yielding compound **27** (224 mg, 82%) a yellow solid; m.p. 129-131 °C; HPLC: 95%;

HRMS (EI): m/z 478.1540 $[M+H]^+$, $C_{25}H_{30}Cl_2NO_4$ requires 478.1552;^{1}H NMR (400 MHz, $CDCl_3$) δ 7.32 (1H, d, *J* = 2.1 Hz, H-2'), 7.27 (1H, d, *J* = 8.0 Hz, H-5'), 7.12 (1H, dd, *J* = 8.0, 2.0 Hz, H-6'), 5.60 (1H, bs, NH), 5.17-5.14 (2H, m, H-1''), 4.89 (1H, s, H-4), 2.33 (6H, s, Me), 1.90-1.75 (8H, m, H-2''), 1.70-1.60 (8H, m, H-3''); ^{13}C NMR (100 MHz, $CDCl_3$) δ 166.9 (CO), 147.9 (C-2), 144.0 (C-1'), 130.3 (C-3'), 130.1 (C-4'), 130.0 (C-6'), 129.8 (C-5'), 127.5 (C-6'), 103.9 (C-3), 78.9 (C-1"), 39.4 (C-4), 32.7 (C-2''), 23.6 (C-3''), 19.6 (Me).

Dicyclohexyl-4-(3,4-dichlorophenyl)-2,6-dimethyl-1,4-dihydropyridine-3,5-dicarboxylate (28)

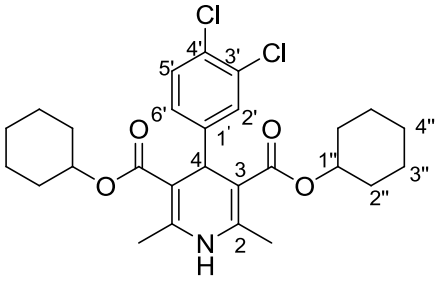

The reaction was performed on a 0.568 mmol scale. The mixture was refluxed under N_2 yielding compound **28** (230 mg, 80%) as a yellow solid; m.p. 145-147°C; HPLC purity: 97%; HRMS (EI): m/z 504.1713 $[M-H]^-$, $C_{27}H_{32}Cl_2NO_4$ requires 504.1708; ^{1}H NMR (400 MHz, $CDCl_3$) δ 7.32 (1H, d, *J* = 1.9 Hz, H-2'), 7.26 (1H, d, *J* = 8.3 Hz, H-5'), 7.13 (1H, dd, *J* = 8.3, 1.9 Hz, H-6'), 5.55 (1H, bs, NH), 4.99 (1H, s, H-4), 4.75 (2H, m, H-1''), 2.34 (6H, s, Me), 1.90-1.76 (8H, m, H-2''), 1.54-1.50 (4H, m, H-4''), 1.37-1.34 (8H, m, H-3''); ^{13}C NMR (100 MHz, $CDCl_3$) δ 166.6 (CO), 148.0 (C-2), 144.0 (C-1'), 131.6 (C-3'), 137.3 (C-4'), 130.2 (C-2'), 129.7(C-5'), 127.6 (C-6'), 103.9 (C-3), 72.1 (C-1"), 39.4 (C-4), 31.7 (C-2''), 25.5 (C-4''), 23.6 (C-3''), 19.7 (Me); v_{max}/ cm^{-1} 3339 (N-H), 3109 (C-H aromatic), 2935 (C-H alkane), 1676 (C=O), 1652 (C=C aromatic), 1107 (C-O ester).

Dibenzyl- 4-(3,4-dichlorophenyl)-2,6-dimethyl-1,4-dihydropyridine-3,5-dicarboxylate (29)

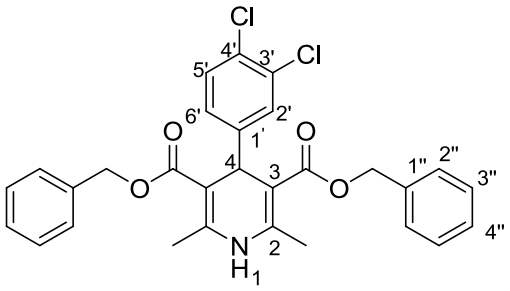

The reaction mixture was refluxed under N_2 yielding compound **29** (138 mg, 96%) as yellow crystals; m.p. 117-119 °C; HPLC purity: 95%; HRMS (EI): m/z 522.1241 $[M+H]^+$, $C_{29}H_{26}Cl_2NO_4$ requires 522.1239; ^{1}H NMR (400 MHz, $CDCl_3$) δ 7.30,7.20 (10H, m, H_{Ar} (benzyl group)), 7.20 (1H, d, *J* = 2.3 Hz, H-2'), 7.14 (1H, d, *J* = 8.3 Hz, H-5'), 6.97 (1H, dd, *J* = 8.3, 2.1 Hz, H-6'), 5.65 (1H, bs, N<u>H</u>), 5.06 (2H, d, J_{AB} = 12.4 Hz, OCH_2), 4.96 (2H, d, J_{AB} = 12.4 Hz, OCH_2), 4.99 (1H, s, H-4), 2.35 (6H, s, Me); ^{13}C NMR (100 MHz, $CDCl_3$) δ 167.1 (CO), 148.0 (C-2), 144.9 (C-1'), 136.4 (C-1''), 132.0 (C-3'), 130.3 (C-2'), 130.0 (C-4'), 129.9 (C-5'), 128.7 (C-3''), 128.4 (C-2''), 128.3 (C-4''), 127.9 (C-6'), 103.6 (C-3), 66.1 (OCH_2), 39.6 (C-4), 20.1 (Me); v_{max}/ cm^{-1} 3371 (N-H, two broad peaks), 3036 (C-H aromatic), 2935 (C-H alkane), 1692 (C=O), 1651 (C=C aromatic), 1097 (C-O ester).

***Bis*(4-methylbenzyl)-4-(3,4-dichlorophenyl)-2,6-dimethyl-1,4-dihydropyridine-3,5-dicarboxylate (30)**

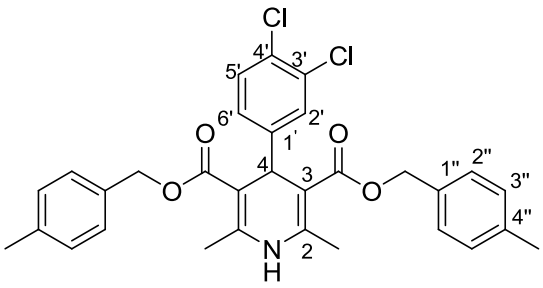

The reaction yielded compound **30** (133 mg, 87%) as colourless crystals; m.p. 174-176 °C; HPLC purity: 98%; HRMS (EI): m/z 550.1556 $[M+H]^+$, $C_{30}H_{31}Cl_2NO_4$ requires 550.1552; ^{1}H NMR (400 MHz, $CDCl_3$) δ 7.39 (4H, s, H-2''), 7.34 (1H, d, *J* = 2.1 Hz, H-2'), 7.27 (1H, d, *J* = 8.3 Hz, H-5'), 7.23 (4H, s, H-3''), 7.10 (1H, dd, *J* = 8.3, 2.1, Hz, H-6'), 5.72 (1H, bs, N<u>H</u>), 5.15 (2H, d, J_{AB} = 12.4 Hz, OCH_2), 5.05 (2H, d, J_{AB} = 12.3 Hz, OCH_2), 5.09 (1H, s, H-4), 2.48 (6H, s, Ar_{Me}), 2.46 (6H, s, Me); ^{13}C NMR (100 MHz, $CDCl_3$) δ 166.2 (CO), 147.1 (C-2), 143.8 (C-1'), 137.1 (C-

4''), 132.6 (C-1''), 131.1 (C-3'), 131.0 (C-4'), 129.5 (C-2'), 129.1 (C-5'), 128.5 (C-2''), 127.6 (C-3''), 127.1 (C-6'), 102.8 (C-3), 65.2 (OCH_2), 39.7 (C-4), 20.6 (Ar_{Me}), 19.8 (Me); v_{max}/ cm^{-1} 3313 (N-H, two broad peaks), 3101 (C-H aromatic), 2947 (C-H alkane), 1685 (C=O), 1652 (C=C aromatic), 1093 (C-O ester).

***Bis*(3-methylbenzyl)-4-(3,4-dichlorophenyl)-2,6-dimethyl-1,4-dihydropyridine-3,5-dicarboxylate (31)**

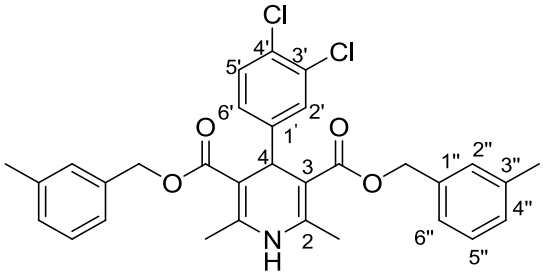

The reaction yielded compound **31** (120 mg, 78%) as colourless crystals; m.p. 107-109 °C; HPLC purity: 98%; HRMS (EI): m/z 550.1543 $[M+H]^+$, $C_{31}H_{30}Cl_2NO_4$ requires 550.1552; ^1H NMR (400 MHz, $CDCl_3$) δ 7.25 (1H, d, *J* = 2.1 Hz, H-2'), 7.19 (2H, t, *J* = 8.2 Hz, H-5''), 7.15 (1H, d, *J* = 8.3 Hz, H-5'), 7.10 (2H, d, *J* = 7.6 Hz, H-2''), 7.00 (2H, m, H-4''), 6.98 (2H, m, H-6''), 6.98-6.95 (1H, m, H-6'), 5.61 (1H, bs, NH-1), 5.05 (2H,d, J_{AB} = 12.0 Hz, OCH_2), 5.00 (2H, d, J_{AB} = 12.1 Hz, OCH_2), 4.97 (1H, s, H-4), 2.35 (6H, s, Ar_{Me}); 2.30 (6H, s, Me); ^{13}C NMR (100 MHz, $CDCl_3$) δ 166.8 (CO), 147.8 (C-2), 144.6 (C-1'), 138.1 (C-3''), 136.2 (C-1''), 131.8 (C-3'), 130.1 (C-2'), 130.0 (C-4'), 129.8 (C-5'), 128.7 (C-2''), 128.6 (C-5''), 128.4 (C-4''), 127.2(C-6'), 125.1 (C-6''), 103.5 (C-3), 65.9 (OCH_2), 39.3 (C-4), 21.3 (Ar_{Me}), 19.8 (Me); v_{max}/ cm^{-1} 3314 (N-H), 3049 (C-H aromatic), 2925 (C-H alkane), 1683 (C=O), 1641 (C=C aromatic), 1093 (C-O ester).

***Bis*(3,4-dimethylbenzyl)-4-(3,4-dichlorophenyl)-2,6-dimethyl-1,4-dihydropyridine-3,5-dicarboxylate (32)**

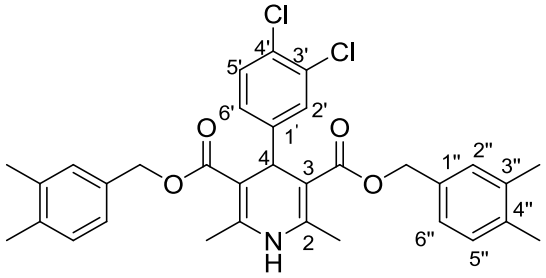

The reaction yielded compound **32** (157 mg, 97%) as yellow crystals; m.p. 111-112 °C; HPLC purity: 95%; HRMS (EI): m/z 578.1860 $[M+H]^+$, $C_{33}H_{34}Cl_2NO_4$ requires 578.1865; ^{1}H NMR (400 MHz, $CDCl_3$) δ 7.23 (1H, d, *J* = 2.1 Hz, H-2'), 7.14 (1H, d, *J* = 8.3 Hz, H-5'), 7.06 (2H, d, *J* = 8.3 Hz, H-5''), 6.98(1H, dd, *J* = 8.3, 2.1 Hz, H-6'), 6.95 (2H, bs, H-6''), 6.93 (2H, bs, H-2''), 5.59 (1H, bs, NH), 5.02 (2H, d, J_{AB} = 12.5 Hz, OCH_2),5.00,4.96 (2H, d, J_{AB} = 12.4 Hz, OCH_2), 4.98 (1H, s, H-4), 2.34 (6H, s, Me), 2.25 (6H, s, Ar_{Me}-3''), 2.21 (6H, s, Ar_{Me}-4''); ^{13}C NMR (100 MHz, $CDCl_3$) δ 166.9 (CO), 147.8 (C-2), 144.4 (C-1'), 136.6 (C-3''), 136.3 (C-4''), 133.7 (C-1''), 131.7 (C-2') 130.1 (C-5'), 129.9 (C-3'), 129.7 (C-5''), 129.6 (C-4'), 129.4 (C-2''), 127.8 (C-6'), 125.6 (C-6''), 103.5 (C-3), 65.8 (OCH_2), 39.3 (C-4), 19.8 (Me), 19.6 (Ar_{Me}-3''), 19.4 (Ar_{Me}-4'');ν_{max}/cm^{-1} 3323 (N-H), 3101 (C-H aromatic), 2935 (C-H alkane), 1686 (C=O), 1654 (C=C aromatic), 1089 (C-O ester).

***Bis*(4-chlorobenzyl)-4-(3,4-dichlorophenyl)-2,6-dimethyl-1,4-dihydropyridine-3,5-dicarboxylate (33)**

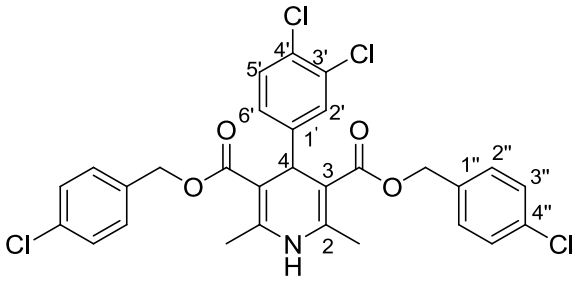

The reaction yielded compound **33** (146 mg, 89%) as colourless crystals; m.p. 176-178 °C; HPLC purity: 97%; HRMS (EI): m/z 590.0452, $[M+H]^+$, $C_{29}H_{24}Cl_4NO_4$ requires 590.0459; ^{1}H NMR (400 MHz, $CDCl_3$) δ 7.28 (4H, d, *J* = 6.5, H-3''), 7.18,7.16 (1H, d, *J* = 8.2 Hz, H-5'), 7.17 (1H, d, *J* = 2.0 Hz, H-2'), 7.12 (4H, d, *J* = 6.6, H-2''), 6.96 (1H, dd, *J* = 8.2, 2.0 Hz, H-6'), 5.65 (1H, bs, NH), 5.07, 4.94 (2H, d, J_{AB} = 12.5 Hz, OCH_2),4.97 (2H, d, J_{AB} = 12.5 Hz, OCH_2), 4.89 (1H, s, H-4), 2.34 (6H, s, Me); ^{13}C NMR (100 MHz, $CDCl_3$) δ 166.6 (C-O), 147.6 (C-2), 144.8 (C-1'), 134.7(C-1''134.0 (C-4''), 131.8 (C-3'), 130.1 (C-4'), 130.0 (C-2'), 129.9(C-5'), 129.5 (C-3''), 128.7 (C-2''), 127.6 (C-6'), 103.9 (C-3), 65.1 (OCH_2), 39.4 (C-4), 19.8 (Me); ν_{max}/ cm^{-1} 3316 (N-H, two broad peaks), 3105 (C-H aromatic), 2949 (C-H alkane), 1685 (C=O), 1652 (C=C aromatic), 1088 (C-O ester).

***Bis*(3-chlorobenzyl)-4-(3,4-dichlorophenyl)-2,6-dimethyl-1,4-dihydropyridine-3,5-dicarboxylate (34)**

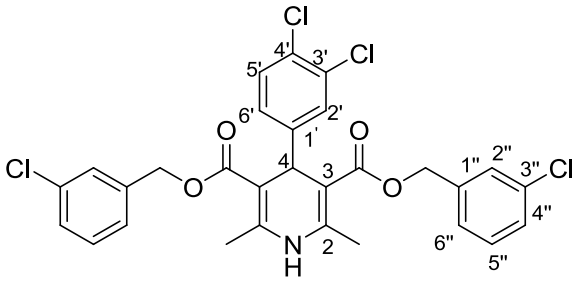

The reaction yielded compound **34** (162 mg, 96%) as colourless crystals; m.p. 142-144 °C; HPLC purity: 98%; HRMS (EI): m/z 590.0433, $[M+H]^+$, $C_{29}H_{24}Cl_4NO_4$ requires 590.0459 ^{1}H NMR (400 MHz, $CDCl_3$) δ 7.25 (2H, d, *J* = 1.8 Hz, H-6''), 7.24,7.18 (1H, d, *J* = 8.2 Hz, H-5'), 7.22 (2H, d, *J* = 1.9 Hz, H-4''), 7.20 (1H, d, *J* = 2.4 Hz, H-2'), 7.16 (2H, bs, H-2''), 7.05 (2H, d, *J* = 7.6 Hz, H-5'') 6.96 (1H, dd, *J* = 8.2, 2.0 Hz, H-6'), 5.69 (1H, bs, NH), 5.11 (2H, d, J_{AB} = 12.0 Hz, OCH_2),5.01 (2H, d, J_{AB} = 12.0 Hz, OCH_2), 4.97 (1H, s, H-4), 2.35 (6H, s, Me); ^{13}C NMR (100 MHz, $CDCl_3$) δ 166.5 (CO), 147.5 (C-2), 145.0 (C-1'), 138.3 (C-1''), 134.4 (C-3''), 132.2 (C-3'), 130.3 (C-4'), 129.9 (C-2'), 129.8(C-5'), 129.7 (C-4''), 128.2(C-6''), 128.0 (C-2''), 127.6 (C-6'), 126.0 (C-5''), 103.2 (C-3), 65.0 (OCH_2), 39.2 (C-4), 19.8 (Me); v_{max}/ cm^{-1} 3346 (N-H), 3107 (C-H aromatic), 2936 (C-H alkane), 1703 (C=O), 1649 (C=C aromatic), 1114 (C-O ester).

***Bis*(2-chlorobenzyl)-4-(3,4-dichlorophenyl)-2,6-dimethyl-1,4-dihydropyridine-3,5-dicarboxylate (35)**

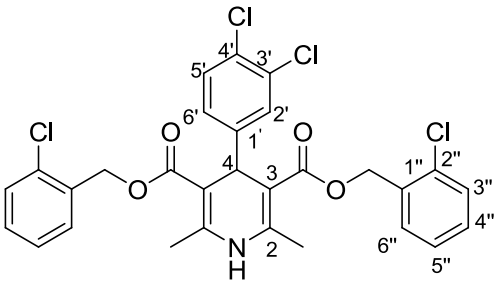

The reaction yielded compound **35** (129 mg, 83%) as yellow crystals; m.p. 122-123 °C; HPLC purity: 96%; HRMS (EI): m/z 590.0434, $[M+H]^+$, $C_{29}H_{24}Cl_4NO_4$ requires 590.0459; ^{1}H NMR (400 MHz, $CDCl_3$) δ 7.35 (2H, d, *J* = 8.0 Hz, H-3''), 7.27-7.23 (2H, m, H-6''), 7.21 (1H, d, *J* = 2.0

Hz, H-2'), 7.17 (2H, t, *J* = 2.4 Hz, H-4''), 7.16 (2H, d, *J* = 1.1 Hz, H-5''), 7.12 (1H, d, *J* = 8.3 Hz, H-5') 6.99 (1H, dd, *J* = 8.2, 2.2 Hz, H-6'), 5.67 (1H, bs, NH), 5.18 (2H, d, J_{AB} = 12.9 Hz, H-13), 5.05(2H, d, J_{AB} = 12.8 Hz, OCH_2), 5.0 (1H, s, H-4), 2.35 (6H, s, H-5); ^{13}C NMR (100 MHz, $CDCl_3$) δ 166.6 (CO), 147.7 (C-2), 144.9 (C-1'), 133.9(C-1''), 133.7 (C-3'), 131.8 (C-4'), 130.1 (C-4''), 130.0 (C-5'), 129.8 (C-2'), 129.5(C-6''), 129.3 (C-3''), 127.6 (C-6'), 126.8 (C-5''), 103.4 (C-3), 63.2 (OCH_2), 39.2 (C-4), 19.8 (Me); v_{max}/ cm^{-1} 3365 (N-H), 3066 (C-H aromatic), 2951 (C-H alkane), 1703 (C=O), 1679 (C=C aromatic), 1085 (C-O ester).

***Bis*(4-bromobenzyl)-4-(3,4-dichlorophenyl)-2,6-dimethyl-1,4-dihydropyridine-3,5-dicarboxylate (36)**

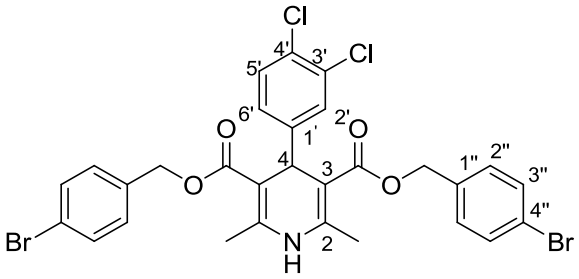

The reaction yielded compound **36** (139 mg, 73%) as colourless crystals; m.p. 178-179 °C; HPLC purity: 95%; HRMS (EI): m/z 677.9428, $[M+H]^+$, $C_{29}H_{24}Cl_2NO_4Br_2$ requires 677.9449;^{1}H NMR (400 MHz, $CDCl_3$) δ 7.28 (4H, d, *J* = 6.4 Hz, H-3''), 7.19,7.16 (1H, d, *J* = 8.6 Hz, H-5'), 7.17 (1H, d, *J* = 2.2 Hz, H-2'), 7.06 (4H, d, *J* = 6.4 Hz, 2''), 6.96 (1H, dd, *J* = 8.3, 2.1 Hz, H-6'), 5.65 (1H, bs, NH), 5.07 (2H, d, J_{AB} = 12.6 Hz, OCH_2),4.97 (2H, d, J_{AB} = 12.6 Hz, OCH_2), 4.93 (1H, s, H-4), 2.34 (6H, s, Me); ^{13}C NMR (100 MHz, $CDCl_3$) δ 166.6 (CO), 147.6 (C-2), 144.8 (C-1'), 135.2(C-1''), 131.8 (C-3'), 131.7 (C-3''), 130.2 (C-4'), 130.1 (C-2'), 129.9(C-5'), 129.8 (C-2''), 127.5 (C-6'), 122.5 (C-4''), 103.4 (C-3), 65.1 (OCH_2), 39.3 (C-4), 19.8 (Me); v_{max}/ cm^{-1} 3317 (N-H), 3101 (C-H aromatic), 2947 (C-H alkane), 1687 (C=O), 1651 (C=C aromatic), 1097 (C-O ester).

***Bis*(3,4-dichlorobenzyl)-4-(3,4-dichlorophenyl)-2,6-dimethyl-1,4-dihydropyridine-3,5-dicarboxylate (37)**

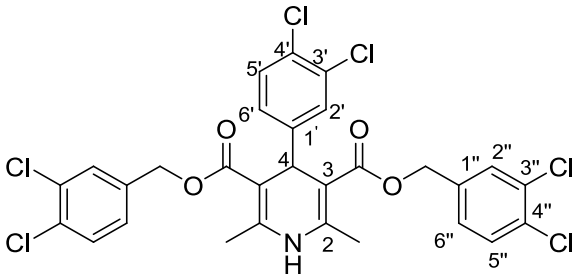

The reaction was performed on a 0.568 mmol scale. The reaction yielded compound **37** (231 mg, 62%) as colourless crystals; m.p. 167-169 °C; HPLC: 95%; HRMS (EI): m/z 655.9504, $[M-H]^-$, $C_{29}H_{20}Cl_6NO_4$ requires 655.9523; ^{1}H NMR (400 MHz, $CDCl_3$) δ 7.30 (2H, d, *J* = 8.3 Hz, H-5''), 7.19 (1H, d, *J* = 2.1 Hz, H-2'), 7.17 (2H, d, *J* = 2.1 Hz, H-2''), 7.14 (1H, d, *J* = 10.1 Hz, H-5'), 6.94 (2H, dd, *J* = 10.3, 2.1 Hz, H-6'), 6.91 (2H, dd, *J* = 8.2, 2.1 Hz, H-6''), 5.65 (1H, bs, NH), 5.08 (2H, d, J_{AB} = 12.8 Hz, OCH_2), 4.92 (2H, d, J_{AB} = 12.8 Hz, OCH_2), 4.87 (1H, s, H-4), 2.24 (6H, s, Me); ^{13}C NMR (100 MHz, $CDCl_3$) δ 166.4 (CO), 147.4 (C-2), 145.1 (C-1'), 136.5 (C-1''), 132.7 (C-3''), 132.1 (C-4'') 132.0 (C-3'), 130.5 (C-5''), 130.4 (C-4'), 130.0 (C-2'), 129.9 (C-5'), 129.8 (C-2''), 127.5 (C-6'), 127.2 (C-6''), 103.0 (C-3), 64.5 (OCH_2), 39.2 (C-4), 19.8 (Me); v_{max}/cm^{-1} 3350 (N-H), 3076 (C-H aromatic), 2950 (C-H alkane), 1699 (C=O), 1651 (C=C aromatic), 1095 (C-O ester).

***Bis*(2,4-dichlorobenzyl-4-(3,4-dichlorophenyl)-2,6-dimethyl-1,4-dihydropyridine-3,5-dicarboxylate (38)**

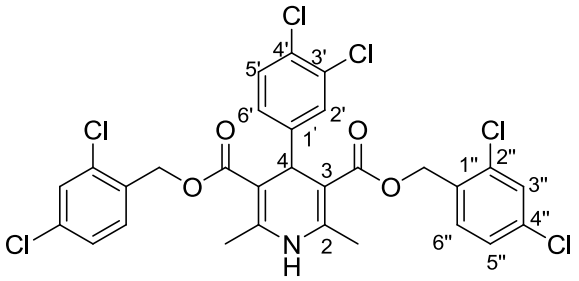

The reaction was performed on a 0.568 mmol scale. The reaction yielded compound **38** (231 mg, 62%) as colourless crystals; m.p. 162-164 °C; HPLC: 99%; HRMS (EI): m/z 657.9674, $[M-H]^-$, $C_{29}H_{22}Cl_6NO_4$ requires 657.9680; ^{1}H NMR (400 MHz, $CDCl_3$) δ 7.39 (2H, d, *J* = 2.8 Hz, H-3''), 7.18 (1H, d, *J* = 2.0 Hz, H-2'), 7.16 (1H, d, *J* = 8.3 Hz, H-5'), 7.14 (2H, dd, *J* = 9.0, 2.8 Hz, H-5''), 7.09 (2H, d, *J* = 9.0 Hz, H-6''), 6.97 (1H, dd, *J* = 8.3, 2.0 Hz, H-6'), 5.70 (1H, bs, NH), 5.15

(2H, d, J_{AB} = 12.8 Hz, OCH_2), 5.04 (2H, d, J_{AB} = 12.6 Hz, OCH_2), 4.93 (1H, s, H-4), 2.35 (6H, s, Me); ^{13}C NMR (100 MHz, $CDCl_3$) δ 166.4 (CO), 147.4 (C-2), 145.1 (C-1'), 134.7 (C-4''), 134.5 (C-2''), 132.5 (C-1''), 131.8 (C-3'), 131.0 (C-3''), 130.2 (C-4'), 130.0 (C-6''), 129.9 (C-2'), 129.4 (C-5'), 127.5 (C-6'), 127.1 (C-5''), 103.3 (C-3), 62.5 (OCH_2), 39.2 (C-4), 19.8 (Me);
v_{max}/ cm^{-1} 3350 (N-H), 3076 (C-H aromatic), 2950 (C-H alkane), 1699 (C=O), 1651 (C=C aromatic), 1095 (C-O ester).

Dimethyl 4-(3,4-dichlorophenyl)-2,6-diethyl-1,4-dihydropyridine-3,5-dicarboxylate (39)

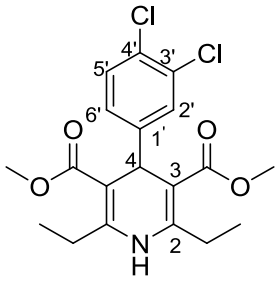

The reaction was performed on a 0.568 mmol scale. The reaction yielded compound **39** (210 mg, 93%) as colourless crystals; m.p. 147-149 °C; HPLC purity: 96%; HRMS (EI): m/z 398.0920, $[M+H]^+$, $C_{19}H_{22}Cl_2NO_4$ requires 398.0926; ^1H NMR (400 MHz, $CDCl_3$) δ 7.31 (1H, d, *J* = 2.1 Hz, H-2'), 7.27 (1H, d, *J* = 8.2 Hz, H-5'), 7.11 (1H, dd, *J* = 8.4 Hz, 2.2 Hz, H-6'), 5.74 (1H, bs, N<u>H</u>), 4.97 (1H, s, H-4), 3.67 (6H, s, OMe), 2.64-2.56 (4H, m, CH_2), 1.25 (6H, t, *J* = 7.5 Hz, Me); ^{13}C NMR (100 MHz, $CDCl_3$) δ 167.1 (CO), 150.3 (C-2), 147.7 (C-1'), 131.9 (C-3'), 129.9 (C-2'), 129.7 (C-4'), 129.6 (C-5'), 127.1 (C-6'), 102.3 (C-3), 51.1 (OMe), 38.8 (C-4), 26.0 (CH_2), 12.7 (Me); v_{max}/ cm^{-1} 3335 (N-H), 3238 (C-H aromatic), 2986-2880 (C-H alkane), 1701 (C=O), 1647 (C=C aromatic), 1119 (C-O ester).

Diethyl-4-(3,4-dichlorophenyl)-2,6-diethyl-1,4-dihydropyridine-3,5-dicarboxylate(40)

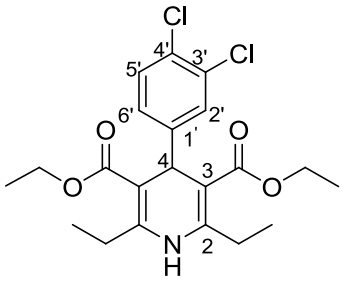

The reaction was performed on a 0.568 mmol scale. The reaction yielded compound **40** (239 mg, 98%) as colourless crystals; m.p. 119-121 °C; HPLC: 99%; HRMS (EI): m/z 426.1243,

$[M+H]^+$, $C_{21}H_{26}Cl_2NO_4$ requires 426.1239; ^{1}H NMR (400 MHz, $CDCl_3$) δ 7.34 (1H, d, *J* = 2.1 Hz, H-2'), 7.27 (1H, d, *J* = 8.3 Hz, H-5'), 7.12 (1H, dd, *J* = 8.3 Hz, 2.1 Hz, H-6'), 5.66 (1H, bs, NH), 4.95-4.60 (1H, s, H-4), 4.10-3.86 (4H, m, OCH_2), 2.70-2.30 (4H, m, CH_2), 1.25 (6H, t, *J* = 7.1, Me $_{ester}$), 1.20 (6H, t, *J* = 7.5 Hz, Me); ^{13}C NMR (100 MHz, $CDCl_3$) δ 166.8 (CO), 149.9 (C-2), 148.1 (C-1'), 130.1 (C-4'), 130.0 (C-2'), 129.9 (C-4'), 129.8 (C-5'), 127.4 (C-6'), 102.6 (C-3), 59.9 (OCH_2), 39.4 (C-4), 26.1 (CH_2), 14.2 (Me $_{ester}$), 12.7 (Me); ν_{max}/ cm^{-1} 3350 (N-H), 3240 (C-H aromatic), 2983-2881 (C-H alkane), 1695 (C=O), 1645 (C=C aromatic), 1119 (C-O ester).

3-*tert*-butyl-5-ethyl-4-(3,4-dichlorophenyl))-2,6-dimethyl-1,4-dihydropyridine-3,5-dicarboxylate (41)

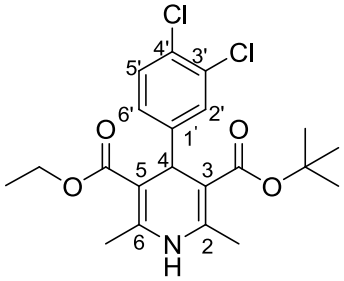

***Method*:** *tert*-Butyl acetoacete (0.568 mmol, 2.00 eq) and 3,4-dichlorobenzaldehyde (0.284 mmol, 1.00 eq) in ethanol (1.00 mL) were added to a microwave reaction vial, a few drops of triethylamine were then added and the mixture was microwave irradiated for a minute at 60 °C. Ethyl-3-aminocrotonate (0.568 mmol, 2.00 eq) was added followed by a few drops of glacial acetic acid and the resultant mixture was further irradiated at 60 °C, for 15 minutes. The general extraction and purification for 1,4-dihydropyridines was then followed to yield compound **41** (43.0 mg, 36%) as an orange oil; HPLC: 95%; HRMS (EI): m/z 426.1223, $[M+H]^+$, $C_{21}H_{26}Cl_2NO_4$ requires 426.1239; ^{1}H NMR (400 MHz, $CDCl_3$) δ 7.34 (1H, d, *J* = 2.1 Hz, H-2'), 7.27 (1H, d, *J* = 8.3 Hz, H-5'), 7.12 (1H, dd, *J* = 8.3 Hz, 2.1 Hz, H-6'), 5.52 (1H, bs, NH-1), 4.90 (1H, s, H-4), 4.10 (2H, q, *J* = 7.2 Hz, OCH_2), 2.32(3H, s, Me-2), 2.30 (3H, s, Me-6), 1.40 (9H, s, Me$_{t\text{-butyl}}$), 1.22 (3H, t, *J* = 7.1 Hz, Me $_{ester}$); ^{13}C NMR (100 MHz, $CDCl_3$) δ 167.2 (CO_{ethyl}) 166.5 ($CO_{t\text{-butyl}}$), 148.1 (C-2), 144.3 (C-1'), 143.1 (C-6), 131.7 (C-3'), 130.1 (C-2'), 129.7 (C-4'), 129.6 (C-5'), 127.5 (C-6'), 105.0 (C-5), 103.8 (C-3), 80.1 (OC-*t*-butyl), 59.8 (OCH_2), 39.7 (C-4), 28.3 (Me$_{t\text{-butyl}}$), 19.6 (Me-2), 19.5 (Me-6), 14.2 (Me $_{ester}$) .

Diethyl 4-(3,4-dichlorophenyl)-1,2,6-trimethyl-1,4-dihydropyridine-3,5-dicarboxylate (42)

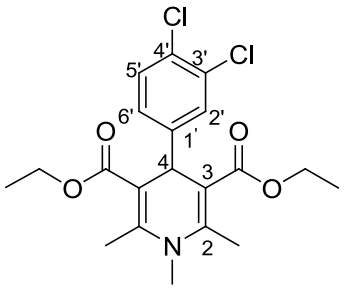

***Method*:** Sodium hydride (2.51 mmol, 2.00 eq) was dissolved in anhydrous THF (2.00 mL) and the mixture cooled to 0 °C under N_2 atmoshpere. A solution of compound **23** (0.752 mmol, 1.00 eq) in THF (2.00 mL) was then added slowly to the cooled mixture for a period of 10 minutes and the resultant mixture warmed up to room temperature and left stiring for further 20 minutes before being cooled to 0 °C again. Dimethyl sulfate (0.903 mmol, 1.20 eq) was then added drop-wise for another 10 minutes and the mixture stirred to room temperature for further 5 minutes. Removal of THF was then done under reduced pressure and the resultant crude mixture quenched with sodium bicarbonate (5.00 mL) and washed with brine (10.0 mL). Ethyl acetate (3x 15.0 mL) was used to extract the organic extracts which were then dried with $MgSO_4$ and the solvent removed on the rotary-evaporator to yield crude product that was purified using column chromatography (solvent system hexane/ethyl acetate (3:1)) to yield compound **42** (304 mg, 98%) as a yellow solid; m.p. 74-76 °C; HPLC: 97%; HRMS (EI): m/z 412.1080, $[M+H]^+$, $C_{20}H_{24}Cl_2NO_4$ requires 412.1082; ^{1}H NMR (400 MHz, $CDCl_3$) δ 7.25 (1H, d, *J* = 8.4 Hz, H-5'), 7.23 (1H, d, *J* = 2.4 Hz, H-2'), 7.03 (1H, dd, *J* = 8.3 Hz, 2.2 Hz, H-6'), 5.01 (1H, s, H-4), 4.18-4.12 (4H, m, OCH_2), 3.18 (3H, s, N<u>Me</u>), 2.48 (6H, s, Me), 1.27 (6H, t, *J* = 7.1 Hz, Me $_{ester}$). ^{13}C NMR (100 MHz, $CDCl_3$) δ 167.3 (CO), 149.5 (C-2), 146.3 (C-1'), 131.7 (C-3'), 129.8 (C-2'), 129.7 (C-4'), 129.1 (C-5'), 126.4 (C-6'), 105.5 (C-3), 59.9(OCH_2), 37.8 (C-4), 33.9 (NHMe), 16.3 (Me), 14.1 (Me $_{ester}$). v_{max}/ cm^{-1} 3063 (C-H aromatic), 2978-2880 (C-H alkane), 1685 (C=O), 1637 (C=C aromatic), 1101 (C-O ester).

***Bis*(2-(4-(tert-butoxycarbonyl)piperazin-1-yl)ethyl)-4-(3,4-dichlorophenyl)-2,6-dimethyl-1,4-dihydropyridine-3,5-dicarboxylate (43)**

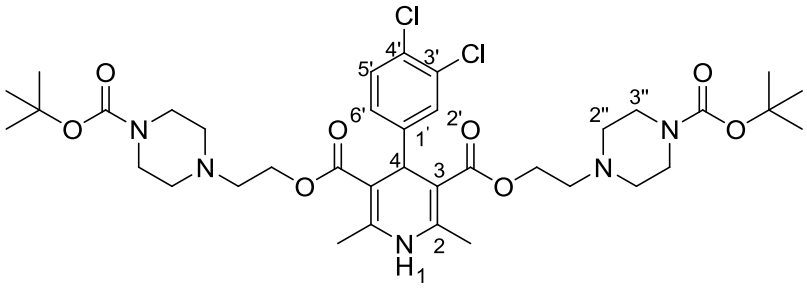

The reaction yielded compound **43** (136 mg, 62%) as a yellow solid; m.p. 62-64 °C; HPLC: 97% HRMS (EI): m/z 766.3346 [M+H$^+$], $C_{37}H_{54}Cl_2N_5O_8$ requires 776.3349; ^{1}H NMR (400 MHz, $CDCl_3$) δ 7.34 (1H, d, *J* = 2.0 Hz, H-2'), 7.27 (1H, d, *J* = 8.1 Hz, H-5'), 7.15 (1H, dd, *J* = 8.2 Hz, 2.0 Hz, H-6'), 5.69 (1H, s, NH-1), 4.95 (1H, s, H-4), 4.18-3.98 (4H, m, OCH_2), 3.38 (8H, t, *J* = 5.20 Hz, H-3''), 2.58 (4H, td, *J* = 12.0, 5.8 Hz, NCH_2), 2.39 (8H, t, *J* = 5.20 Hz, H-2''), 2.35 (6H, s, Me), 1.46 (18H, s, $Me_{t\text{-butyl}}$). ^{13}C NMR (100 MHz, $CDCl_3$) δ 166.9 (CO),154.8 (NCO), 147.8 (C-2), 144.63 (C-1'), 131.7 (C-3'), 130.0 (C-4'), 129.9 (C-2'),129.8 (C-5'), 127.5 (C-6'), 103.5 (C-3), 79.7 (OC-*t*-butyl), 61.2 (CH_2), 56.5 (NCH_2), 53.7 (C-3''), 43.6 (C-2''), 39.1 (C-4), 28.5 ($Me_{t\text{-butyl}}$), 19.7 (Me).

Bis(2-(piperidin-1-yl)ethyl)-4-(3,4-dichlorophenyl)-2,6-dimethyl-1,4-dihydropyridine-3,5-dicarboxylate (44)

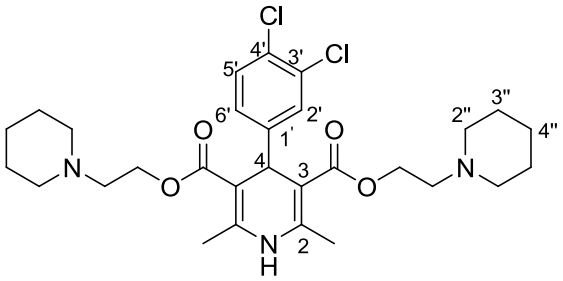

The reaction was performed on a 0.568 mmol scale. The reaction yielded compound **44** (267 mg, 83%) as an orange oil; HPLC: 99%; HRMS (EI): m/z 564.2393, [M+H]$^+$, $C_{21}H_{26}Cl_2N_3O_4$ requires 564.2396; ^{1}H NMR (400 MHz, $CDCl_3$) δ 7.34 (1H, d, *J* = 2.0 Hz, H-2'), 7.25 (1H, d, *J* = 8.3 Hz, H-5'), 7.17 (1H, dd, *J* = 8.3 Hz, 2.1 Hz, H-6'), 5.63 (1H, s, NH-1), 4.96 (1H, s, H-4), 4.20 (4H, q, *J* = 7.2 Hz, OCH_2), 2.59 (4H, t, *J* = 6.0 Hz, NCH_2), 2.40 (8H, t, *J* = 5.4 Hz, H-2''), 2.35 (6H, s, Me), 1.58 (8H, m, H-3''), 1.50-1.43 (4H, m, H-4''); ^{13}C NMR (100 MHz, $CDCl_3$) δ 167.0 (CO), 147.7 (C-2), 144.6 (C-1'), 131.7 (C-3'), 130.0 (C-4'), 129.9 (C-2'),129.8

(C-5'), 127.6 (C-6'), 103.3 (C-3), 61.7 (CH_2), 57.3 (C-2''), 54.7 (NCH_2), 39.1 (C-4), 25.9 (C-3''), 24.1 (C-4''), 19.7 (Me).

General Procedure for the syntheses of the 1,4-pyridine derivatives:

A suspension of a 1,4-dihydropyridine (0.502 mmol, 1.00 eq), oxone® (0.753 mmol, 1.50 eq), wet silica (50 % *w*/*w*) (0.753 mmol, 1.50 eq) and $NaNO_2$ (1.51 mmol, 3.00 eq) in DCM (2.00 mL) was taken into a round bottom flask and stirred at room temperature for the required time (60-120 minutes). The mixture was then filtered and the residue washed with DCM (3x 10 mL) followed by filtrate being dried with $MgSO_4$. The solvent was then evaporated under reduced pressure and crude mixture purified by column chromatography followed by recrystallization from DCM/ hexane to yield the required product.

Diethyl 4-(3,4-dichlorophenyl)-2,6-dimethylpyridine-3,5-dicarboxylate (45)

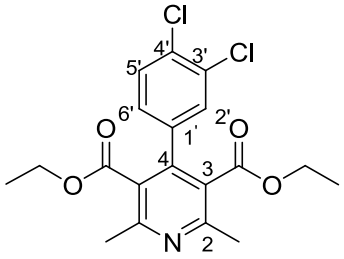

The reaction yielded compound **45** (139 mg, 70%) as colourless crystals; m.p. 62-64 °C; ^{1}H NMR (400 MHz, $CDCl_3$) δ 7.45 (1H, d, *J* = 8.3 Hz, H-5'), 7.38 (1H, d, *J* = 2.0 Hz, H-2'), 7.10 (1H, dd, *J* = 8.3 Hz, 2.0 Hz, H-6'), 4.08 (4H, q, *J* = 9.4 Hz, OCH_2), 2.60 (6H, s, , Me), 1.05 (6H, t, *J* = 7.2 Hz, ester Me); ^{13}C NMR (100 MHz, $CDCl_3$) δ 167.4 (CO), 155.8 (C-2), 143.5 (C-4), 136.3 (C-1'), 133.0 (C-4'), 132.5 (C-3'), 130.2 (C-5'), 130.1 (C-5'), 127.7 (C-6'), 126.6 (C-3), 61.6 (OCH_2), 23.0 (Me), 13.8 (ester Me). v_{max}/cm^{-1} 3059 (C-H aromatic), 2959 (C-H alkane), 1726 (C=O), 1664 (C=C aromatic), 1545 (C=N), 1122 (C-O ester).

Diethyl-4-(4-chloro-3-(trifluoromethyl)phenyl)-2,6-dimethylpyridine-3,5-dicarboxylate (46)

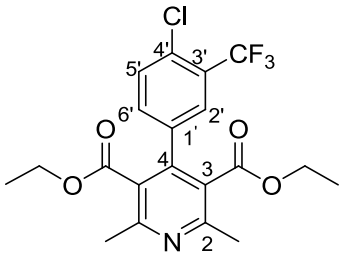

The reaction yielded compound **46** (142 mg, 66%) as yellow crystals; m.p. 71-73 °C; HPLC: 98% HRMS (EI): m/z 430.1031 [M^+H^+], $C_{20}H_{20}F_3ClNO_4$ requires 430.1033; ^{1}H NMR (400 MHz, $CDCl_3$) δ 7.63 (1H. d, *J* = 2.0 Hz, H-2'), 7.53 (1H, d, *J* = 8.4 Hz, H-5'), 7.38 (1H, dd, *J* = 8.4, 2.0 Hz, H-6'), 4.06 (4H, q, *J* = 7.1 Hz, OCH_2), 2.38 (6H,s, Me), 1.22 (6H, t, *J* = 7.2 Hz, Me $_{ester}$); ^{13}C NMR (100 MHz, $CDCl_3$) δ 167.4 (CO), 156.2 (C-2), 143.5 (C-4), 135.6 (C-1'), 132.9 (C-4'), 132.8 (C-2'), 131.4 (C-5'), 128.5 (q, J_{CF} = 30 Hz, C-3'),127.6 (C-6'), 126.7 (C-3), 122.0 (q, J_{CF} = 200 Hz $\underline{C}F_3$), 61.8 (OCH_2), 23.5 (Me), 13.8 (Me $_{ester}$). ν_{max}/ cm^{-1} 3063 (C-H aromatic), 2965 (C-H alkane), 1730 (C=O), 1566 (C=C aromatic), 1547 (C=N), 1102 (C-O ester).

Diethyl 2,6-dimethyl-4-(4-nitrophenyl)pyridine-3,5-dicarboxylate (47)

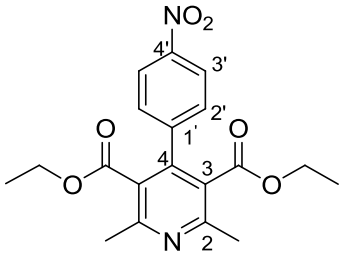

The reaction yielded compound **47** (129 mg, 69%) as yellow crystals; m.p. 114-115 °C; HPLC: 97%; ^{1}H NMR (400 MHz, $CDCl_3$) δ= 8.24 (2H, d, *J* = 8.8 Hz, H-3'), 7.50 (2H, d, *J* = 8.8 Hz, H-2'), 4.04 (4H, q, *J* = 7.2 Hz, OCH_2), 2.60 (6H, s, Me), 0.98 (6H, t, *J* = 7.2 Hz, Me $_{ester}$); ^{13}C NMR (100 MHz, $CDCl_3$) δ 167.1 (CO), 156.2 (C-2), 145.0 (C-4), 144.0 (C-4'), 143.3 (C-1'), 129.4 (C-2'), 126.2 (C-3), 123.3 (C-3'), 61.5 (OCH_2), 23.1 (Me), 13.7 (Me $_{ester}$). ν_{max}/ cm^{-1} 3067 (C-H aromatic), 2960 (C-H alkane), 1726 (C=O), 1565 (C=C aromatic), 1547 (C=N), 1103 (C-O ester).

***Bis*(2-chlorobenzyl) 4-(3,4-dichlorophenyl)-2,6-dimethylpyridine-3,5-dicarboxylate (48)**

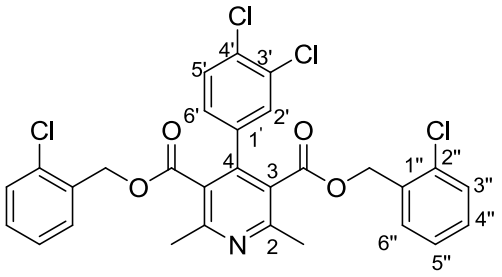

The reaction was performed on a 0.109 mmol scale. The reaction yielded compound **48** (40 mg, 63%) as yellow crystals; m.p. 123-125 °C; HPLC: 96% HRMS (EI): m/z 588.0306 [M^+H^+], $C_{29}H_{22}Cl_4NO_4$ requires 588.0303; ^{1}H NMR (400 MHz, $CDCl_3$) δ 7.31 (2H, d, *J* = 8.0 Hz, H-3''), 7.29 (1H, d, *J* = 2.1 Hz, H-2'), 7.22 (2H, t, *J* = 9.2 Hz, H-5''), 7.16 (2H, d, *J* = 7.1 Hz, H-6''), 7.09 (2H, d, *J* = 7.5, H-4''), 7.02 (1H, d, *J* = 8.3 Hz, H-5'), 6.89 (1H, dd, *J* = 8.3, 2.1 Hz, H-6'), 5.15 (4H, s, OCH_2), 2.60 (6H, s, Me); ^{13}C NMR (100 MHz, $CDCl_3$) δ 167.1 (CO), 156.1 (C-2), 146.3 (C-4), 135.6 (C-1'), 134.3 (C-1''), 132.6 (C-4'), 132.0 (C-3'), 131.0 (C-3''), 130.1 (C-6''), 130.0 (C-2'), 129.8 (C-5'), 129.7 (C-2''), 129.6 (C-4''), 126.9 (C-6'), 126.2 (C-5''), 64.6 (OCH_2), 23.0 (Me); ν_{max}/ cm^{-1} 3068 (C-H aromatic), 2956 (C-H alkane), 1729 (C=O), 1680 (C=C aromatic), 1548 (C=N), 1101 (C-O ester).

Dibenzyl 4-(3,4-dichlorophenyl)-2,6-dimethylpyridine-3,5-dicarboxylate (49)

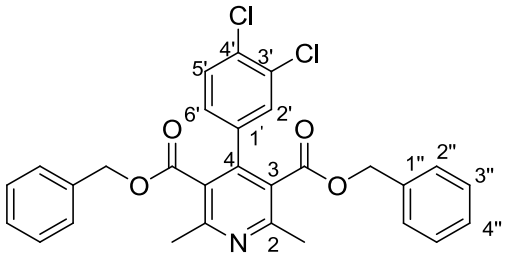

The reaction was performed as for the previously described general procedure for syntheses of 1,4-dihydropyrines, however, the reaction yielded compound **49** (140 mg, 95%) as colourless powder; m.p. 106-108 °C; HPLC: 95% HRMS (EI): m/z 520.1087 [$M+H^+$], $C_{29}H_{24}Cl_2NO_4$ requires 520.1082; ^{1}H NMR (400 MHz, $CDCl_3$) δ 7.30 (6H, m, H-3'' and H-4''), 7.18 (1H, d, *J* = 2.2 Hz, H-2'), 7.06 (1H, d, *J* = 8.4 Hz, H-5'), 7.05, 7.03 (4H, m, H-2''), 6.87 (1H, dd, *J* = 8.4, 2.2 Hz, H-6'), 5.01 (4H, s, OCH_2), 2.55 (6H, s, Me); ^{13}C NMR (100 MHz, $CDCl_3$) δ 167.3 (CO), 156.1 (C-2), 143.5 (C-4), 137.8 (C-1'), 134.3 (C-1''), 133.0 (C-4'), 132.5 (C-3'), 130.1 (C-2'), 129.8 (C-5'), 128.7 (C-3''), 128.6 (C-4''), 128.5 (C-2''), 127.3 (C-6'), 126.3 (C-3),

67.6 (OCH_2), 23.0 (Me); v_{max}/ cm^{-1} 3061 (C-H aromatic), 2964 (C-H alkane), 1730 (C=O), 1563 (C=C aromatic), 1550 (C=N), 1107 (C-O ester).

5.2 β-haematin inhibition assay method

The β-haematin inhibition assay was measured using the method described by Carter et. al.[99] Modifications were done for manual liquid delivery. A 20 ml stock solution containing water/acetone/NP-40 (305.5 µM)/DMSO 35%/35%/20%/10% (*v*/*v*) was prepared. Using a multichannel pipette, 100µM of the detergent solution was added to each well (columns 1-11) in the plate. The compounds were dissolved in DMSO to give final concentration of 20 mM thereafter followed by delivery of the compound to the wells (column 12). A serial dilution of the solution using a multichannel pipette to give final concentrations of 0 -1000 µM was done. A solution of 25 mM haematin was prepared by dissolving 8 mg of haemin in 0.5 mL of dimethyl sulfoxide (DMSO) and sonicated for complete dissolution. For a final 222.2 µM buffered solution, 178.8 µM of the 25 mM haematin solution was added to 20 mL solution of 1 M sodium acetate buffer (pH 4.9) prepared by dissolving sodium acetate in H_2O with 2.4 ml acetic acid to make a 50 ml solution. Addition of buffered solution to the wells gave final haematin and acetate buffer concentrations of 100 µM and 1 M respectively, followed by incubation of plate at 37 °C in a water bath for 5 hours. The β-haematin inhibition assay analysis was done using the colorimetric pyridine-ferrichrome method developed by Ncokazi and Egan.[123] A solution of 50% (v/v) pyridine, 20 % (v/v) acetone, 30% (v/v) H_2O and 0.2 M HEPES buffer (pH 7.4) was prepared and 32 µL added to each of the well plate to give a final pyridine concentration of 5% (v/v). Acetone (60 µL) was then added to each well. To determine the drug response against β-haematin formation, absorbance of the pyridine-haem complex in the plate wells was measured at 405 nm using a SpectaMax plate reader. The data were then fitted to a sigmoidal dose-response curve using the GraphPad Prism v3.02 programme and the IC_{50} (amount of drug needed to inhibit β-haematin formation by 50%) of the compound determined.

5.3 The parasite growth inhibition assay.

The antiplasmodium activity was measured using a method described previously. [125]A 20mg/ml stock solution of test sample was prepared by dissolving each analogue in 100% DMSO followed by sonication of the mixture. Thereafter delivery of the compound to the well plate containing the *P. falciparum* infected RBC was carried out. A serial dilution using a multichannel pipette from 100 µg/nL to final concentration of 0.2 µg/nL was then done. The test samples were tested against *P. falciparum* infected RBC and quantitative assessment of the activity was determined using the lactate dehydrogenase assay.[127]

Equations[135]

$$\boldsymbol{VAR = 10^{(logD_{pH\ 7.4}\ logD_{pHv})}}$$

Assuming pH_v = 5.0

$$\boldsymbol{LAR = VAR\ 10^{logD_{pH7.4}}}$$

References

1. W. H. O., *The World Malaria Report 2014*, WHO Global Malaria Programme, Geneva, 2014.
2. L. M. Prescott, J. P. Harley and D. A. Klein, *Microbiology*, McGraw-Hill, New York, sixth edn., 2005.
3. F. E. G. Cox, *Parasites & Vectors*, 2010, 3, 1-9.
4. R. I. Chima, C. A. Goodman and A. Mills, *Health Policy*, 2003, 63, 17-36.
5. W. H. O., *The World Malaria Report 2011*, WHO Global Malaria Programme, Geneva, 2011.
6. L. H. Bannister and I. W. Sherman, *Encyclopedia of Life Sciences*, 2009, 1-12.
7. L. H. Miller, D. I. Baruch, K. Marsh and O. K. Doumbo, *Nature* 2002, 415, 672-679.
8. M. Rueping, A. R. Antonchick and T. Theissmann, *Angewandte Chemie-International Edition*, 2006, 45, 3683-3686.
9. N. I. A. I. D., *Understanding Malaria* http://www.niaid.nih.gov/topics/Malaria/Documents/malaria.pdf access 04/03/2015, NIAID Science Education U.S. Department of Health and Human Services, National Institutes of Health, National Institute of Allergy and Infectious Diseases, 2007.
10. R. D. Gosling, L. Okell, J. Mosha and D. Chandramohan, *Clinical Microbiology and Infection*, 2011, 17, 1617-1623.
11. C. E. Shulman and E. K. Dorman, *Transactions of the Royal Society of Tropical Medicine and Hygiene*, 2003, 97, 30-35.
12. N. F. Walker, B. Nadjm and C. J. M. Whitty, *Medicine*, 2014 42, 100-106.
13. J. F. Trape, G. Pison, M. P. Preziosi, C. Enel, A. D. du Lou, V. Delaunay, B. Samb, E. Lagarde, J. F. Molez and F. Simondon, *Comptes Rendus De l'Académie Des Sciences Serie iii-Sciences De La Vie-Life Sciences*, 1998, 321, 689-697.
14. M. Melcher, R. A. Muhle, P. P. Henrich, S. M. Kraemer, M. Avril, I. Vigan-Womas, O. Mercereau-Puijalon, J. D. Smith and D. A. Fidock, *Cellular Microbiology*, 2010, 12, 1446-1462.
15. D. I. Baruch, *Baillière's Clinical Haemotology*, 1999, 12, 747-761.

16. J. C. Hafalla, O. Silvie and K. Matuschewski, *Immunological Reviews*, 2011, 240, 297-316.
17. N. Gerald, B. Mahajan and S. Kumar, *Eukaryotic Cell*, 2011, 10, 474-482.
18. L. Tilley, M. W. A. Dixon and K. Kirk, *International Journal of Biochemistry & Cell Biology*, 2011, 43, 839-842.
19. M. A. Ambele, B. T. Sewell, F. R. Cummings, P. J. Smith and T. J. Egan, *Crystal Growth & Design*, 2013, 13, 4442-4452.
20. T. J. Egan, *Molecular and Biochemical Parasitology*, 2008, 157, 127-136.
21. T. J. Egan, *Journal of Inorganic Biochemistry*, 2008, 102, 1288-1299.
22. A. K. Tripathi, S. K. Garg and B. L. Tekwani, *Biochemical and Biophysical Research Communications*, 2002, 290, 595-601.
23. H. Ginsburg, O. Famin, J. M. Zhang and M. Krugliak, *Biochemical Pharmacology*, 1998, 56, 1305-1313.
24. P. Loria, S. Miller, M. Foley and L. Tilley, *Biochemical Journal*, 1999, 339, 363-370.
25. M. Krugliak, J. M. Zhang and H. Ginsburg, *Molecular and Biochemical Parasitology*, 2002, 119, 249-256.
26. G. M. Lancisi, *De Noxiis Paludum Effluvius Eorumque Remediis*, J.M. Salvioni, Rome, 1717.
27. S. Litsios, *Social History of Medicine*, 2000, 13, 341-342.
28. R. Thome, S. C. Pinto Lopes, F. T. Maranhao Costa and L. Verinaud, *Immunology Letters*, 2013, 153, 50-57.
29. K. Bendrat, B. J. Berger and A. Cerami, *Nature*, 1995, 378, 138-139.
30. S. Kumar, M. Guha, V. Choubey, P. Maity and U. Bandyopadhyay, *Life Sciences*, 2007, 80, 813-828.
31. A. Dorn, R. Stoffel, H. Matile, A. Bubendorf and R. G. Ridley, *Nature*, 1995, 374, 269-271.
32. A. Dorn, S. R. Vippagunta, H. Matile, A. Bubendorf, J. L. Vennerstrom and R. G. Ridley, *Biochemical Pharmacology*, 1998, 55, 737-747.
33. C. D. Fitch, G. Z. Cai, Y. F. Chen and J. D. Shoemaker, *Biochimica Et Biophysica Acta-Molecular Basis of Disease*, 1999, 1454, 31-37.
34. C. D. Fitch, G. Z. Cai and J. D. Shoemaker, *Biochimica Et Biophysica Acta-Molecular Basis of Disease*, 2000, 1535, 45-49.

35. J. M. Pisciotta, I. Coppens, A. K. Tripathi, P. F. Scholl, J. Shuman, S. Bajad, V. Shulaev and D. J. Sullivan, Jr., *Biochemical Journal*, 2007, 402, 197-204.
36. N. T. Huy, Y. Shima, A. Maeda, T. T. Men, K. Hirayama, A. Hirase, A. Miyazawa and K. Kamei, *Plos One*, 2013, 8, e70025.
37. A. N. Hoang, R. D. Sandlin, A. Omar, T. J. Egan and D. W. Wright, *Biochemistry*, 2010, 49, 10107-10116.
38. S. Pagola, P. W. Stephens, D. S. Bohle, A. D. Kosar and S. K. Madsen, *Nature*, 2000, 404, 307-310.
39. A. Hamsik, *Zeitschrift fur Physiologische Chemie*, 1936, 190, 199-215.
40. M. A. Ambele and T. J. Egan, *Malaria Journal*, 2012, 11, 337.
41. A. N. Hoang, K. K. Ncokazi, K. A. de Villiers, D. W. Wright and T. J. Egan, *Dalton Transactions*, 2010, 39, 1235-1244.
42. C. D. Fitch and P. Kanjananggulpan, *Journal of Biological Chemistry*, 1987, 262, 15552-15555.
43. R. G. Ridley, *Nature*, 2002, 415, 686-693.
44. S. A. Ward, E. J. P. Sevene, I. M. Hastings, F. Nosten and R. McGready, *Lancet Infectious Diseases*, 2007, 7, 136-144.
45. S. Chusacultanachai, P. Thiensathit, B. Tarnchompoo, W. Sirawaraporn and Y. Yuthavong, *Molecular and Biochemical Parasitology*, 2002, 120, 61-72.
46. J. K. Baird, *New England Journal of Medicine*, 2005, 352, 1565-1577.
47. W. R. J. Taylor and N. J. White, *Drug Safety*, 2004, 27, 25-61.
48. C. Roper, R. Pearce, B. Bredenkamp, J. Gumede, C. Drakeley, F. Mosha, D. Chandramohan and B. Sharp, *Lancet*, 2003, 361, 1174-1181.
49. O. Skold, *Drug Resistance Updates*, 2000, 3, 155-160.
50. T. Triglia, J. G. T. Menting, C. Wilson and A. F. Cowman, *Proceedings of the National Academy of Sciences of the United States of America*, 1997, 94, 13944-13949.
51. T. Gebru, A. Hailu, P. G. Kremsner, J. F. J. Kun and M. P. Grobusch, *Malaria Journal*, 2006, 5, 112.
52. J. Krungkrai, *Parasitology*, 2004, 129, 511-524.
53. H. J. Painter, J. M. Morrisey and A. B. Vaidya, *Antimicrobial Agents and Chemotherapy*, 2010, 54, 5281-5287.

54. A. L. Baggish and D. R. Hill, *Antimicrobial Agents and Chemotherapy*, 2002, 46, 1163-1173.

55. M. Korsinczky, N. H. Chen, B. Kotecka, A. Saul, K. Rieckmann and Q. Cheng, *Antimicrobial Agents and Chemotherapy*, 2000, 44, 2100-2108.

56. I. K. Srivastava, H. Rottenberg and A. B. Vaidya, *Journal of Biological Chemistry*, 1997, 272, 3961-3966.

57. X. C. Ding, H.-P. Beck and G. Raso, *Trends in Parasitology*, 2011, 27, 73-81.

58. A. M. Dondorp, F. Nosten, P. Yi, D. Das, A. P. Phyo, J. Tarning, K. M. Lwin, F. Ariey, W. Hanpithakpong, S. J. Lee, P. Ringwald, K. Silamut, M. Imwong, K. Chotivanich, P. Lim, T. Herdman, S. S. An, S. Yeung, P. Singhasivanon, N. P. J. Day, N. Lindegardh, D. Socheat and N. J. White, *New England Journal of Medicine*, 2009, 361, 455-467.

59. A. M. Dondorp, S. Yeung, L. White, C. Nguon, N. P. J. Day, D. Socheat and L. von Seidlein, *Nature Reviews Microbiology*, 2010, 8, 272-280.

60. A. Robert, C. Bonduelle, S. A. L. Laurent and B. Meunier, *Journal of Physical Organic Chemistry*, 2006, 19, 562-569.

61. Y. Tu, *Nature Medicine*, 2011, 17, 1217-1220.

62. E. A. Ashley, M. Dhorda, R. M. Fairhurst, C. Amaratunga, P. Lim, S. Suon, S. Sreng, J. M. Anderson, S. Mao, B. Sam, C. Sopha, C. M. Chuor, C. Nguon, S. Sovannaroth, S. Pukrittayakamee, P. Jittamala, K. Chotivanich, K. Chutasmit, C. Suchatsoonthorn, R. Runcharoen, T. T. Hien, N. T. Thuy-Nhien, N. V. Thanh, N. H. Phu, Y. Htut, K. T. Han, K. H. Aye, O. A. Mokuolu, R. R. Olaosebikan, O. O. Folaranmi, M. Mayxay, M. Khanthavong, B. Hongvanthong, P. N. Newton, M. A. Onyamboko, C. I. Fanello, A. K. Tshefu, N. Mishra, N. Valecha, A. P. Phyo, F. Nosten, P. Yi, R. Tripura, S. Borrmann, M. Bashraheil, J. Peshu, M. A. Faiz, A. Ghose, M. A. Hossain, R. Samad, M. R. Rahman, M. M. Hasan, A. Islam, O. Miotto, R. Amato, B. MacInnis, J. Stalker, D. P. Kwiatkowski, Z. Bozdech, A. Jeeyapant, P. Y. Cheah, T. Sakulthaew, J. Chalk, B. Intharabut, K. Silamut, S. J. Lee, B. Vihokhern, C. Kunasol, M. Imwong, J. Tarning, W. J. Taylor, S. Yeung, C. J. Woodrow, J. A. Flegg, D. Das, J. Smith, M. Venkatesan, C. V. Plowe, K. Stepniewska, P. J. Guerin, A. M. Dondorp, N. P. Day and N. J. White, *New England Journal of Medicine*, 2014, 371, 411-423.

63. A.-C. Uhlemann and D. A. Fidock, *Lancet*, 2012, 379, 1928-1930.

64. R. M. Fairhurst, G. M. L. Nayyar, J. G. Breman, R. Hallett, J. L. Vennerstrom, S. Duong, P. Ringwald, T. E. Wellems, C. V. Plowe and A. M. Dondorp, *American Journal of Tropical Medicine and Hygiene*, 2012, 87, 231-241.
65. J. Achan, A. O. Talisuna, A. Erhart, A. Yeka, J. K. Tibenderana, F. N. Baliraine, P. J. Rosenthal and U. D'Alessandro, *Malaria Journal*, 2011, 10.
66. A. R. Renslo, *ACS Medicinal Chemistry Letters*, 2013, 4, 1126-1128.
67. R. Buller, M. L. Peterson, O. Almarsson and L. Leiserowitz, *Crystal Growth & Design*, 2002, 2, 553-562.
68. A. F. Slater, *Pharmacology & Therapeutics*, 1993, 57, 203-235.
69. G. R. Coatney, *American Journal of Tropical Medicine and Hygiene*, 1963, 12, 121-128.
70. J. M. Combrinck, T. E. Mabotha, K. K. Ncokazi, M. A. Ambele, D. Taylor, P. J. Smith, H. C. Hoppe and T. J. Egan, *ACS Chemical Biology*, 2013, 8, 133-137.
71. M. S. Walczak, K. Lawniczak-Jablonska, A. Wolska, A. Sienkiewicz, L. Suarez, A. J. Kosar and D. S. Bohle, *Journal of Physical Chemistry B*, 2011, 115, 1145-1150.
72. A. V. Pandey, H. Bisht, V. K. Babbarwal, J. Srivastava, K. C. Pandey and V. S. Chauhan, *Biochemical Journal*, 2001, 355, 333-338.
73. T. J. Egan, R. Hunter, C. H. Kaschula, H. M. Marques, A. Misplon and J. Walden, *Journal of Medicinal Chemistry*, 2000, 43, 283-291.
74. D. J. Sullivan, I. Y. Gluzman, D. G. Russell and D. E. Goldberg, *Proceedings of the National Academy of Sciences of the United States of America*, 1996, 93, 11865-11870.
75. I. Weissbuch and L. Leiserowitz, *Chemical Reviews*, 2008, 108, 4899-4914.
76. E. Y. Klein, *International Journal of Antimicrobial Agents*, 2013, 41, 311-317.
77. T. J. Egan, *Trends in Parasitology*, 2006, 22, 235-237.
78. G. Awasthi and A. Das, *Memorias Do Instituto Oswaldo Cruz*, 2013, 108, 947-961.
79. R. E. Martin, R. V. Marchetti, A. I. Cowan, S. M. Howitt, S. Broer and K. Kirk, *Science*, 2009, 325, 1680-1682.
80. H. O. Alkadi, *Chemotherapy*, 2007, 53, 385-391.
81. M. Botta, F. Corelli, F. Manetti and A. Tafi, *Farmaco*, 2002, 57, 153-165.
82. E. L. Flannery, A. K. Chatterjee and E. A. Winzeler, *Nature Reviews Microbiology*, 2013, 11, 849-862.

83. I. Gashaw, P. Ellinghaus, A. Sommer and K. Asadullah, *Drug Discovery Today*, 2011, 16, 1037-1043.

84. A. C. Good, S. R. Krystek and J. S. Mason, *Drug Discovery Today*, 2000, 5, S61-S69.

85. P. L. Olliaro and Y. Yuthavong, *Pharmacology & Therapeutics*, 1999, 81, 91-110.

86. G. L. Patrick, *An introduction to Medicinal Chemistry*, Oxford University press Oxford, Fourth edn., 2009.

87. J. G. Topliss, *Journal of Medicinal Chemistry*, 1972, 15, 1006.

88. J. G. Topliss, *Journal of Medicinal Chemistry*, 1977, 20, 463-469.

89. J. G. Topliss, *Topliss Sets in Drug Design*, Maybridge MedChem 2, Maybridge.

90. R. D. Sandlin, M. D. Carter, P. J. Lee, J. M. Auschwitz, S. E. Leed, J. D. Johnson and D. W. Wright, *Antimicrobial Agents and Chemotherapy*, 2011, 55, 3363-3369.

91. R. D. Sandlin, K. Y. Fong, K. J. Wicht, H. M. Carrell, T. J. Egan and D. W. Wright, *International Journal for Parasitology-Drugs and Drug Resistance*, 2014, 4, 316-325.

92. E. M. P. Silva, P. A. M. M. Varandas and A. M. S. Silva, *Synthesis*, 2013, 45 3053-3089.

93. G. Swarnalatha, G. Prasanthi, N. Sirisha and C. Madhusudhana Chetty, *International Journal of ChemTech Research*, 2011, 3, 75-89.

94. C. Bladen, M. G. Gunduz, R. Simsek, C. Safak and G. W. Zamponi, *Pflugers Archiv-European Journal of Physiology*, 2014, 466, 1355-1363.

95. J. J. V. Eynde and A. Mayence, *Molecules*, 2003, 8, 381-391.

96. M. Filipan-Litvic, M. Litvic, I. Cepanec and V. Vinkovic, *Molecules*, 2007, 12, 2546-2558.

97. A. M. Vijesh, A. M. Isloor, S. K. Peethambar, K. N. Shivananda, T. Arulmoli and N. A. Isloor, *European Journal of Medicinal Chemistry*, 2011, 46, 5591-5597.

98. N. Mvumvu, BSc(Hons) Chemistry, University of Cape Town, 2012.

99. M. D. Carter, V. V. Phelan, R. D. Sandlin, B. O. Bachmann and D. W. Wright, *Combinatorial Chemistry & High Throughput Screening*, 2010, 13, 285-292.

100. H. J. Schneider and M. Wang, *Journal of Organic Chemistry*, 1994, 59, 7464-7472.

101. D. Kuter, K. Chibale and T. J. Egan, *Journal of Inorganic Biochemistry*, 2011, 105, 684-692.

102. J. Clayden, N. Greeves, S. Warren and P. Wothers, *Organic Chemistry*, Oxford University Press Inc., New York, United States, 2001.

103. S. Benetti, R. Romagnoli, C. Derisi, G. Spalluto and V. Zanirato, *Chemical Reviews*, 1995, 95, 1065-1114.
104. J. Christoffers and N. Onal, *European Journal of Organic Chemistry*, 2000, 1633-1635.
105. R. J. Clemens, *Chemical Reviews*, 1986, 86, 241-318.
106. R. Gomez-Bombarelli, M. Gonzalez-Perez, M. T. Perez-Prior, J. A. Manso, E. Calle and J. Casado, *Chemical Research in Toxicology*, 2008, 21, 1964-1969.
107. W. Bo, Y. L. Ming and S. J. Shuan, *Tetrahedron Letters*, 2003, 44, 5037-5039.
108. M. L. Kantam, V. Neeraja, B. Bharathi and C. V. Reddy, *Catalysis Letters*, 1999, 62, 67-69.
109. J. S. Yadav, B. V. S. Reddy, A. D. Krishna, C. S. Reddy and A. V. Narsaiah, *Journal of Molecular Catalysis A: Chemical*, 2007, 261, 93-97.
110. S. P. Chavan, K. Pasupathy, S. Shengule, V. Shinde and R. Anand, *Arkivoc*, 2005, 162-168.
111. S. P. Chavan, K. Shivasankar, R. Sivappa and R. Kale, *Tetrahedron Letters*, 2002, 43, 8583-8586.
112. H. R. Memarian, M. Abdoli-Senejani and D. Dopp, *Zeitschrift Fur Naturforschung Section B-a Journal of Chemical Sciences*, 2006, 61, 50-56.
113. Z. Wang, Q. Liu, W. Zhang and Q. Chen, *Journal of Chemical Research*, 2013, DOI: 10.3184/174751913x13843392957323, 748-750.
114. M. A. Zolfigol, M. Bagherzadeh, K. Niknam, F. Shirini, I. Mohammadpoor-Baltork, A. G. Choghamarani and M. Baghbanzadeh, *Journal of the Iranian Chemical Society*, 2006, 3, 73-80.
115. M. A. Zolfigol, M. Kiany-Borazjani, M. M. Sadeghi, I. Mohammadpoor-Baltork and H. R. Memarian, *Synthetic Communications*, 2000, 30, 3919-3923.
116. M. Karelson, V. S. Lobanov and A. R. Katritzky, *Chemical Reviews*, 1996, 96, 1027-1043.
117. ChemAxon, MarvinSketch v 6.3.1, Hungary, Europe.
118. D. C. Kombo, K. Tallapragada, R. Jain, J. Chewning, A. A. Mazurov, J. D. Speake, T. A. Hauser and S. Toler, *Journal of Chemical Information and Modeling*, 2013, 53, 327-342.
119. F. Lovering, J. Bikker and C. Humblet, *Journal of Medicinal Chemistry*, 2009, 52, 6752-6756.

120. J. M. Wang, X. Q. Xie, T. J. Hou and X. J. Xu, *Journal of Physical Chemistry A*, 2007, 111, 4443-4448.

121. J. A. Padron, R. Carrasco and R. F. Pellon, *Journal of Pharmacy and Pharmaceutical Sciences*, 2002, 5, 267-274.

122. Y. H. Zhao, M. H. Abraham and A. M. Zissimos, *Journal of Organic Chemistry*, 2003, 68, 7368-7373.

123. K. K. Ncokazi and T. J. Egan, *Analytical Biochemistry*, 2005, 338, 306-319.

124. H. Motulsky, *GraphPad Prism v3.02*, GraphPad Software Inc., San Diego, California.

125. V. K. Zishiri, M. C. Joshi, R. Hunter, K. Chibale, P. J. Smith, R. L. Summers, R. E. Martin and T. J. Egan, *Journal of Medicinal Chemistry*, 2011, 54, 6956-6968.

126. W. Trager and J. B. Jensen, *Science*, 1976, 193, 673-675.

127. M. T. Makler, J. M. Ries, J. A. Williams, J. E. Bancroft, R. C. Piper, B. L. Gibbins and D. J. Hinrichs, *American Journal of Tropical Medicine and Hygiene*, 1993, 48, 739-741.

128. C. A. Lipinski, F. Lombardo, B. W. Dominy and P. J. Feeney, *Advanced Drug Delivery Reviews*, 1997, 23, 3-25.

129. C. A. Lipinski, F. Lombardo, B. W. Dominy and P. J. Feeney, *Advanced Drug Delivery Reviews*, 2001, 46, 3-26.

130. C. A. Lipinski, F. Lombardo, B. W. Dominy and P. J. Feeney, *Advanced Drug Delivery Reviews*, 2012, 64, 4-17.

131. S. J. Marrink and H. J. C. Berendsen, *Journal of Physical Chemistry*, 1996, 100, 16729-16738.

132. A. Dorn, S. R. Vippagunta, H. Matile, C. Jaquet, J. L. Vennerstrom and R. G. Ridley, *Biochemical Pharmacology*, 1998, 55, 727-736.

133. P. G. Bray, S. R. Hawley and S. A. Ward, *Molecular Pharmacology*, 1996, 50, 1551-1558.

134. S. R. Hawley, P. G. Bray, P. M. O'Neill, B. K. Park and S. A. Ward, *Biochemical Pharmacology*, 1996, 52, 723-733.

135. D. C. Warhurst, J. C. Craig, P. S. Adagu, R. K. Guy, P. B. Madrid and Q. L. Fivelman, *Biochemical Pharmacology*, 2007, 73, 1910-1926.

136. D. J. Triggle, *Drug Discovery Today*, 1997, 2, 138-147.

137. L. A. Nguyen, H. He and C. Pham-Huy, *International Journal of Biomedical Science : IJBS* 2006, 2, 85-100.

138. D. Setamdideh and B. Zeynizadeh, *Zeitschrift Fur Naturforschung Section B: A Journal of Chemical Sciences*, 2006, 61, 1275-1281.

139. L. Koren-Selfridge, H. N. Londino, J. K. Vellucci, B. J. Simmons, C. P. Casey and T. B. Clark, *Organometallics*, 2009, 28, 2085-2090.

140. Y. Ogata and K. Tomizawa, *Journal of Organic Chemistry*, 1980, 45, 785-788.

141. L. J. Zhang, S. W. Wang, S. L. Zhou, G. S. Yang and E. H. Sheng, *Journal of Organic Chemistry*, 2006, 71, 3149-3153.

142. M. Iman, A. Davood, A. R. Nematollahi, A. R. Dehpoor and A. Shafiee, *Archives of Pharmacal Research*, 2011, 34, 1417-1426.

143. P. Lacotte, D.-A. Buisson and Y. Ambroise, *European Journal of Medicinal Chemistry*, 2013, 62, 722-727.

144. G. B. D. Rao, B. N. Acharya and M. P. Kaushik, *Tetrahedron Letters*, 2013, 54, 6644-6647.

145. F. Bossert, E. Wehinger, K. Stoepel, W. Vater and S. Kasda, *German Offen*, 1976, DE25081 A25081 19760909.

146. H. Hong, M. Jianguo, J. Li, C Dong, L. Zhang and Z. S. Faming, 2014, CN103553995 A 120140205.

147. B. Kohl, R. W. Ulrich and D. Flockerzi, *Patent Cooperation Treaty Application*, 1988, W08809331 A08809331 19881201.

148. J. T. Nguyen, C. A. Velazquez and E. E. Knaus, *Bioorganic & Medicinal Chemistry*, 2005, 13, 1725-1738.

149. G. Quadro and J. Cahn, *European Patent Application*, 1987, EP218996 A218992 19870422.

150. N. Pedemonte, D. Boido, O. Moran, M. Giampieri, M. Mazzei, R. Ravazzolo and L. J. V. Galietta, *Molecular Pharmacology*, 2007, 72, 197-207.